POLITECNICO DI TORINO

SCUOLA DI DOTTORATO
Dottorato in Ingegneria Aerospaziale - XXII ciclo
Doctorat en mécanique de l'Université Paris Ouest - Nanterre La Défense,
Laboratoire de Mécanique de Paris X (LMpX)

Ph.D. Dissertation

Modeling and validation of multilayered structures for spacecraft, including multifield interactions

Pietro Nali

Tutors
Prof. Erasmo Carrera
Prof. Olivier Polit
Dr. Adriano Calvi

Settembre 2010

a mio padre Nino

Summary

This work deals with classical and mixed variational statements for the analysis of layered structures under the effect of four different fields: mechanical, thermal, electrical and magnetic. Constitutive equations, in terms of coupled mechanical-thermal-electrical-magnetic field variables, are obtained on the basis of a thermodynamics approach. The Principle of Virtual Displacements (PVD) and the Reissner's Mixed Variational Theorem (RMVT) are employed. The latter permits interlaminar variables, such as transverse stresses, transverse electrical displacements etc. to be assumed "a priori". A number of particular cases of the considered variational statements are proposed. The Finite Element case for multilayerd plates is addressed to. A new condensed notation is introduced into the Carrera's Unified Formulation (CUF) framework, which leads to governing equations and Finite Element (FE) matrices in terms of a few fundamental nuclei. Variable kinematics, as well as layer-wise and equivalent single layer descriptions, have been implemented for the considered FEs according to the CUF. The presented benchmarks and the assessments show the effectiveness of the proposed approach.
The accuracy of the mechanical analysis performed in this work would imply a commercial implementation in order to make available advanced FEs for the calculation of the stress field and to properly apply failure criteria to multilayered structures.
The accurate results obtained in the multifield coupled analysis demonstrate that the proposed multifield plate FEs furnish the same results obtainable only using solid FEs in commercial software and then with a higher computational effort. In addition, some advanced fully coupled thermo-mechanical static, modal and buckling analysis which are possible in the framework of the proposed approach are currently not available at the commercial level, even employing solid FEs.
The showed FEM results are obtained in MUL2 FEM code, which has been developed coherently with the presented formulation.

Résumé

Cette thèse s'intéresse aux principes variationels classiques et mixtes pour l'étude des structures stratifiées dans lesquelles agissent quatre champs différents: mécanique, thermique, électrique et magnétique. Les équations constitutives, obtenues par une approche thermodynamique, sont présentées sous forme couplée pour les champs mécanique, thermique, électrique et magnétique. Le principe des puissances virtuelles et le théorème variationel mixte de Reissner sont appliquées. Ce dernier permet d'assurer "a priori" la continuité des variables significatives aux intercouches pour les contraintes transversales, le déplacement électrique, etc. Plusieurs cas particuliers du principe variationel considéré sont ainsi proposés. On considére l'analyse par la méthode des éléments finis (E.F) pour les structures multicouches. Une nouvelle notation condensée est introduite dans le contexte de la formulation unifiée, laquelle permet d'obtenir les matrices élémentaires à partir des nucleus fondamentaux propres à cette approche. En accord avec la formulation unifiée, les E.F sont implémentés avec une cinématique variable et en utilisant les descriptions *layer-wise* (par couche) et *equivalent single layer* (couche équivalente). L'approche présentée est évaluée à travers plusieurs exemples et par comparaisons avec des solutions exactes. La précision numérique des analyses mécaniques nécessite l'implémentation dans des codes E.F commerciaux d'E.F appropriés pour calculer les champ de contrainte dans l'épaisseur des structures multicouches afin de pouvoir appliquer proprement des critères de rupture pour ces problèmes.
Les résultats obtenus dans les analyses multiphysiques couplées démontrent que les E.F multiphysiques pour structures multicouches proposées fournissent les mêmes résultats qu'avec les codes commerciaux, mais en utilisant des E.F solides qui s'avèrent beaucoup plus coûteux en temps de modélisation et de calcul. De plus, les analyses thermomécaniques statique, modale et de flambement, possible en utilisant les outils présentés dans ce travail, ne peuvent être effectués dans les codes commerciaux, même en utilisant des E.F solides.
Enfin, les résultats numériques présentés dans cette thèse ont été obtenus avec le code MUL2, implémenté conformément à la formulation présentée.

Acknowledgments

To me this PhD means three years of interesting cooperation with many different people and organizations. I would like to acknowledge everybody who worked with me during this period, with the awareness that we will continue to be together involved in many other future scientific activities. A special thanks is to my family that supported me during my studies and to my girlfriend Silvia for the quality time together and for her suggestions concerning the illustrations of this work. I would like to express my gratitude to my collegues Axel, Saverio and Marco for the nice collaboration on many interesting subjects. I would like also to thank my friends Giuseppe, Carlo, Franco, Stefano, Fabio, Antonio and Vincenzo for the closenees showed keeping in touch with me during my studies and to some of them for having visited me in Netherlands or in Torino during these years. One more thanks is to my friend Morciano for the cool convivial time spent in Torino having often lunch or dinner together.
Last but not least, I'm very grateful to Prof. Erasmo Carrera, Prof. Olivier Polit and Dr. Adriano Calvi, respectively my tutor at the *Politecnico di Torino*, my tutor at *Université Paris Ouest - Nanterre La Défense* and my supervisor at the European Space Agency, for all the kind suggestions that they punctually provided me with and for the interest devoted to present activity and to future developments.

Endorsers of the Activity

This activity is the result of a cooperation between the *Politecnico di Torino (Dipartimento di Ingegneria Aeronautica e Spaziale, DIASP)* and the European Space Agency (ESA), within the frame of the ESA D/TEC Networking and Partnering Initiative (NPI), ESTEC-Contract No. 21082/06/NL/PA.

Table of contents

Nomenclature

B	magnetic field
C	specific heat per unit mass
C_{ijkl}	elastic coefficients - Hooke's law
D	electrical displacement
$\boldsymbol{D}$	differential operator
e_{ijn}	piezoelectric coefficients
E	electric field
$\boldsymbol{\mathcal{E}}$	intensive variable vector
F	dissipation function
F_τ	set of polynomials independent functions, employed to describe *var* along the thickness direction
G	Gibbs free energy per unit of volume
$\boldsymbol{G}$	vector of unknowns in mixed formulation
h	layer thickness
$\boldsymbol{H}$	constitutive matrix
H	auxiliary magnetic field
$\mathcal{H}$	thermodynamic enthalpy density
k	(superscript) quantity related to the k-th layer
$\boldsymbol{K}$	stiffness matrix
$\boldsymbol{K}^{k\tau sij}$	stiffness fundamental nucleus
$\boldsymbol{K_G}^{k\tau sij}$	buckling fundamental nucleus
L_e	work made by external loads
$\boldsymbol{M}$	mass matrix
$\boldsymbol{M}^{k\tau sij}$	mass fundamental nucleus
N_i	shape functions
p_n	pyroelectric coefficients
$\boldsymbol{P}^k$	vector of nodal external loads
q_i	heat flux component
q_{ij}	piezomagnetic coefficients
$\boldsymbol{Q}$	nodal unknown vector in PVD formulation
r_n	pyromagnetic coefficients
$\boldsymbol{R}$	nodal unknown vector in RMVT formulation
$\boldsymbol{\mathcal{S}}$	extensive variable vector
U	internal energy per unit of volume
$\boldsymbol{U}$	primary unknowns vector in PVD formulation
V	volume
$\boldsymbol{V}$	primary unknowns vector in RMVT formulation
δ	the variational symbol;
ϵ	strain;
ε_{ij}	permittivity coefficients
ζ	dimensionless plate-thickness coordinate
η	variation of entropy per unit of volume
θ	temperature variation respect to θ_{ref}
ϑ	heat strain
κ_{ij}	conductivity tensor
λ_{ij}	stress-temperature coefficients
μ_{ij}	magnetic permeability coefficients
ρ	density

σ	stress
ς_n	E-H coupling coefficients
ϕ	electric potential
φ	magnetic potential
Ω	layer middle surface

Acronyms

CLT	Classical Laminate Theory (Kirchhoff plate theory)
DOF	Degree Of Freedom
EDn	ESL modeling based on the PVD, with thickness expansion of order n
ESL	Equivalent Single Layer
FE	Finite Element
FEM	Finite Element Method
$FSDT$	First order Shear Deformation Theory (Mindlin plate theory)
LDn	LW modeling based on the PVD, with thickness expansion of order n
LMn	LW modeling based on the RMVT, with thickness expansion of order n
LW	Layer Wise
$MDOF$	Multi Degree Of Freedom
MFP	MultiField Problem
$MITC$	Mixed Interpolated Tensorial Components
MLS	MultiLayered Structure
PVD	Principle of Virtual Displacements
$RMVT$	Reissner's Mixed Variational Theorem
$SDOF$	Single Degree Of Freedom
CUF	Carrera's Unified Formulation

0.1 Introduction

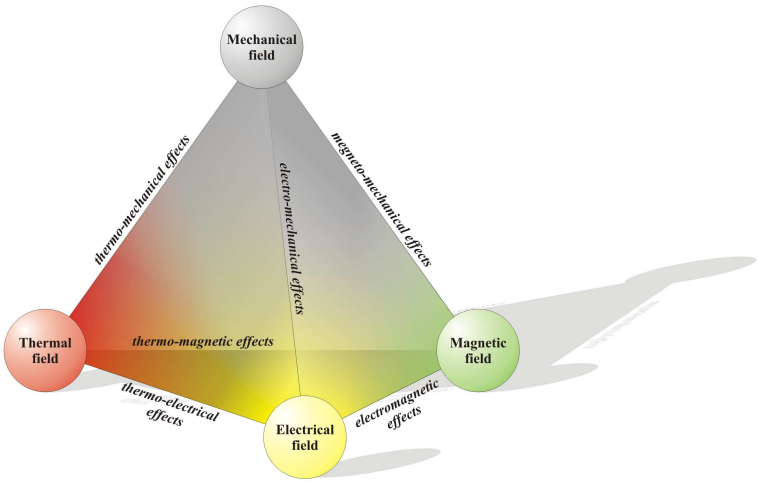

Figure 1. Interaction processes between the mechanical, thermal, electrical, and magnetic fields

In recent decades, Scientists have identified four fundamental physical forces that act in nature: weak, strong, gravitational and electromagnetic. Each one of these forces can be associated to a fundamental physical field. Due to both computational reasons and the Heisenberg uncertainty principle, a deterministic modeling of systems is not possible when referring to these four fields, which concern subatomic scales and relativistic quantities. In order to make a modeling of structures possible without reference to subatomic dimensions, other fields have been defined to substitute the four fundamental ones: mechanical, thermal, electrical and magnetic fields. Interaction processes are in Fig. 1. These all are based on measurable material properties (e.g. the Young modulus for the mechanical case). Such properties describe the behavior of the material in a suitable scale for engineering purposes. It is widely believed that much of the next generation aircraft and spacecraft will be manufactured as multilayered structures (MLSs - Fig. 2) under the action of a combination of two or more of the four fields. Two examples of MultiField Problem (MFP) application are: the so-called “smart structures” in which layers of piezo-electric or piezo-magnetic materials are used as sensors or actuators to develop electro-magnetic fields that are able to counteract thermo-mechanical deformations; inflatable structures that have been planned to be used for the future space exploration missions, which consist of a very special multilayered-made structure subjected to thermo-mechanical loadings and in some cases to electro-magnetic loadings as well. These two examples also show that structures typically employed in MFPs appear as assemblies of flat or curved MLSs.
A number of requirements must be taken into account for an accurate analysis of MFPs and MLSs. The following points dealt with in this work:

1. The Constitutive equations must be derived in a consistent form.
2. The Coupling among the various fields should be accurately described.
3. Inter-layer continuity of the relevant variables must be guaranteed.
4. The employed kinematic model must be rich enough to describe the localized through-the-thickness-distribution of the involved variables in the various layers.

Reference to a thermodynamic basis is mandatory for what at point 1 [1].
As far as point 2 is concerned, the coupling could be introduced as in a *partial* or *full* form. When the coupling is partial, the constitutive laws are uncoupled and the effect of coupling is only introduced as an external loading. If the coupling is full, the constitutive relations are coupled. For instance, if the electro-mechanical coupling is fully included in the formulation of a piezoelectric problem, an electro-mechanic stiffness appears in the governing equations.
As far as point 3 is concerned, it should be pointed out that a classical choice of primary variables for the various fields could violate some interlaminar continuities. This is the case of transverse shear and normal stresses, which for equilibrium reasons, must be continuous at each layer interface, Fig. 3. Such continuity is not enforced in classical modeling which only makes use of displacement variables [2]. The same could be said for transverse electrical displacements or transverse magnetic inductance [3], [4]. As far as point 4 is concerned, it is well known that the use

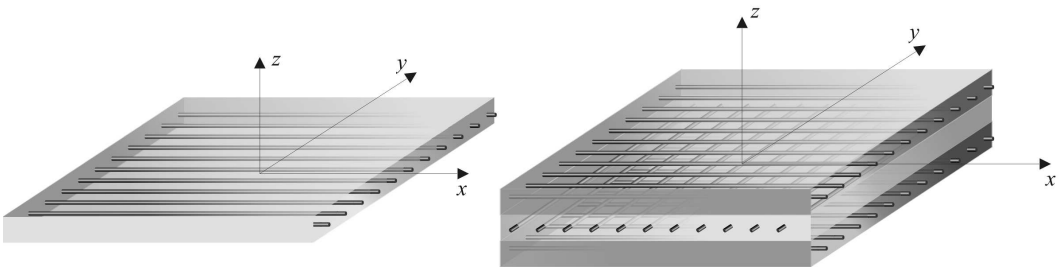

Figure 2. Example of fiber reinforced panels: a Single Layer (on the left) and a Multi Layered Structure (on the right)

of variable kinematic models is mandatory in MLSs subjected to MFP loadings. These loadings, in fact, have an *isotropic/anisotropic* and *localized* nature. For instance, the thermal field, being scalar, is isotropic by definition while the electrical and magnetic fields, being vectorial, can be isotropic or anisotropic. Loadings from these fields are completely different from those from mechanical cases. Consequently, kinematical models that were originally proposed for plate and shell structures subjected to mechanical loading could undergo difficulties analyzing MFPs. Modelings that permits the use of both Equivalent Single Layer (ESL) models, and Layer Wise (LW) models, are mandatory in these cases.
A few pioneering works on the topic are mentioned below. Multilayered composite structures made by orthotropic laminae with embedded piezoelectric patches/layers were studied early on by Mindlin in the contest of displacement formulation [5]. Coupled, two-field formulations with generalized displacements, mechanical displacements and electric potential as independent variables, have been proposed, among others, by Tiersten and Mindlin [6], EerNisse [7] and Tiersten [8]. A first Finite Element (FE) relying on these formulations was proposed by Allik and Hughes [9]. Mindlin [10] and Dokmeci [11] proposed coupled variational principles for the vibration analysis of thermo-piezoelectric plates.
The present work represents a contribution to the analysis of MLSs in case of MFPs, according to the above points 1-4. Under assumption of the field variables, constitutive equations are derived from the Gibbs free energy for fully coupled cases. Classical variational statements, e.g. the principle of virtual displacements (PVD) is extended to MFPs. Fully coupled and partially coupled cases are considered. The necessary continuity of secondary variables at the interface between two adjacent layers is imposed by extending Reissner's Mixed Variational Theorem (RMVT) to MFPs (in work [12] such C_z^0 requirements are illustrated for the pure mechanical case). Variable kinematics models are derived according to the Carrera's Unified Formulation

(CUF) proposed in earlier works by the first author [13], [12], [14]. With respect to previous works ([3], [4], [13], [15]), which were restricted to 2-3 fields, the derivation is herein presented in a compact form and for all the four involved fields. The dimension of the fundamental nuclei related to CUF is given according to the number of the variables involved in the variational statements. The whole notation (e.g. geometrical relations, constitutive equations, variational statements) has been therefore rearranged. By doing this, a number of new significant formulations have been proposed in the framework of both PVD and RMVT. The subcases related to RMVT, which can restrict the interface continuity only to those variables that are of particular significance for the considered problem, are of particular interest.

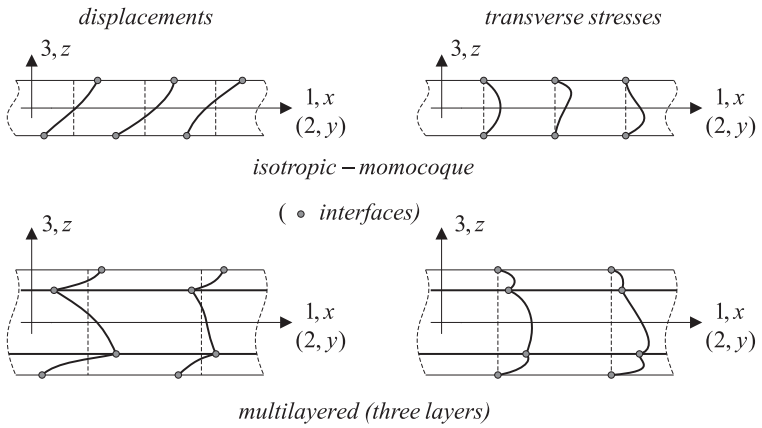

Figure 3. Displacement and transverse stress distribution in the plate thickness direction z. Comparison between a one-layered and a three-layered plate structure

Part I

Theory

Chapter 1

Constitutive and geometrical equations for multifield problems

1.1 Constitutive equations from thermodynamic approach

The constitutive equations are derived, in this section, in the linear case for the considered multifield problems. Standard tensor notation is used and Einstein's summation convention is implied over repeated indices. A cartesian reference system is considered, with the z-axis along the plate-thickness direction, Fig. 2. A set of intensive variables θ, ϵ, E and H, which are respectively the increment in temperature with respect to the reference temperature θ_{ref}, strain, electric field and auxiliary magnetic field, are first assumed as independent variables. The relevant thermodynamic functions are the Gibbs free energy-per-unit of volume G [1], the dissipation F and the thermodynamic enthalpy density $\mathcal{H}$:

$$G = U - \theta\eta + \sigma_{ij}\epsilon_{ij} - E_i D_i - H_i B_i, \tag{1.1}$$

$$F(\vartheta_i) = \frac{1}{2}\kappa_{ij}\vartheta_i\vartheta_j - \tau_0\dot{q}_i, \tag{1.2}$$

$$\mathcal{H}(U,\epsilon_{ij},\theta,\vartheta_i) = G - F, \tag{1.3}$$

where:
U = internal energy per unit of volume;
σ_{ij} = stress tensor;
η = variation of entropy per unit of volume;
D_i = electrical displacements vector;
B_i = magnetic inductance vector;
κ_{ij} = conductivity tensor;
ϑ_i = heat strain vector;
τ_0 = thermal relaxation parameter;
$\dot{q}_i$ = is the temporal derivative of the heat flux q_i.
The dissipation function F has to be used only if a certain temperature is imposed on the surfaces of the structure and the steady-state temperature profile needs to be calculate. Differently, if the interest is in the instantaneous temperature profile caused by a mechanical deformation, the contribution of F has to be neglected [16]. The temporal derivative of the heat flux is set to zero in the present work since only stationary fluxes are considered as boundary conditions.

The Gibbs free energy can be written as a quadratic form according to [1]:

$$\begin{aligned} G = \frac{1}{2}\Bigg(&\theta^2\frac{\partial^2 G}{\partial\theta^2} + \epsilon_{ij}\epsilon_{lm}\frac{\partial^2 G}{\partial\epsilon_{ij}\partial\epsilon_{lm}} + E_iE_l\frac{\partial^2 G}{\partial E_i\partial E_l} + H_iH_l\frac{\partial^2 G}{\partial H_i\partial H_l} + \theta\epsilon_{lm}\frac{\partial^2 G}{\partial\theta\partial\epsilon_{lm}} + \\ &+\theta E_l\frac{\partial^2 G}{\partial\theta\partial E_l} + \theta H_l\frac{\partial^2 G}{\partial\theta\partial H_l} + \epsilon_{ij}\theta\frac{\partial^2 G}{\partial\epsilon_{ij}\partial\theta} + \epsilon_{ij}E_l\frac{\partial^2 G}{\partial\epsilon_{ij}\partial E_l} + \epsilon_{ij}H_l\frac{\partial^2 G}{\partial\epsilon_{ij}\partial H_l} + \\ &+E_i\theta\frac{\partial^2 G}{\partial E_i\partial\theta} + E_i\epsilon_{lm}\frac{\partial^2 G}{\partial E_i\partial\epsilon_{lm}} + E_iH_l\frac{\partial^2 G}{\partial E_i\partial H_l} + H_i\theta\frac{\partial^2 G}{\partial H_i\partial\theta} + H_i\epsilon_{lm}\frac{\partial^2 G}{\partial H_i\partial\epsilon_{lm}} + \\ &+H_iE_l\frac{\partial^2 G}{\partial H_i\partial E_l}\Bigg). \end{aligned} \tag{1.4}$$

Consequently, $\mathcal{H}$ takes the following form:

$$\mathcal{H} = \frac{1}{2}\left(\theta^2\frac{\partial^2 H}{\partial\theta^2} + \epsilon_{ij}\epsilon_{lm}\frac{\partial^2 H}{\partial\epsilon_{ij}\partial\epsilon_{lm}} + \theta\epsilon_{lm}\frac{\partial^2 H}{\partial\theta\partial\epsilon_{lm}} + \epsilon_{ij}\theta\frac{\partial^2 H}{\partial\epsilon_{ij}\partial\theta} - \kappa_{ij}\vartheta_i\vartheta_j\right). \tag{1.5}$$

The exact differential of $\mathcal{H}$ is:

$$d\mathcal{H} = -\eta d\theta + \sigma_{ij}d\epsilon_{ij} - D_i dE_i - B_i dH_i - q_i d\vartheta_i, \tag{1.6}$$

where:

$$\eta = -\left[\frac{\partial\mathcal{H}}{\partial\theta}\right]_{\epsilon,E,H}, \sigma_{ij} = \left[\frac{\partial\mathcal{H}}{\partial\epsilon_{ij}}\right]_{\theta,E,H}, D_i = -\left[\frac{\partial\mathcal{H}}{\partial E_i}\right]_{\theta,\epsilon,H}, B_i = -\left[\frac{\partial\mathcal{H}}{\partial H_i}\right]_{\theta,\epsilon,E}, q_i = \left[\frac{\partial\mathcal{H}}{\partial\vartheta_i}\right]. \tag{1.7}$$

Subscripts refer to the quantities to be kept constant in the differentiation.
Substituting Eq. 1.4 into Eq. 1.7 one has:

$$\eta = \theta\left[-\frac{\partial^2\mathcal{H}}{\partial\theta^2}\right]_{\epsilon,E,H} + \epsilon_{ij}\left[-\frac{\partial^2\mathcal{H}}{\partial\theta\partial\epsilon_{ij}}\right]_{E,H} + E_i\left[-\frac{\partial^2\mathcal{H}}{\partial\theta\partial E_i}\right]_{\epsilon,H} + H_i\left[-\frac{\partial^2\mathcal{H}}{\partial\theta\partial H_i}\right]_{\epsilon,E}; \tag{1.8}$$

$$\sigma_{ij} = \theta\left[\frac{\partial^2\mathcal{H}}{\partial\epsilon_{ij}\partial\theta}\right]_{E,H} + \epsilon_{ij}\left[\frac{\partial^2\mathcal{H}}{\partial\epsilon_{ij}\partial\epsilon_{lm}}\right]_{\theta,E,H} + E_l\left[\frac{\partial^2\mathcal{H}}{\partial\epsilon_{ij}\partial E_l}\right]_{\theta,H} + H_l\left[\frac{\partial^2\mathcal{H}}{\partial\epsilon_{ij}\partial H_l}\right]_{\theta,E}; \tag{1.9}$$

$$D_i = \theta\left[-\frac{\partial^2\mathcal{H}}{\partial E_i\partial\theta}\right]_{\epsilon,H} + \epsilon_{ij}\left[-\frac{\partial^2\mathcal{H}}{\partial E_l\partial\epsilon_{ij}}\right]_{\theta,H} + E_i\left[-\frac{\partial^2\mathcal{H}}{\partial E_i\partial E_j}\right]_{\theta,\epsilon,H} + H_i\left[-\frac{\partial^2\mathcal{H}}{\partial E_i\partial H_j}\right]_{\theta,\epsilon}; \tag{1.10}$$

$$B_i = \theta\left[-\frac{\partial^2\mathcal{H}}{\partial H_i\partial\theta}\right]_{\epsilon,E} + \epsilon_{ij}\left[-\frac{\partial^2\mathcal{H}}{\partial H_l\partial\epsilon_{ij}}\right]_{\theta,E} + E_i\left[-\frac{\partial^2\mathcal{H}}{\partial H_i\partial E_j}\right]_{\theta,\epsilon} + H_i\left[-\frac{\partial^2\mathcal{H}}{\partial H_i\partial H_j}\right]_{\theta,\epsilon,E}. \tag{1.11}$$

$$q_i = \vartheta_i\left[-\frac{\partial^2\mathcal{H}}{\partial\vartheta_i\partial\vartheta_j}\right]. \tag{1.12}$$

The following coefficients can be defined:

$$
\begin{aligned}
\frac{\rho C^{\epsilon,E,H}}{\theta_{ref}} &= -\left[\frac{\partial^2\mathcal{H}}{\partial\theta^2}\right]_{\epsilon,E,H} = \left[\frac{\partial\eta}{\partial\theta}\right]_{\epsilon,E,H}, \\
C_{ijlm}^{\theta,E,H} &= \left[\frac{\partial^2\mathcal{H}}{\partial\epsilon_{ij}\partial\epsilon_{lm}}\right]_{\theta,E,H} = \left[\frac{\partial\sigma_{ij}}{\partial\epsilon_{lm}}\right]_{\theta,E,H}, \\
\varepsilon_{ij}^{\theta,\epsilon,H} &= -\left[\frac{\partial^2\mathcal{H}}{\partial E_i\partial E_j}\right]_{\theta,\epsilon,H} = \left[\frac{\partial D_i}{\partial E_j}\right]_{\theta,\epsilon,H}, \\
\mu_{ij}^{\theta,\epsilon,E} &= -\left[\frac{\partial^2\mathcal{H}}{\partial H_i\partial H_j}\right]_{\theta,\epsilon,E} = \left[\frac{\partial B_i}{\partial H_j}\right]_{\theta,\epsilon,E}, \\
\lambda_{ij}^{E,H} &= -\left[\frac{\partial^2\mathcal{H}}{\partial\theta\partial\epsilon_{ij}}\right]_{E,H} = \left[\frac{\partial\sigma_{ij}}{\partial\theta}\right]_{\epsilon,E,H} = \left[\frac{\partial\eta}{\partial\epsilon_{ij}}\right]_{\theta,E,H}, \\
p_i^{\epsilon,H} &= -\left[\frac{\partial^2\mathcal{H}}{\partial\theta\partial E_i}\right]_{\epsilon,H} = \left[\frac{\partial D_i}{\partial\theta}\right]_{\epsilon,E,H} = \left[\frac{\partial\eta}{\partial E_i}\right]_{\theta,\epsilon,H}, \\
e_{lij}^{\theta,H} &= -\left[\frac{\partial^2\mathcal{H}}{\partial\epsilon_{ij}\partial E_l}\right]_{\theta,H} = \left[\frac{\partial\sigma_{ij}}{\partial E_l}\right]_{\theta,\epsilon,H} = \left[\frac{\partial D_l}{\partial\epsilon_{ij}}\right]_{\theta,E,H}, \\
r_i^{\epsilon,E} &= -\left[\frac{\partial^2\mathcal{H}}{\partial\theta\partial H_i}\right]_{\epsilon,E} = \left[\frac{\partial\eta}{\partial H_i}\right]_{\theta,\epsilon,E} = \left[\frac{\partial B_i}{\partial\theta}\right]_{\epsilon,E,H}, \\
q_{lij}^{\theta,E} &= -\left[\frac{\partial^2\mathcal{H}}{\partial\epsilon_{ij}\partial H_l}\right]_{\theta,E} = \left[\frac{\partial\sigma_{ij}}{\partial H_l}\right]_{\theta,\epsilon,E} = \left[\frac{\partial B_l}{\partial\epsilon_{ij}}\right]_{\theta,E,H}, \\
d_{ij}^{\theta,\epsilon} &= -\left[\frac{\partial^2\mathcal{H}}{\partial E_i\partial H_j}\right]_{\theta,\epsilon} = \left[\frac{\partial D_i}{\partial H_j}\right]_{\theta,\epsilon,E} = \left[\frac{\partial B_i}{\partial E_j}\right]_{\theta,\epsilon,H}, \\
\kappa_{ij} &= -\left[\frac{\partial^2\mathcal{H}}{\partial\vartheta_i\partial\vartheta_j}\right] = -\left[\frac{\partial q_i}{\partial\vartheta_j}\right],
\end{aligned}
\tag{1.13}
$$

with:
ρ = density;
$C^{\epsilon,E,H}$ = specific heat per unit mass;
θ_{ref} = reference temperature;
C_{ijlm} = elastic coefficients - Hookes'law;
ε_{ij} = permittivity coefficients;
μ_{ij} = magnetic permeability coefficients;
λ_{ij} = stress-temperature coefficients;
p_i = pyroelectric coefficients;
e_{lij} = piezoelectric coefficients;
r_i = pyromagnetic coefficients;
q_{lij} = piezomagnetic coefficients;
d_i = magneto-electric coupling coefficients.
The first four constants in Eqs. 1.13 are principal constants in the respective individual systems; the latter six are coupling constants between two of the four considered fields. Introducing the constants of Eqs. 1.13 , the following constitutive equations in the coupled four-field system are

obtained by Eqs. 1.12-1.11:

$$\begin{aligned}
\eta &= \frac{\rho}{\theta_{ref}} C^{\epsilon,E,H}\theta + \lambda_{ij}^{E,H}\epsilon_{ij} + p_i^{\epsilon,H}E_i + r_i^{\epsilon,E}H_i,\\
\sigma_{ij} &= -\lambda_{ij}^{E,H}\theta + C_{ijlm}^{\theta,E,H}\epsilon_{lm} - e_{ijl}^{\theta,H}E_l - q_{ijl}^{\theta,E}H_l,\\
D_l &= p_l^{\epsilon,H}\theta + e_{lij}^{\theta,H}\epsilon_{ij} + \varepsilon_{lm}^{\theta,\epsilon,H}E_m + d_{lm}^{\theta,\epsilon}H_m,\\
B_l &= r_l^{\epsilon,E}\theta + q_{lij}^{\theta,E}\epsilon_{ij} + d_{lm}^{\theta,\epsilon}E_m + \mu_{lm}^{\theta,\epsilon,E}H_m,\\
q_i &= \kappa_{ij}\vartheta_j.
\end{aligned} \tag{1.14}$$

As emphasized in [1], physical constants are introduced by second derivative of the relevant thermodynamic function. Each coupling constant is a second derivative with respect to two different variables, and is therefore considered to have a different meaning when interchanging the order of differentiation. For instance, from the definition given above, two kind of piezoelectric constant,

$$e_{lij}^{\theta,H} = \left[\frac{\partial D_l}{\partial \epsilon_{ij}}\right]_{\theta,E,H} \quad \text{and} \quad \widetilde{e}_{lij}^{\theta,H} = \left[\frac{\partial \sigma_{ij}}{\partial E_l}\right]_{\theta,\epsilon,H},$$

are derived. The former e represents the electric flux density versus unit strain, whereas the latter $\widetilde{e}$ represents stress versus unit electric field. It turn out that these correspond to the direct and converse piezoelectric effect, respectively. The piezoelectric coupling term in the third of Eqs. 1.14 indicates the direct effect; that in the second of Eqs. 1.14 represents the converse effect. The equality of direct and converse effect is thus self-evident. Similar facts are found for the other coupling constants (λ_{ij}, p_i, r_i, q_{lij}, and d_{lm}).
Let's anticipate that by using the RMVT, only extensive variables can be modeled through-the-thickness plate z-direction (σ_{zz}, σ_{xz}, σ_{yz} D_z, B_z, q_z).

1.2 Generalized Hooke's law for anysotropic materials and condensed notation

Passing from indices to vectors, it is useful to introduce the so-called "condensed notation", collecting vectors $\boldsymbol{\sigma}$,$\mathbf{D}$,$\mathbf{B}$,η and $\boldsymbol{\epsilon}$,$\mathbf{E}$,$\mathbf{H}$,θ in $\boldsymbol{\mathcal{E}}$ and $\boldsymbol{\mathcal{S}}$ respectively; $\boldsymbol{\mathcal{S}}$ is the vector of extensive variables while $\boldsymbol{\mathcal{E}}$ is the vector of intensive ones. Bold letters denote arrays. ϵ_{ij} components in vectorial notation correspond to $2\epsilon_{ij}$ components in tensorial notation, when $i \neq j$):

$$\boldsymbol{\mathcal{S}}^T = \left\{ \begin{array}{cccccccccccccc} \sigma_{xx} & \sigma_{yy} & \sigma_{xy} & -D_x & -D_y & -B_x & -B_y & -\eta & \sigma_{zz} & \sigma_{xz} & \sigma_{yz} & -D_z & -B_z \end{array} \right\}, \tag{1.15}$$

$$\boldsymbol{\mathcal{E}}^T = \left\{ \begin{array}{cccccccccccccc} \epsilon_{xx} & \epsilon_{yy} & \gamma_{xy} & E_x & E_y & H_x & H_y & \theta & \epsilon_{zz} & \gamma_{xz} & \gamma_{yz} & E_3 & H_3 \end{array} \right\}. \tag{1.16}$$

Note that dealing with plates, subscript "z" indicates the through-the-thickness z-direction while subscripts "x" and "y" are for the two in-plane directions. Non-mechanical quantities appear under negative sign in vector $\boldsymbol{\mathcal{S}}$ and this is due to the fact non-mechanical quantities are negative in Eq. 1.1.
The material is considered to be orthotropic, homogeneous and operating in the linear elastic range. Considering the four-field linear coupling, constitutive coefficient in Eq. 1.14 can be organized in matrix $\boldsymbol{H}$, that can be named generalized Hooke's law for anisotropic materials:

$$\boldsymbol{\mathcal{S}} = \boldsymbol{H}\boldsymbol{\mathcal{E}}, \tag{1.17}$$

where $\boldsymbol{H}$ is the matrix in Eq. 1.18. To be noted that thermal conductivities are neglected at the moment. See in Sec. 4.3.2 how thermal conductivities can be included into the proposed formulation.

$$\boldsymbol{H} = \begin{pmatrix}
C_{11} & C_{12} & C_{16} & 0 & 0 & 0 & 0 & -\lambda_1 & C_{13} & 0 & 0 & -e_{31} & -q_{31} \\
C_{12} & C_{22} & C_{26} & 0 & 0 & 0 & 0 & -\lambda_2 & C_{23} & 0 & 0 & -e_{32} & -q_{32} \\
C_{16} & C_{26} & C_{66} & 0 & 0 & 0 & 0 & -\lambda_6 & C_{36} & 0 & 0 & -e_{36} & -q_{36} \\
0 & 0 & 0 & -\varepsilon_{11} & -\varepsilon_{12} & -d_{11} & -d_{12} & -p_1 & 0 & -e_{15} & -e_{14} & 0 & 0 \\
0 & 0 & 0 & -\varepsilon_{12} & -\varepsilon_{22} & -d_{12} & -d_{22} & -p_2 & 0 & -e_{25} & -e_{24} & 0 & 0 \\
0 & 0 & 0 & -d_{11} & -d_{12} & -\mu_{11} & -\mu_{12} & -r_1 & 0 & -q_{15} & -q_{14} & 0 & 0 \\
0 & 0 & 0 & -d_{12} & -d_{22} & -\mu_{12} & -\mu_{22} & -r_2 & 0 & -q_{25} & -q_{24} & 0 & 0 \\
-\lambda_1 & -\lambda_2 & -\lambda_6 & -p_1 & -p_2 & -r_1 & -r_2 & -(\frac{\rho \mathrm{C}}{\theta_{ref}}) & -\lambda_3 & 0 & 0 & -p_3 & -r_3 \\
C_{13} & C_{23} & C_{36} & 0 & 0 & 0 & 0 & -\lambda_3 & C_{33} & 0 & 0 & -e_{33} & -q_{33} \\
0 & 0 & 0 & -e_{15} & -e_{25} & -q_{15} & -q_{25} & 0 & 0 & C_{55} & C_{45} & 0 & 0 \\
0 & 0 & 0 & -e_{14} & -e_{24} & -q_{14} & -q_{24} & 0 & 0 & C_{45} & C_{44} & 0 & 0 \\
-e_{31} & -e_{32} & -e_{36} & 0 & 0 & 0 & 0 & -p_3 & -e_{33} & 0 & 0 & -\varepsilon_{33} & -d_{33} \\
-q_{31} & -q_{32} & -q_{36} & 0 & 0 & 0 & 0 & -r_3 & -q_{33} & 0 & 0 & -d_{33} & -\mu_{33}
\end{pmatrix} \tag{1.18}$$

1.3 Rotation of constitutive coefficients from material to laminate reference system

Multilayered panels are built bonding together different laminae, according to a given staking sequence. Each lamina represents a certain layer made of a particular orthotropic material. As example, in case of one-directional fiber reinforced layers, each lamina can have a different principal direction for its fibres, once superposed to the other laminae. Material constitutive coefficient are commonly given in the material reference system 1,2,3. Fig. 1.1 shows that the axis 3 corresponds to the axis z in the laminate reference system, while α is the angle of clockwise rotation needed to superpose the 1,2 axes of the material reference system to the x,y axes laminated reference system. It is useful to introduce the rotation matrices $\boldsymbol{T}_1$,$\boldsymbol{T}_2$,$\boldsymbol{T}_3$.

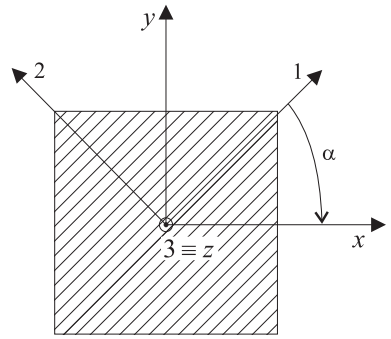

Figure 1.1. Rotation angle α from material to laminate reference system

$$\boldsymbol{T}_1 = \begin{pmatrix}
cos^2(\alpha) & sin^2(\alpha) & -sin(2\alpha) & 0 & 0 & 0 \\
sin^2(\alpha) & cos^2(\alpha) & sin(2\alpha) & 0 & 0 & 0 \\
sin(\alpha)cos(\alpha) & -sin(\alpha)cos(\alpha) & cos^2(\alpha) - sin^2(\alpha) & 0 & 0 & 0 \\
0 & 0 & 0 & 1 & 0 & 0 \\
0 & 0 & 0 & 0 & cos(\alpha) & -sin(\alpha) \\
0 & 0 & 0 & 0 & sin(\alpha) & cos(\alpha)
\end{pmatrix} \tag{1.19}$$

$$\boldsymbol{T}_2 = \begin{pmatrix} 1 & 0 & 0 \\ 0 & cos(\alpha) & -sin(\alpha) \\ 0 & sin(\alpha) & cos(\alpha) \end{pmatrix} \tag{1.20}$$

$$\boldsymbol{T}_3 = \begin{pmatrix} 1 \end{pmatrix} \tag{1.21}$$

The coefficients in the laminate reference system can be calculated from those given the material reference system by the following rotations in Eqs. 1.22-1.31. Matrix subscripts x,y,z and 1,2,3 indicate that the coefficients are in the laminate and in the material reference system respectively.

$$\begin{pmatrix} C_{11} & C_{12} & C_{16} & C_{13} & 0 & 0 \\ C_{12} & C_{22} & C_{26} & C_{23} & 0 & 0 \\ C_{16} & C_{26} & C_{66} & C_{36} & 0 & 0 \\ C_{13} & C_{23} & C_{36} & C_{33} & 0 & 0 \\ 0 & 0 & 0 & 0 & C_{55} & C_{45} \\ 0 & 0 & 0 & 0 & C_{45} & C_{44} \end{pmatrix}_{x,y,z} = \boldsymbol{T}_1 \begin{pmatrix} C_{11} & C_{12} & 0 & C_{13} & 0 & 0 \\ C_{12} & C_{22} & 0 & C_{23} & 0 & 0 \\ 0 & 0 & C_{66} & C_{36} & 0 & 0 \\ C_{13} & C_{23} & C_{36} & C_{33} & 0 & 0 \\ 0 & 0 & 0 & 0 & C_{55} & 0 \\ 0 & 0 & 0 & 0 & 0 & C_{44} \end{pmatrix}_{1,2,3} \boldsymbol{T}_1^T \tag{1.22}$$

$$\begin{pmatrix} 0 & 0 & 0 & 0 & -e_{15} & -e_{14} \\ 0 & 0 & 0 & 0 & -e_{25} & -e_{24} \\ -e_{31} & -e_{32} & -e_{36} & -e_{33} & 0 & 0 \end{pmatrix}_{x,y,z} = \boldsymbol{T}_2 \begin{pmatrix} 0 & 0 & 0 & 0 & -e_{15} & 0 \\ 0 & 0 & 0 & 0 & & -e_{24} \\ -e_{31} & -e_{32} & 0 & -e_{33} & 0 & 0 \end{pmatrix}_{1,2,3} \boldsymbol{T}_1^T \tag{1.23}$$

$$\begin{pmatrix} 0 & 0 & 0 & 0 & -q_{15} & -q_{14} \\ 0 & 0 & 0 & 0 & -q_{25} & -q_{24} \\ -q_{31} & -q_{32} & -q_{36} & -q_{33} & 0 & 0 \end{pmatrix}_{x,y,z} = \boldsymbol{T}_2 \begin{pmatrix} 0 & 0 & 0 & 0 & -q_{15} & 0 \\ 0 & 0 & 0 & 0 & & -q_{24} \\ -q_{31} & -q_{32} & 0 & -q_{33} & 0 & 0 \end{pmatrix}_{1,2,3} \boldsymbol{T}_1^T \tag{1.24}$$

$$\begin{pmatrix} -\varepsilon_{11} & -\varepsilon_{12} & 0 \\ -\varepsilon_{12} & -\varepsilon_{22} & 0 \\ 0 & 0 & -\varepsilon_{33} \end{pmatrix}_{x,y,z} = \boldsymbol{T}_2 \begin{pmatrix} -\varepsilon_{11} & 0 & 0 \\ 0 & -\varepsilon_{22} & 0 \\ 0 & 0 & -\varepsilon_{33} \end{pmatrix}_{1,2,3} \boldsymbol{T}_2^T \tag{1.25}$$

$$\begin{pmatrix} -\mu_{11} & -\mu_{12} & 0 \\ -\mu_{12} & -\mu_{22} & 0 \\ 0 & 0 & -\mu_{33} \end{pmatrix}_{x,y,z} = \boldsymbol{T}_2 \begin{pmatrix} -\mu_{11} & 0 & 0 \\ 0 & -\mu_{22} & 0 \\ 0 & 0 & -\mu_{33} \end{pmatrix}_{1,2,3} \boldsymbol{T}_2^T \tag{1.26}$$

$$\begin{pmatrix} -d_{11} & -d_{12} & 0 \\ -d_{12} & -d_{22} & 0 \\ 0 & 0 & -d_{33} \end{pmatrix}_{x,y,z} = \boldsymbol{T}_2 \begin{pmatrix} -d_{11} & 0 & 0 \\ 0 & -d_{22} & 0 \\ 0 & 0 & -d_{33} \end{pmatrix}_{1,2,3} \boldsymbol{T}_2^T \tag{1.27}$$

$$\begin{pmatrix} -p_1 \\ -p_2 \\ -p_3 \end{pmatrix}_{x,y,z} = \boldsymbol{T}_2 \begin{pmatrix} -p_1 \\ -p_2 \\ -p_3 \end{pmatrix}_{1,2,3} \boldsymbol{T}_3^T \tag{1.28}$$

$$\begin{pmatrix} -r_1 \\ -r_2 \\ -r_3 \end{pmatrix}_{x,y,z} = \boldsymbol{T}_2 \begin{pmatrix} -r_1 \\ -r_2 \\ -r_3 \end{pmatrix}_{1,2,3} \boldsymbol{T}_3^T \tag{1.29}$$

$$\left(\begin{array}{c} -\frac{\rho \mathrm{C}}{\theta_{ref}} \end{array} \right)_{x,y,z} = \boldsymbol{T}_3 \left(\begin{array}{c} -\frac{\rho \mathrm{C}}{\theta_{ref}} \end{array} \right)_{1,2,3} \boldsymbol{T}_3^T \tag{1.30}$$

$$\begin{pmatrix} -\lambda_1 & -\lambda_2 & -\lambda_6 & -\lambda_3 & 0 & 0 \end{pmatrix}_{x,y,z} = \boldsymbol{T}_3 \begin{pmatrix} -\lambda_1 & -\lambda_2 & 0 & -\lambda_3 & 0 & 0 \end{pmatrix}_{1,2,3} \boldsymbol{T}_1^T \tag{1.31}$$

It can be noted that Eq. 1.30 is an identity.

1.4 Geometrical relations

The primary unknowns of the problem can be collected in vector $\boldsymbol{U}$ in Eq. 1.32.

$$\boldsymbol{U}^T = \begin{Bmatrix} u_1 & u_2 & u_3 & \phi & \varphi & \theta \end{Bmatrix}, \tag{1.32}$$

where superscripts T indicates the array transposition. The intensive variables $\boldsymbol{\mathcal{E}}$ are linearly related to the unknowns $\boldsymbol{U}$ according to the following geometrical relations:

$$\boldsymbol{\mathcal{E}} = \boldsymbol{D}\boldsymbol{U}, \tag{1.33}$$

where $\boldsymbol{D}$ denotes the following differential operator:

$$\boldsymbol{D} = \begin{pmatrix} \partial_x & 0 & 0 & 0 & 0 & 0 \\ 0 & \partial_y & 0 & 0 & 0 & 0 \\ \partial_y & \partial_x & 0 & 0 & 0 & 0 \\ 0 & 0 & 0 & -\partial_x & 0 & 0 \\ 0 & 0 & 0 & -\partial_y & 0 & 0 \\ 0 & 0 & 0 & 0 & -\partial_x & 0 \\ 0 & 0 & 0 & 0 & -\partial_y & 0 \\ 0 & 0 & 0 & 0 & 0 & 1 \\ 0 & 0 & \partial_z & 0 & 0 & 0 \\ \partial_z & 0 & \partial_x & 0 & 0 & 0 \\ 0 & \partial_z & \partial_y & 0 & 0 & 0 \\ 0 & 0 & 0 & -\partial_z & 0 & 0 \\ 0 & 0 & 0 & 0 & -\partial_z & 0 \end{pmatrix}. \tag{1.34}$$

Chapter 2

Two-dimensional plate theories

This chapter does not consists in a description of two-dimensional plate theories since very exhaustive literature is available on this subject. To the contraire, various two-dimensional plate theories are critically discussed in order to emphasize advantage or disadvantages of each one of them. The discussion encompasses a complete set of theories, starting from the classical ones and ending with the advanced modeling proposed in this activity.

2.1 Classical theories

2.1.1 Kirchhoff plate theory

The Kirchhoff plate theory is a classical theory useful to model single layered thin panels. In same simple case it can be applied to model multilayered plates, where each layer is orthotropic and rotated according to the chosen stacking sequence. Present theory does not consider the transverse shear and normal stresses. Distributed loading can be properly included in modeling, while the inclusion of concentrated loads could not lead to consistent results. The kinematic description of the displacement field is the following:

$$\begin{cases} u_x(x,y,z) = \bar{u}_x(x,y) + z\bar{u}_{z,x}(x,y) \\ u_y(x,y,z) = u_y(x,y) + z\bar{u}_{z,y}(x,y) \\ u_z(x,y,z) = u_z(x,y), \end{cases} \tag{2.1}$$

where $\bar{u}_x$,$\bar{u}_y$,$\bar{u}_z$ are the displacements on the plate reference surface, which is usually chosen as coincident with the middle surface. Primary unknowns appear both in normal form and under space derivative in the kinematic assumption. With the Kirchhoff plate theory the plate displacement field can be calculated for the above mentioned case studies, while results concerning stresses can be very inaccurate, also considering that the theory neglect transverse stresses.
The acronym commonly used to indicate the application of Kirchhoff plate theory is CLT: Classical Laminate Theory.

2.1.2 Mindlin plate theory

The Mindlin plate theory is a classical theory useful to model single layered thin/relatively thick panels. In same simple case it can be applied to model multilayered plates, where each layer

is orthotropic and rotated according to the chosen stacking sequence. Present theory does not consider the stress. Distributed loading can be properly included in modeling, while the inclusion of concentrated loads could not lead to consistent results. With the Mindlin plate theory the plate displacement field can be calculated for the above mentioned case studies, while results concerning transverse can be quite inaccurate. The kinematic description of the displacement field is the following:

$$\begin{cases} u_x(x,y,z) = \bar{u}_x(x,y) + z\bar{\varphi}_x(x,y) \\ u_y(x,y,z) = u_y(x,y) + z\bar{\varphi}_y(x,y) \\ u_z(x,y,z) = u_z(x,y), \end{cases} \tag{2.2}$$

where $\bar{u}_x$,$\bar{u}_y$,$\bar{u}_z$ and $\bar{\varphi}_x$,$\bar{\varphi}_y$ are respectively displacements and z-derivative of $\bar{u}_x$,$\bar{u}_y$ on the plate reference surface, which is usually chosen as coincident with the middle surface.
The acronym commonly used to indicate the application of Kirchhoff plate theory is FSDT: First order Shear Deformation Theory.

2.2 Carrera's Unified Formulation, CUF: advanced theories

Both Kirchhoff and Mindlin plate theories are reasonably appropriate to model single-layered panels. Mindlin kinematic description accounts a linear shear deformation through the thickness of the plate and then provide a more accurate modeling than Kirchhoff theory. The difference is evident only when relatively thick panels are considered.
However, a linear description of the shear deformation could not be sufficient, depending on the considered case-study. As a consequence, higher order thickness expansions should be considered in the kinematic assumptions. Kinematic assumption can be written under the form of a thickness expansion of generic order and generic base:

$$\begin{cases} u_x(x,y,z) = F_1(z)u_x^1 + F_2(z)u_x^2 + F_3(z)u_x^3 + ... \\ u_y(x,y,z) = F_1(z)u_y^1 + F_2(z)u_y^2 + F_3(z)u_y^3 + ... \\ u_z(x,y,z) = F_1(z)u_z^1 + F_2(z)u_z^2 + F_3(z)u_z^3 + ... \end{cases} \tag{2.3}$$

$F_\tau(z)$ can be called thickness function (function of z). In case of first order expansion, setting $F_1(z) = 1$, $F_2(z) = z$ and $F_2(z) = 0$ for displacement u_z, the description in Eq. 2.3 is coincident to the Mindlin description in Eq. 2.2 and the only formal difference is that the primary variables are indicated via different symbols.
If multilayered structures are addressed to, more refined mathematical models are needed in order to include the effects caused by the layer-interfaces. In fact, adjacent layers can differ in material properties and/or in fiber orientation. This leads to the so-called through-the-thickness *zig-zag* trend of quantities that describe the problem, Fig. 3. Layer Wise (LW) kinematic descriptions are able to reproduce the *zig-zag* effect considering each layer independently from the others. The continuity of relevant quantities can be imposed at the interfaces between different layers. Superscript k is introduced in order to distinguish between quantities related to different layers. LW kinematic description can be written as it follows:

$$\begin{cases} u^k(x,y,z) = F_1(z)u_1^k + F_2(z)u_2^k + F_3(z)u_3^k + ... \\ v^k(x,y,z) = F_1(z)v_1^k + F_2(z)v_2^k + F_3(z)v_3^k + ... \\ w^k(x,y,z) = F_1(z)w_1^k + F_2(z)w_2^k + F_3(z)w_3^k + ... \end{cases}, \tag{2.4}$$

where primary unknowns u_x,u_y,u_z are indicated with u,v,w to simplify the notation. A more compact form of Eq. 2.4 can be written using vectors and the repeated index τ:

$$\boldsymbol{u}^k = \boldsymbol{F}_\tau \boldsymbol{u}_\tau^k \tag{2.5}$$

It is convenient to use Lagrange polynomials as thickness functions $F_\tau(z)$. This allows to have only physical quantities of some well-known locations through the thickness of the plate. Moreover all the primary unknowns are of the same unit of measurement, whatever is the order of the thickness expansion and the continuity of relevant quantities at the layer interfaces can be imposed adding a number of additional conditions equal to the number of layer interfaces:

$$\boldsymbol{u}_\tau^{k+} = \boldsymbol{u}_\tau^{k-}, \tag{2.6}$$

where $\boldsymbol{u}_\tau^{k+}$ and $\boldsymbol{u}_\tau^{k-}$ stand for primary unknowns of the upper-layer and of the lower-layer respectively, in the laminate reference system.
Eq. 2.5 is representative of the Carrera's Unified Formulation and is the heart of the proposed modeling technique. It is clear that the same equation is valid both ESL description (without index k) and for LW theories (with index k). In addition, whatever order of expansion and polynomial choice can be considered.
To be underlined that if a first order through-the-thickness expansion is employed, constitutive coefficient in the material reference system can be modified as in the following in order to avoid the thickness locking:

$$\begin{aligned} C_{11}^{'} &= C_{11} - \frac{C_{13}^2}{C_{33}}; \\ C_{22}^{'} &= C_{22} - \frac{C_{23}^2}{C_{33}}; \\ C_{12}^{'} &= C_{12} - \frac{C_{13}C_{23}}{C_{33}}. \end{aligned} \tag{2.7}$$

In case of LW theory such correction is not needed if more that one layer are considered in the staking sequence.
In this chapter, only the mechanical field has been discussed, while in the next chapter it will be evident that the CUF can be easily applied also to multifield problems, if the appropriate variational statement is applied.

Chapter 3

Variational statements for multifield problems

3.1 Principle of Virtual Displacements, PVD

In this section PVD is derived for the fully coupled multifield case. It means that complete coupling among mechanical, thermal, electrical and magnetic variables is considered. It is convenient to start the derivation directly from Hamilton's principle:

$$\delta \int_{t_0}^{t} (K - \Pi)\, dt \;=\; 0 \qquad \Rightarrow \qquad \delta \int_{t_0}^{t} K\, dt - \delta \int_{t_0}^{t} \Pi\, dt \;=\; 0, \tag{3.1}$$

where K is the kinetic energy and Π is the potential energy; δ is the variational symbol; t denotes time, t_0 and t_1 are the initial and generic instant. The kinetic energy variation can be treated as it follows:

$$\begin{aligned} \delta \int_{t_0}^{t} K\, dt \;&=\; \delta \int_{t_0}^{t} dt \int_V \Big(\frac{1}{2}\,\rho\, \dot{u}_i\, \dot{u}_i\Big)\, dV \;=\; \int_{t_0}^{t} \int_V (\rho\, \dot{u}_i\, \delta \dot{u}_i)\, dV\, dt \;= \\ &=\; \int_V (\rho\, \dot{u}_i\, \delta u_i)\, dV \Big|_{t_0}^{t_1} \;-\; \int_{t_0}^{t_1} \int_V (\rho\, \ddot{u}_i\, \delta u_i)\, dV\, dt. \end{aligned} \tag{3.2}$$

V is the plate volume, u_i is a displacement component and dot denotes differentiation with respect to time. δu is equal zero in $t = t_0$ and $t = t_1$, so that:

$$\delta \int_{t_0}^{t} K\, dt \;=\; -\delta \int_{t_0}^{t_1} \int_V (\rho\, \ddot{u}_i\, \delta u_i)\, dV\, dt. \tag{3.3}$$

It follows that:

$$\delta \int_{t_0}^{t} K\, dt \;=\; -\int_{t_0}^{t} \delta L_{in}\, dt, \tag{3.4}$$

in which δL_{in} denotes the variation of the work done by inertial forces.
The variation of potential energy is written in Eq. 3.5 as algebraic sum of the variation of $\mathcal{H}$ and the variation of the work made by applied mechanical/multifield loading. Any hypothetical load due to magnetic field is here neglected. For practical reasons, body forces and volumetric

electrical charges are neglected too. Thermal loading are not appearing in Eq. 3.5 since the eventual temperature distributions can be imposed in direct manner on the mathematical model.

$$\begin{aligned}\delta \int_{t_0}^{t} \Pi \, dt = \delta \int_{t_0}^{t} \left[\int_V \mathcal{H} \, dV - \int_A \left(\bar{t}_j \, u_j - \bar{Q} \, \Phi \right) \, dA \right] dt = \\ = \delta \int_{t_0}^{t} \int_V \mathcal{H} \, dV \, dt - \int_{t_0}^{t} \delta L_e \, dt,\end{aligned} \tag{3.5}$$

where:
A is the surface involved by loading;
$\bar{t}_j$ is the mechanical loading in j-direction;
$\bar{Q}$ is the charge density on the plate surface;
ϕ is the electric potential;
δL_e denotes the variation of the work done by external loads.

Upon substitution of Eq. 3.4 and Eq. 3.5 in Eq. 3.1 it follows that:

$$\delta \int_{t_0}^{t} \int_V \mathcal{H} \, dV \, dt \; = \; \int_{t_0}^{t} \delta L_e \, dt - \int_{t_0}^{t} \delta L_{in} \, dt. \tag{3.6}$$

Differentiating $\mathcal{H}$ and neglecting F, Eq. 3.6 takes the following form:

$$\int_{t_0}^{t} \int_V \left(\frac{\partial \mathcal{H}}{\partial T} \delta T + \frac{\partial \mathcal{H}}{\partial \epsilon_{ij}} \delta \epsilon_{ij} + \frac{\partial \mathcal{H}}{\partial E_l} \delta E_l + \frac{\partial \mathcal{H}}{\partial H_l} \delta H_l \right) dV \, dt = \int_{t_0}^{t} \delta L_e \, dt - \int_{t_0}^{t} \delta L_{in} \, dt. \tag{3.7}$$

Substituting in Eq. 3.7 the coefficients in Eqs. 1.7 and eliminating the time integral, the PVD for a three dimensional continua is obtained:

$$\int_V \left(-\eta \delta \theta + \sigma_{ij} \delta \epsilon_{ij} - D_l \delta E_l - B_l \delta H_l \right) dV \; = \; \delta L_e - \delta L_{in}. \tag{3.8}$$

By using the condensed notation, the PVD statement for a multilayered plate results in the following compact form:

$$\int_V \left(\delta \boldsymbol{\mathcal{E}}_G^T \boldsymbol{\mathcal{S}}_H \right) dV \; = \; \delta L_e - \delta L_{in}, \tag{3.9}$$

where subscripts "G" and "H" indicate variables obtained by Geometrical relations and by constitutive/Hooke's relations respectively. For multilayered structures, the volume integral, has to be intended as:

$$\int_V (...) \; dV \; = \; \sum_{k=1}^{N_l} \int_{\Omega_k} \int_{h_k} (...) \; d\Omega_k \, dz, \tag{3.10}$$

where Ω_k is the layer middle surface and h_k denotes the k^{th} layer-thickness domain
PVD can also be written in the following form:

$$\begin{aligned}&\int_V (\delta \boldsymbol{\epsilon}_{pG}^T \boldsymbol{\sigma}_{pH} + \delta \boldsymbol{\epsilon}_{nG}^T \boldsymbol{\sigma}_{nH} + \boldsymbol{H}_{pG}^T \boldsymbol{B}_{pH} + \delta H_{nG} B_{nH} + \\ &+ \delta \boldsymbol{E}_{pG}^T \boldsymbol{D}_{pH} + \delta E_{nG} D_{nH} + \delta \theta_G \eta_H) \, dV \; = \; \delta L_e - \delta L_{in},\end{aligned} \tag{3.11}$$

where notation already used in previous work [4] is referred to: subscript "p" denotes in-plane unknowns and subscript "n" denotes out-of-plane unknowns.

Particular cases

In practical applications, not all the intensive variables (θ,ϵ,E,H) are considered in the problem. Considering all the possible combinations of virtual variation active in the model, many different governing equations can be obtained. For the PVD, virtual variations here addressed to are six: δu_1, δu_2, δu_3, $\delta\phi$, $\delta\varphi$, $\delta\theta$; where $\delta\phi$ and $\delta\varphi$ indicate the variations of electric and magnetic potential, respectively[1]. In general, a virtual variation can be considered alone or can be coupled with the others. A few examples of variational statements for different case of coupling are proposed in the following. Reference is made to the form of PVD at Eq. 3.11.

PVD-u_x,u_y,u_z: pure Mechanical case.
If only virtual variations of displacements δu_x, δu_y, δu_z are considered, Eq. 3.8 is reduced to:

$$\int_V (\delta\boldsymbol{\epsilon}_{pG}^T\boldsymbol{\sigma}_{pH} + \delta\boldsymbol{\epsilon}_{nG}^T\boldsymbol{\sigma}_{nH})\, dV \;=\; \delta L_e - \delta L_{in}. \tag{3.12}$$

That is a pure mechanical problem is described.

PVD-u_x,u_y,u_z,θ: coupled Thermo-Mechanical case.
By adding the variation of temperature: δu_x, δu_y, δu_z, $\delta\theta$, Eq. 3.8 becomes:

$$\int_V (\delta\boldsymbol{\epsilon}_{pG}^T\boldsymbol{\sigma}_{pH} + \delta\boldsymbol{\epsilon}_{nG}^T\boldsymbol{\sigma}_{nH} + \delta\theta_G\eta_H)\, dV \;=\; \delta L_e - \delta L_{in}. \tag{3.13}$$

That is a coupled thermo-mechanical problem is described: a variation in temperature can cause a variation in the displacement field and viceversa).
The thermal field can be also intended as partially coupled with the mechanical field, that is the extensive variable concerning thermal field (η) is not considered in constitutive relations. The thermal field impacts the system under form of thermal stresses σ_θ and thermal load vector, while temperature variations due to the mechanical field are not considered. The advantage of using a partially coupled system lies in the reduction of the number of system degrees of freedoms. The disadvantage is that thermal effect due to strain is neglected and the temperature has to be imposed at any point of the considered continuum. Corresponding Eq. 3.8 is:

$$\int_V (\delta\boldsymbol{\epsilon}_{pG}^T(\boldsymbol{\sigma}_{pH} - \boldsymbol{\sigma}_{p\theta}) + \delta\boldsymbol{\epsilon}_{nG}^T(\boldsymbol{\sigma}_{nH} - \boldsymbol{\sigma}_{n\theta}))\, dV \;=\; \delta L_e - \delta L_{in}. \tag{3.14}$$

PVD-u_x,u_y,u_z,ϕ: coupled Electro-Mechanical case.
The considered virtual variations are: δu_x, δu_y, δu_z, $\delta\phi$ and the PVD reduces to:

$$\int_V (\delta\boldsymbol{\epsilon}_{pG}^T\boldsymbol{\sigma}_{pH} + \delta\boldsymbol{\epsilon}_{nG}^T\boldsymbol{\sigma}_{nH} + \delta\boldsymbol{E}_{pG}^T\boldsymbol{D}_{pH} + \delta E_{nG}D_{nH})\, dV \;=\; \delta L_e - \delta L_{in}. \tag{3.15}$$

PVD-u_x,u_y,u_z,φ: coupled Magneto-Mechanical case. The considered virtual variations are: δu_1, δu_2, δu_3, $\delta\varphi$ and the PVD reduces to:

$$\int_V (\delta\boldsymbol{\epsilon}_{pG}^T\boldsymbol{\sigma}_{pH} + \delta\boldsymbol{\epsilon}_{nG}^T\boldsymbol{\sigma}_{nH} + \delta\boldsymbol{H}_{pG}^T\boldsymbol{B}_{pH} + \delta H_{nG}B_{nH})\, dV \;=\; \delta L_e - \delta L_{in}. \tag{3.16}$$

PVD-u_x,u_y,u_z,ϕ,φ: coupled Magneto-Electro-Mechanical case.
The considered virtual variations are: δu_x, δu_y, δu_z, $\delta\phi$, $\delta\varphi$ and the PVD statement is:

$$\int_V (\delta\boldsymbol{\epsilon}_{pG}^T\boldsymbol{\sigma}_{pH} + \delta\boldsymbol{\epsilon}_{nG}^T\boldsymbol{\sigma}_{nH} + \boldsymbol{H}_{pG}^T\boldsymbol{B}_{pH} + \delta H_{nG}B_{nH} + \delta\boldsymbol{E}_{pG}^T\boldsymbol{D}_{pH} + \delta E_{nG}D_{nH})\, dV \;=\; \delta L_e - \delta L_{in}.$$

[1] To be noticed that δu_1, δu_2, δu_3 come from the strain $\delta\epsilon$, $\delta\phi$ from δE and $\delta\varphi$ from δH.

PVD-θ: pure Thermal case.
In this case only virtual variation of temperature $\delta\theta$ is considered and the PVD reduces to:

$$\int_V (\delta\theta_G \eta_H)\, dV \;=\; \delta L_e. \tag{3.17}$$

A pure thermal problem is obtained that is equivalent to heat conduction problems and where δL_e has to be written including the thermal loading in explicit manner.

3.2 Reissner's mixed variational theorem, RMVT

As stated in the introduction, the advantage of using RMVT consists in the possibility of assuming two independent set of variables: a set of primary unknowns and a set of extensive variables which are modeled in the thickness plate z-direction. The main advantage of using RMVT is the "a priori" and complete fulfillment of the C_z^0 requirements for the modeled extensive mechanical variables. In this section RMVT for the multifield case is written. All the normal components (those in the z-direction) of extensive variables are modeled in the thickness plate z-direction. By referring to the condensed notation and considering that subscript "a" indicates "not modeled quantities", while subscript "b" pertains to "modeled quantities", the following vectors can be introduced:

$\boldsymbol{\mathcal{S}}_a = \left\{ \begin{array}{cccccccc} \sigma_{xx} & \sigma_{yy} & \sigma_{xy} & -D_x & -D_y & -B_x & -B_y & -\eta \end{array} \right\}$ is the vector of not-modeled extensive variables, which are calculated by constitutive relations;
$\boldsymbol{\mathcal{S}}_b = \left\{ \begin{array}{cccccc} \sigma_{zz} & \sigma_{xz} & \sigma_{yz} & -D_z & -B_z \end{array} \right\}$ is the vector of modeled extensive variables;
$\boldsymbol{\mathcal{E}}_{aG} = \left\{ \begin{array}{cccccccc} \epsilon_{xx} & \epsilon_{yy} & \epsilon_{xy} & E_x & E_y & H_x & H_y & \theta \end{array} \right\}_G$ is the vector of intensive variables associated to $\boldsymbol{\mathcal{S}}_a$ and calculated by geometrical relations;
$\boldsymbol{\mathcal{E}}_{bG} = \left\{ \begin{array}{ccccc} \epsilon_{zz} & \epsilon_{xz} & \epsilon_{yz} & E_z & H_z \end{array} \right\}_G$ is the vector of intensive variables associated to $\boldsymbol{\mathcal{S}}_b$ and calculated by geometrical relations;
$\boldsymbol{\mathcal{E}}_{bH} = \left\{ \begin{array}{ccccc} \epsilon_{zz} & \epsilon_{xz} & \epsilon_{yz} & E_z & H_z \end{array} \right\}_H$ is the vector of intensive variables associated to $\boldsymbol{\mathcal{S}}_b$ and calculated by constitutive relations.

The application of RMVT requires the rearrangement of constitutive and geometrical relations and this is described in Sec. 3.3 and Sec. 3.4 respectively. Non-mechanical quantities appear under negative sign in vectors of extensive variables for the same reason already explained in Sec. 3.1.

Since $\boldsymbol{\mathcal{S}}_b$ are unknown variables, Lagrange multiplier associated to $\boldsymbol{\mathcal{S}}_b$ should be introduced (see [17] for the pure mechanical case, and [18] for more explanations about the generic multifield case). The first member of Eq. 3.6 results changed as it follows.

$$\delta \int_{t_0}^{t} \int_V \mathcal{H}\, dV\, dt \longrightarrow \delta \int_{t_0}^{t} \int_V \left[\mathcal{H} + \delta\boldsymbol{\mathcal{S}}_b^T \left(\boldsymbol{\mathcal{E}}_{bG} - \boldsymbol{\mathcal{E}}_{bH} \right) \right] dV\, dt. \tag{3.18}$$

For our purpose it is convenient to differentiate and the Eq. 3.6 takes the following form:

$$\int_{t_0}^{t} \int_V \left[\delta\boldsymbol{\mathcal{E}}_{aG}^T \frac{\partial \mathcal{H}}{\partial \boldsymbol{\mathcal{E}}_{aG}^T} + \delta\boldsymbol{\mathcal{E}}_{bG}^T \frac{\partial \mathcal{H}}{\partial \boldsymbol{\mathcal{E}}_{bG}^T} + \delta\boldsymbol{\mathcal{S}}_b^T \left(\boldsymbol{\mathcal{E}}_{bG} - \boldsymbol{\mathcal{E}}_{bH} \right) \right] dV\, dt = \int_{t_0}^{t} \delta L_e\, dt - \int_{t_0}^{t} \delta L_{in}\, dt. \tag{3.19}$$

By eliminating the time integral, the RMVT statement for a MLS in MFP is obtained:

$$\int_V \left[\delta\boldsymbol{\mathcal{E}}_{aG}^T \boldsymbol{\mathcal{S}}_{aH} + \delta\boldsymbol{\mathcal{E}}_{bG}^T \boldsymbol{\mathcal{S}}_b^k + \delta\boldsymbol{\mathcal{S}}_b^T \left(\boldsymbol{\mathcal{E}}_{bG} - \boldsymbol{\mathcal{E}}_{bH} \right) \right] dV = \delta L_e - \delta L_{in}. \tag{3.20}$$

If the through-the-thickness modeled variables are $\boldsymbol{\sigma}_n$, D_n and B_n (that is $\boldsymbol{\sigma}_{zz}$, $\boldsymbol{\sigma}_{xz}$, $\boldsymbol{\sigma}_{yz}$, D_z and B_z), RMVT can also be written in the following form:

$$\begin{aligned}\int_V (\delta\boldsymbol{\epsilon}_{pG}^T\boldsymbol{\sigma}_{pH} + \delta\boldsymbol{\epsilon}_{nG}^T\boldsymbol{\sigma}_n + \delta\boldsymbol{\sigma}_n^T(\boldsymbol{\epsilon}_{nG} - \boldsymbol{\epsilon}_{nH}) + \delta\theta_G\eta_H + \delta\boldsymbol{E}_{pG}^T\boldsymbol{D}_{pH} + \delta E_{nG}D_n + \\ +\delta D_n(E_{nG} - E_{nH}) + \delta\boldsymbol{H}_{pG}^T\boldsymbol{B}_{pH} + \delta H_{nG}B_n + \delta B_n(H_{nG} - H_{nH}))\, dV \;=\; \delta L_e - \delta L_{in}.\end{aligned} \tag{3.21}$$

Particular cases

As done for the PVD, several RMVT particular case form can be obtained. These all can be of particular interest in practical applications. By considering all the possible combination of virtual variation active in the model, problem's unknowns can be thought as grouped in two sets: primary unknowns and unknowns modeled through-the-thickness z-direction, which are intensive variables (Fig. 3.1). Combinations of these two set of virtual variations can be considered. If only

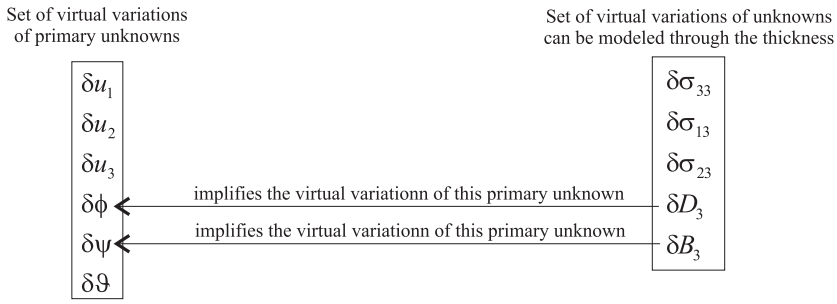

Figure 3.1. The two set of unknowns

variations associated to primary unknowns are chosen, PVD is obtained, otherwise a particular case of RMVT is given. In this section, a few examples of RMVT particular cases are formulated, also considering a different number of involved fields. For sake of clarity, the same notation used in the PVD cases is reconsidered. Between brackets are the quantities modeled via RMVT.

RMVT-u_x,u_y,u_z(σ_{zz},σ_{xz},σ_{yz}): pure Mechanical case.
The considered virtual variations are: δu_x, δu_y, δu_z, $\delta\sigma_{zz}$, $\delta\sigma_{xz}$, $\delta\sigma_{yz}$ and the RMVT statement is:

$$\int_V (\delta\boldsymbol{\epsilon}_{pG}^T\boldsymbol{\sigma}_{pH} + \delta\boldsymbol{\epsilon}_{nG}^T\boldsymbol{\sigma}_n + \boldsymbol{\sigma}_n^T(\boldsymbol{\epsilon}_{nG} - \boldsymbol{\epsilon}_{nH}))\, dV \;=\; \delta L_e - \delta L_{in}. \tag{3.22}$$

RMVT-u_x,u_y,u_z(σ_{zz}): pure Mechanical case, only normal transverse stress modeled.
The considered virtual variations are: δu_x, δu_y, δu_z, $\delta\sigma_{zz}$ and the RMVT statement is:

$$\int_V (\delta\boldsymbol{\epsilon}_{pG}^T\boldsymbol{\sigma}_{pH} + \delta\boldsymbol{\epsilon}_{nG}^T\boldsymbol{\sigma}_n + \sigma_{zz}(\epsilon_{zzG} - \epsilon_{zzH}))\, dV \;=\; \delta L_e - \delta L_{in}. \tag{3.23}$$

RMVT-u_x,u_y,u_z(σ_{xz},σ_{yz}): pure Mechanical case, only shear transverse stresses modeled.
The considered virtual variations are: δu_x, δu_y, δu_z, $\delta\sigma_{xz}$, $\delta\sigma_{yz}$ and the RMVT reduces to:

$$\int_V (\delta\boldsymbol{\epsilon}_{pG}^T\boldsymbol{\sigma}_{pH} + \delta\boldsymbol{\epsilon}_{nG}^T\boldsymbol{\sigma}_n + \sigma_{xz}(\epsilon_{xzG} - \epsilon_{xzH}) + \sigma_{yz}(\epsilon_{yzG} - \epsilon_{yzH}))\, dV \;=\; \delta L_e - \delta L_{in}. \tag{3.24}$$

RMVT-u_x,u_y,u_z,θ(σ_{zz},σ_{xz},σ_{yz}): coupled Thermo-Mechanical case.
The considered virtual variations are: δu_x, δu_y, δu_z, $\delta\theta$, $\delta\sigma_{zz}$, $\delta\sigma_{xz}$, $\delta\sigma_{yz}$ and the RMVT reduces to:

$$\int_V (\delta\boldsymbol{\epsilon}_{pG}^T\boldsymbol{\sigma}_{pH} + \delta\boldsymbol{\epsilon}_{nG}^T\boldsymbol{\sigma}_n + \delta\boldsymbol{\sigma}_n^T(\boldsymbol{\epsilon}_{nG} - \boldsymbol{\epsilon}_{nH}) + \delta\theta_G\eta_H)\, dV \;=\; \delta L_e - \delta L_{in}. \tag{3.25}$$

RMVT-u_x,u_y,u_z,ϕ(σ_{zz},σ_{xz},σ_{yz}): coupled Electro-Mechanical case.
If the considered virtual variations are: δu_x, δu_y, δu_z, $\delta\phi$, $\delta\sigma_{zz}$, $\delta\sigma_{xz}$, $\delta\sigma_{yz}$, the RMVT statement is:

$$\begin{aligned}&\int_V (\delta\boldsymbol{\epsilon}_{pG}^T\boldsymbol{\sigma}_{pH} + \delta\boldsymbol{\epsilon}_{nG}^T\boldsymbol{\sigma}_n + \delta\boldsymbol{\sigma}_n^T(\boldsymbol{\epsilon}_{nG} - \boldsymbol{\epsilon}_{nH}) + \delta\boldsymbol{E}_{pG}^T\boldsymbol{D}_{pH} + \delta E_{nG}D_{nH})\, dV \;=\\ &=\; \delta L_e - \delta L_{in}.\end{aligned} \tag{3.26}$$

RMVT-u_x,u_y,u_z,ϕ(σ_{zz},σ_{xz},σ_{yz},D_z): coupled Electro-Mechanical case.
If the considered virtual variations are: δu_x, δu_y, δu_z, $\delta\phi$, $\delta\sigma_{zz}$, $\delta\sigma_{xz}$, $\delta\sigma_{yz}$, δD_z, the RMVT statement is:

$$\begin{aligned}&\int_V (\delta\boldsymbol{\epsilon}_{pG}^T\boldsymbol{\sigma}_{pH} + \delta\boldsymbol{\epsilon}_{nG}^T\boldsymbol{\sigma}_n + \delta\boldsymbol{\sigma}_n^T(\boldsymbol{\epsilon}_{nG} - \boldsymbol{\epsilon}_{nH}) + \delta\boldsymbol{E}_{pG}^T\boldsymbol{D}_{pH} + \delta E_{nG}D_n +\\ &+\delta D_n(E_{nG} - E_{nH}))\, dV \;=\; \delta L_e - \delta L_{in}.\end{aligned} \tag{3.27}$$

RMVT-u_x,u_y,u_z,φ(σ_{zz},σ_{xz},σ_{yz}): coupled Magneto-Mechanical case.
If the considered virtual variations are: δu_x, δu_y, δu_z, $\delta\varphi$, $\delta\sigma_{zz}$, $\delta\sigma_{xz}$, $\delta\sigma_{yz}$, the RMVT reduces to:

$$\begin{aligned}&\int_V (\delta\boldsymbol{\epsilon}_{pG}^T\boldsymbol{\sigma}_{pH} + \delta\boldsymbol{\epsilon}_{nG}^T\boldsymbol{\sigma}_n + \delta\boldsymbol{\sigma}_n^T(\boldsymbol{\epsilon}_{nG} - \boldsymbol{\epsilon}_{nH}) + \delta\boldsymbol{H}_{pG}^T\boldsymbol{B}_{pH} + \delta H_{nG}B_{nH})\, dV \;=\\ &=\; \delta L_e - \delta L_{in}.\end{aligned} \tag{3.28}$$

RMVT-u_x,u_y,u_z,φ(σ_{zz},σ_{xz},σ_{yz},B_z): coupled Magneto-Mechanical case.
If the considered virtual variations are: δu_x, δu_y, δu_z, $\delta\varphi$, $\delta\sigma_{zz}$, $\delta\sigma_{xz}$, $\delta\sigma_{yz}$, δB_z, the RMVT reduces to:

$$\begin{aligned}&\int_V (\delta\boldsymbol{\epsilon}_{pG}^T\boldsymbol{\sigma}_{pH} + \delta\boldsymbol{\epsilon}_{nG}^T\boldsymbol{\sigma}_n + \delta\boldsymbol{\sigma}_n^T(\boldsymbol{\epsilon}_{nG} - \boldsymbol{\epsilon}_{nH}) + \delta\boldsymbol{H}_{pG}^T\boldsymbol{B}_{pH} + \delta H_{nG}B_n +\\ &+\delta B_n(H_{nG} - H_{nH}))\, dV \;=\; \delta L_e - \delta L_{in}.\end{aligned} \tag{3.29}$$

RMVT-u_x,u_y,u_z,ϕ(σ_{zz},σ_{xz},σ_{yz}): coupled Magneto-Electro-Mechanical case.
If the considered virtual variations are: δu_x, δu_y, δu_z, $\delta\phi$, $\delta\varphi$, $\delta\sigma_{zz}$, $\delta\sigma_{xz}$, $\delta\sigma_{yz}$, the RMVT statement is:

$$\begin{aligned}&\int_V (\delta\boldsymbol{\epsilon}_{pG}^T\boldsymbol{\sigma}_{pH} + \delta\boldsymbol{\epsilon}_{nG}^T\boldsymbol{\sigma}_n + \delta\boldsymbol{\sigma}_n^T(\boldsymbol{\epsilon}_{nG} - \boldsymbol{\epsilon}_{nH}) + \delta\boldsymbol{E}_{pG}^T\boldsymbol{D}_{pH} + \delta E_{nG}D_{nH} +\\ &+\delta\boldsymbol{H}_{pG}^T\boldsymbol{B}_{pH} + \delta H_{nG}B_n)\, dV \;=\; \delta L_e - \delta L_{in}.\end{aligned} \tag{3.30}$$

RMVT-u_x,u_y,u_z,ϕ,φ(σ_{zz},σ_{xz},σ_{yz},D_z,B_z): coupled Magneto-Electro-Mechanical case.
If the considered virtual variations are: δu_x, δu_y, δu_z, $\delta\phi$, $\delta\varphi$, $\delta\sigma_{zz}$, $\delta\sigma_{xz}$, $\delta\sigma_{yz}$, δD_z, δB_z, the RMVT reduces to:

$$\begin{aligned}&\int_V (\delta\boldsymbol{\epsilon}_{pG}^T\boldsymbol{\sigma}_{pH} + \delta\boldsymbol{\epsilon}_{nG}^T\boldsymbol{\sigma}_n + \delta\boldsymbol{\sigma}_n^T(\boldsymbol{\epsilon}_{nG} - \boldsymbol{\epsilon}_{nH}) + \delta\boldsymbol{E}_{pG}^T\boldsymbol{D}_{pH} + \delta E_{nG}D_n +\\ &+\delta D_n(E_{nG} - E_{nH}) + \delta\boldsymbol{H}_{pG}^T\boldsymbol{B}_{pH} + \delta H_{nG}B_n + \delta B_n(H_{nG} - H_{nH}))\, dV \;=\; \delta L_e - \delta L_{in}.\end{aligned} \tag{3.31}$$

3.3 Geometrical relations for mixed models

Unknowns variables are collected in the vector $\boldsymbol{V}$, which includes the assumed interlaminar continuous variables:

$$\boldsymbol{V}^{kT} = \left\{ \begin{array}{ccccccccccc} u_1 & u_2 & u_3 & \phi & \varphi & \theta & \sigma_{33} & \sigma_{13} & \sigma_{23} & D_3 & B_3 \end{array} \right\}. \tag{3.32}$$

Considering the vectors introduced in Sec. 3.2, here rewritten:

$$\boldsymbol{\mathcal{E}}_a^T = \left\{ \begin{array}{cccccccc} \epsilon_{11} & \epsilon_{22} & \gamma_{12} & E_1 & E_2 & H_1 & H_2 & \theta \end{array} \right\}; \tag{3.33}$$

$$\boldsymbol{\mathcal{E}}_b^T = \left\{ \begin{array}{ccccc} \epsilon_{33} & \gamma_{13} & \gamma_{23} & E_3 & H_3 \end{array} \right\}; \tag{3.34}$$

$$\boldsymbol{\mathcal{S}}_a^T = \left\{ \begin{array}{ccccccccc} \sigma_{11} & \sigma_{22} & \sigma_{12} & -D_1 & -D_2 & -B_1 & -B_2 & -\eta \end{array} \right\}; \tag{3.35}$$

$$\boldsymbol{\mathcal{S}}_b^T = \left\{ \begin{array}{ccccc} \sigma_{33} & \sigma_{13} & \sigma_{23} & -D_3 & -B_3 \end{array} \right\}, \tag{3.36}$$

following geometrical relations can be written:

$$\boldsymbol{\mathcal{E}}_{aG} = \boldsymbol{D}_a \boldsymbol{V}; \tag{3.37}$$

$$\boldsymbol{\mathcal{E}}_{bG} = \boldsymbol{D}_b \boldsymbol{V}; \tag{3.38}$$

$$\boldsymbol{\mathcal{S}}_{bG} = \boldsymbol{D}_{b'} \boldsymbol{V}. \tag{3.39}$$

In explicit form:

$$\boldsymbol{D}_a = \begin{pmatrix} \partial_x & 0 & 0 & 0 & 0 & 0 & 0 & 0 & 0 & 0 & 0 \\ 0 & \partial_y & 0 & 0 & 0 & 0 & 0 & 0 & 0 & 0 & 0 \\ \partial_y & \partial_x & 0 & 0 & 0 & 0 & 0 & 0 & 0 & 0 & 0 \\ 0 & 0 & 0 & -\partial_x & 0 & 0 & 0 & 0 & 0 & 0 & 0 \\ 0 & 0 & 0 & -\partial_y & 0 & 0 & 0 & 0 & 0 & 0 & 0 \\ 0 & 0 & 0 & 0 & -\partial_x & 0 & 0 & 0 & 0 & 0 & 0 \\ 0 & 0 & 0 & 0 & -\partial_y & 0 & 0 & 0 & 0 & 0 & 0 \\ 0 & 0 & 0 & 0 & 0 & 1 & 0 & 0 & 0 & 0 & 0 \end{pmatrix}; \tag{3.40}$$

$$\boldsymbol{D}_b = \begin{pmatrix} 0 & 0 & \partial_z & 0 & 0 & 0 & 0 & 0 & 0 & 0 & 0 \\ \partial_z & 0 & \partial_x & 0 & 0 & 0 & 0 & 0 & 0 & 0 & 0 \\ 0 & \partial_z & \partial_y & 0 & 0 & 0 & 0 & 0 & 0 & 0 & 0 \\ 0 & 0 & 0 & -\partial_z & 0 & 0 & 0 & 0 & 0 & 0 & 0 \\ 0 & 0 & 0 & 0 & -\partial_z & 0 & 0 & 0 & 0 & 0 & 0 \end{pmatrix}; \tag{3.41}$$

$$\boldsymbol{D}_{b'} = \begin{pmatrix} 0 & 0 & 0 & 0 & 0 & 0 & 1 & 0 & 0 & 0 & 0 \\ 0 & 0 & 0 & 0 & 0 & 0 & 0 & 1 & 0 & 0 & 0 \\ 0 & 0 & 0 & 0 & 0 & 0 & 0 & 0 & 1 & 0 & 0 \\ 0 & 0 & 0 & 0 & 0 & 0 & 0 & 0 & 0 & -1 & 0 \\ 0 & 0 & 0 & 0 & 0 & 0 & 0 & 0 & 0 & 0 & -1 \end{pmatrix}. \tag{3.42}$$

3.4 Constitutive relations for mixed models

Mixed variational statements require the rearrangement of constitutive relations. The Eq. 1.17 is rearranged in the following form:

$$\widetilde{\boldsymbol{\mathcal{S}}}_H = \widetilde{\boldsymbol{H}}\widetilde{\boldsymbol{\mathcal{E}}}_G. \tag{3.43}$$

$\tilde{\boldsymbol{\mathcal{S}}}_H$ is composed by the vector of not modeled extensive variables $\boldsymbol{\mathcal{S}}_{aH}$ and the vector of intensive variables $\boldsymbol{\mathcal{E}}_{bH}$ (which is associated to $\boldsymbol{\mathcal{S}}_b$); $\widetilde{\boldsymbol{\mathcal{E}}}_G$ is composed by the vector of intensive variables $\boldsymbol{\mathcal{E}}_{aG}$ (which is associated to $\boldsymbol{\mathcal{S}}_a$) and the vector of modeled extensive variables $\boldsymbol{\mathcal{S}}_b$, that is considered a geometrical vector by Eq. 3.39:

$$\begin{aligned} \widetilde{\boldsymbol{\mathcal{S}}}_H^T &= \left\{ \begin{array}{cc} \boldsymbol{\mathcal{S}}_{aH}^T & \boldsymbol{\mathcal{E}}_{bH}^T \end{array} \right\}; \\ \widetilde{\boldsymbol{\mathcal{E}}}_G^T &= \left\{ \begin{array}{cc} \boldsymbol{\mathcal{E}}_{aG}^T & \boldsymbol{\mathcal{S}}_{bG}^T \end{array} \right\}. \end{aligned} \tag{3.44}$$

Constitutive matrix $\boldsymbol{H}$ in Eq. 1.17 can be partitioned by dividing cells related to modeled and not modeled quantities:

$$\boldsymbol{H} = \left\{ \begin{array}{cc} \boldsymbol{H}_{aa} & \boldsymbol{H}_{ab} \\ \boldsymbol{H}_{ba} & \boldsymbol{H}_{bb} \end{array} \right\}, \tag{3.45}$$

where $\boldsymbol{H}_{ab} = \boldsymbol{H}_{ba}^T$.
In explicit form:

$$\boldsymbol{H}_{aa} = \begin{pmatrix} C_{11} & C_{12} & C_{16} & 0 & 0 & 0 & 0 & -\lambda_1 \\ C_{12} & C_{22} & C_{26} & 0 & 0 & 0 & 0 & -\lambda_2 \\ C_{16} & C_{26} & C_{66} & 0 & 0 & 0 & 0 & 0 \\ 0 & 0 & 0 & -\varepsilon_{11} & -\varepsilon_{12} & -d_{11} & -d_{12} & 0 \\ 0 & 0 & 0 & -\varepsilon_{12} & -\varepsilon_{22} & -d_{12} & -d_{22} & 0 \\ 0 & 0 & 0 & -d_{11} & -d_{12} & -\mu_{11} & -\mu_{12} & 0 \\ 0 & 0 & 0 & -d_{12} & -d_{22} & -\mu_{12} & -\mu_{22} & 0 \\ -\lambda_1 & -\lambda_2 & 0 & 0 & 0 & 0 & 0 & -(\frac{\rho \mathrm{C}}{\theta_{ref}}) \end{pmatrix}; \tag{3.46}$$

$$\boldsymbol{H}_{ab} = \begin{pmatrix} C_{13} & 0 & 0 & -e_{31} & -q_{31} \\ C_{23} & 0 & 0 & -e_{32} & -q_{32} \\ C_{36} & 0 & 0 & -e_{36} & -q_{36} \\ 0 & -e_{15} & -e_{14} & 0 & 0 \\ 0 & -e_{25} & -e_{24} & 0 & 0 \\ 0 & -q_{15} & -q_{14} & 0 & 0 \\ 0 & -q_{25} & -q_{24} & 0 & 0 \\ -\lambda_3 & 0 & 0 & -p_3 & -r_3 \end{pmatrix}; \tag{3.47}$$

$$\boldsymbol{H}_{ba} = \begin{pmatrix} C_{13} & C_{23} & C_{36} & 0 & 0 & 0 & 0 & -\lambda_3 \\ 0 & 0 & 0 & -e_{15} & -e_{25} & -q_{15} & -q_{25} & 0 \\ 0 & 0 & 0 & -e_{14} & -e_{24} & -q_{14} & -q_{24} & 0 \\ -e_{31} & -e_{32} & -e_{36} & 0 & 0 & 0 & 0 & -p_3 \\ -q_{31} & -q_{32} & -q_{36} & 0 & 0 & 0 & 0 & -r_3 \end{pmatrix}; \tag{3.48}$$

$$\boldsymbol{H}_{bb} = \begin{pmatrix} C_{33} & 0 & 0 & -e_{33} & -q_{33} \\ 0 & C_{55} & C_{45} & 0 & 0 \\ 0 & C_{45} & C_{44} & 0 & 0 \\ -e_{33} & 0 & 0 & -\varepsilon_{33} & -d_{33} \\ -q_{33} & 0 & 0 & -d_{33} & -\mu_{33} \end{pmatrix}. \tag{3.49}$$

The system in Eq. 1.17 can be arranged according to the above partitioning:

$$\begin{aligned} \boldsymbol{\mathcal{S}}_{aH} &= \boldsymbol{H}_{aa}\boldsymbol{\mathcal{E}}_{aG} + \boldsymbol{H}_{ab}\boldsymbol{\mathcal{E}}_{bG}, \\ \boldsymbol{\mathcal{S}}_{bH} &= \boldsymbol{H}_{ba}\boldsymbol{\mathcal{E}}_{aG} + \boldsymbol{H}_{bb}\boldsymbol{\mathcal{E}}_{bG}. \end{aligned} \tag{3.50}$$

From Eq. 3.50 one has:

$$\begin{aligned} \boldsymbol{\mathcal{S}}_{aH} &= \widetilde{\boldsymbol{H}}_{aa}\boldsymbol{\mathcal{E}}_{aG} + \widetilde{\boldsymbol{H}}_{ab}\boldsymbol{\mathcal{S}}_{bG}, \\ \boldsymbol{\mathcal{E}}_{bH} &= \widetilde{\boldsymbol{H}}_{ba}\boldsymbol{\mathcal{E}}_{aG} + \widetilde{\boldsymbol{H}}_{bb}\boldsymbol{\mathcal{S}}_{bG}, \end{aligned} \tag{3.51}$$

with:

$$\begin{aligned} \widetilde{\boldsymbol{H}}_{aa} &= \boldsymbol{H}_{aa} - \boldsymbol{H}_{ab}(\boldsymbol{H}_{bb})^{-1}\boldsymbol{H}_{ba}; \\ \widetilde{\boldsymbol{H}}_{ab} &= \boldsymbol{H}_{ab}(\boldsymbol{H}_{bb})^{-1}; \\ \widetilde{\boldsymbol{H}}_{ba} &= -(\boldsymbol{H}_{bb})^{-1}\boldsymbol{H}_{ab}; \\ \widetilde{\boldsymbol{H}}_{bb} &= (\boldsymbol{H}_{bb})^{-1}. \end{aligned} \tag{3.52}$$

Matrix $\widetilde{\boldsymbol{H}}$ of Eq. 3.43 is:

$$\widetilde{\boldsymbol{H}} = \begin{Bmatrix} \widetilde{\boldsymbol{H}}_{aa} & \widetilde{\boldsymbol{H}}_{ab} \\ \widetilde{\boldsymbol{H}}_{ba} & \widetilde{\boldsymbol{H}}_{bb} \end{Bmatrix}. \tag{3.53}$$

A significant advantage of using the condensed notation is that the showed procedure to obtain geometrical and constitutive relations for mixed models is applicable in all the possible RMVT applications (a few possible particular cases are presented in Sec. 3.2). Consequently, the proposed methodology represents a general and an automatic way to obtain geometrical and constitutive coefficients for many different cases of variational statements, as explained in [18]. As examples, in next sections the geometrical and constitutive relations are explicitly obtained for the application of RMVT-u_x,u_y,u_z,$\phi(D_z)$ and RMVT-u_x,u_y,u_z,$\phi(\sigma_{zz}$,σ_{xz},σ_{yz},$D_z)$.

3.4.1 Geometrical and constitutive relations for RMVT-u_x,u_y,u_z,$\phi(D_z)$

In case of RMVT-u_x,u_y,u_z,$\phi(D_z)$ application, primary unknowns variables are collected in the vector

$$\boldsymbol{V}^T = \left\{ \begin{array}{ccccc} u_x & u_y & u_z & \phi & D_z \end{array} \right\}.$$

It is useful to rewrite vectors introduced in Sec. 3.2 including only the interested variables:

$$\begin{array}{l} \boldsymbol{\mathcal{E}}_a^T = \left\{ \begin{array}{cccccccc} \epsilon_{xx} & \epsilon_{yy} & \epsilon_{xy} & E_x & E_y & \epsilon_{zz} & \epsilon_{xz} & \epsilon_{yz} \end{array} \right\}; \boldsymbol{\mathcal{E}}_b^T = \left\{ \begin{array}{c} E_z \end{array} \right\}; \\ \boldsymbol{\mathcal{S}}_a^T = \left\{ \begin{array}{cccccccc} \sigma_{xx} & \sigma_{yy} & \sigma_{xy} & -D_x & -D_y & \sigma_{zz} & \sigma_{xz} & \sigma_{yz} \end{array} \right\}; \boldsymbol{\mathcal{S}}_b^T = \left\{ \begin{array}{c} -D_z \end{array} \right\}. \end{array}$$

Following geometrical relations can be written:

$$\boldsymbol{\mathcal{E}}_{aG} = \boldsymbol{D}_a\boldsymbol{V}; \tag{3.54}$$

$$\boldsymbol{\mathcal{E}}_{bG} = \boldsymbol{D}_b\boldsymbol{V}; \tag{3.55}$$

$$\boldsymbol{\mathcal{S}}_{bG} = \boldsymbol{D}_{b'}\boldsymbol{V}. \tag{3.56}$$

In explicit form:

$$\boldsymbol{D}_a = \begin{pmatrix} \partial_x & 0 & 0 & 0 & 0 \\ 0 & \partial_y & 0 & 0 & 0 \\ \partial_y & \partial_x & 0 & 0 & 0 \\ 0 & 0 & 0 & -\partial_x & 0 \\ 0 & 0 & 0 & -\partial_y & 0 \\ 0 & 0 & \partial_z & 0 & 0 \\ \partial_z & 0 & \partial_x & 0 & 0 \\ 0 & \partial_z & \partial_y & 0 & 0 \end{pmatrix}; \quad \boldsymbol{D}_b = \begin{pmatrix} 0 & 0 & 0 & -\partial_z & 0 \end{pmatrix}; \quad \boldsymbol{D}_{b'} = \begin{pmatrix} 0 & 0 & 0 & 0 & -1 \end{pmatrix}.$$

The physical constitutive matrix $\boldsymbol{H}$ can be partitioned by dividing cells related to modeled and not modeled quantities:

$$\boldsymbol{H} = \begin{Bmatrix} \boldsymbol{H}_{aa} & \boldsymbol{H}_{ab} \\ \boldsymbol{H}_{ba} & \boldsymbol{H}_{bb} \end{Bmatrix}, \tag{3.57}$$

where $\boldsymbol{H}_{ab} = \boldsymbol{H}_{ba}^T$.
In explicit form:

$$\boldsymbol{H}_{aa} = \begin{pmatrix} C_{11} & C_{12} & C_{16} & 0 & 0 & C_{13} & 0 & 0 \\ C_{12} & C_{22} & C_{26} & 0 & 0 & C_{23} & 0 & 0 \\ C_{16} & C_{26} & C_{66} & 0 & 0 & C_{36} & 0 & 0 \\ 0 & 0 & 0 & -\varepsilon_{11} & -\varepsilon_{12} & 0 & 0 & 0 \\ 0 & 0 & 0 & -\varepsilon_{12} & -\varepsilon_{22} & 0 & 0 & 0 \\ C_{13} & C_{23} & C_{36} & 0 & 0 & C_{33} & 0 & 0 \\ 0 & 0 & 0 & 0 & 0 & 0 & C_{55} & C_{45} \\ 0 & 0 & 0 & 0 & 0 & 0 & C_{45} & C_{44} \end{pmatrix}; \quad \boldsymbol{H}_{ab} = \begin{pmatrix} -e_{31} \\ -e_{32} \\ -e_{36} \\ 0 \\ 0 \\ -e_{33} \\ 0 \\ 0 \end{pmatrix};$$

$$\boldsymbol{H}_{ba} = \begin{pmatrix} -e_{31} & -e_{32} & -e_{36} & 0 & 0 & -e_{33} & 0 & 0 \end{pmatrix}; \quad \boldsymbol{H}_{bb} = \begin{pmatrix} -\varepsilon_{33} \end{pmatrix}.$$

After calculations, matrix $\widetilde{\boldsymbol{H}}$ of becomes:

$$\widetilde{\boldsymbol{H}} = \begin{Bmatrix} \widetilde{\boldsymbol{H}}_{aa} & \widetilde{\boldsymbol{H}}_{ab} \\ \widetilde{\boldsymbol{H}}_{ba} & \widetilde{\boldsymbol{H}}_{bb} \end{Bmatrix}, \tag{3.58}$$

with:

$$\widetilde{\boldsymbol{H}}_{aa} = \begin{bmatrix} C_{11} + e_{31}^2/\varepsilon_{33} & C_{12} + e_{31}e_{32}/\varepsilon_{33} & C_{16} + e_{31}e_{36}/\varepsilon_{33} & 0 & 0 & C_{13} + e_{31}e_{33}/\varepsilon_{33} & 0 & 0 \\ C_{12} + e_{31}e_{32}/\varepsilon_{33} & C_{22} + e_{32}^2/\varepsilon_{33} & C_{26} + e_{32}e_{36}/\varepsilon_{33} & 0 & 0 & C_{23} + e_{32}e_{33}/\varepsilon_{33} & 0 & 0 \\ C_{16} + e_{31}e_{36}/\varepsilon_{33} & C_{26} + e_{32}e_{36}/\varepsilon_{33} & C_{66} + e_{36}^2/\varepsilon_{33} & 0 & 0 & C_{36} + e_{33}e_{36}/\varepsilon_{33} & 0 & 0 \\ 0 & 0 & 0 & -\varepsilon_{11} & -\varepsilon_{12} & 0 & -e_{15} & -e_{14} \\ 0 & 0 & 0 & -\varepsilon_{12} & -\varepsilon_{22} & 0 & -e_{25} & -e_{24} \\ C_{13} + e_{31}e_{33}/\varepsilon_{33} & C_{23} + e_{32}e_{33}/\varepsilon_{33} & C_{36} + e_{33}e_{36}/\varepsilon_{33} & 0 & 0 & C_{33} + e_{33}^2/\varepsilon_{33} & 0 & 0 \\ 0 & 0 & 0 & -e_{15} & -e_{25} & 0 & C_{55} & C_{45} \\ 0 & 0 & 0 & -e_{14} & -e_{24} & 0 & C_{45} & C_{44} \end{bmatrix};$$

$$\widetilde{\boldsymbol{H}}_{ab}^T = \begin{bmatrix} e_{31}/\varepsilon_{33} & e_{32}/\varepsilon_{33} & e_{36}/\varepsilon_{33} & 0 & 0 & e_{33}/\varepsilon_{33} & 0 & 0 \end{bmatrix};$$

$$\widetilde{\boldsymbol{H}}_{ba} = \begin{bmatrix} -e_{31}/\varepsilon_{33} & -e_{32}/\varepsilon_{33} & -e_{36}/\varepsilon_{33} & 0 & 0 & -e_{33}/\varepsilon_{33} & 0 & 0 \end{bmatrix};$$

$$\widetilde{\boldsymbol{H}}_{bb} = \begin{bmatrix} -1/\varepsilon_{33} \end{bmatrix}.$$

3.4.2 Geometrical and constitutive relations for RMVT-u_x,u_y,u_z,$\phi(\sigma_{zz}$,σ_{xz},σ_{yz},$D_z)$

In case of RMVT-u_x,u_y,u_z,$\phi(\sigma_{zz}$,σ_{xz},σ_{yz},$D_z)$ application, primary unknowns variables are collected in the vector

$$\boldsymbol{V}^T = \left\{ \begin{array}{ccccc} u_x & u_y & u_z & \phi & D_z \end{array} \right\}.$$

It is useful to rewrite vectors introduced in Sec. 3.2 including only the interested variables:

$$\begin{array}{ll} \boldsymbol{\mathcal{E}}_a^T = \left\{ \begin{array}{ccccc} \epsilon_{xx} & \epsilon_{yy} & \epsilon_{xy} & E_x & E_y \end{array} \right\}; & \boldsymbol{\mathcal{E}}_b^T = \left\{ \begin{array}{cccc} \epsilon_{zz} & \epsilon_{xz} & \epsilon_{yz} & E_z \end{array} \right\}; \\ \boldsymbol{\mathcal{S}}_a^T = \left\{ \begin{array}{ccccc} \sigma_{xx} & \sigma_{yy} & \sigma_{xy} & -D_x & -D_y \end{array} \right\}; & \boldsymbol{\mathcal{S}}_b^T = \left\{ \begin{array}{cccc} \sigma_{zz} & \sigma_{xz} & \sigma_{yz} & -D_z \end{array} \right\}. \end{array}$$

Following geometrical relations can be written:

$$\boldsymbol{\mathcal{E}}_{aG} = \boldsymbol{D}_a \boldsymbol{V}; \tag{3.59}$$

$$\boldsymbol{\mathcal{E}}_{bG} = \boldsymbol{D}_b \boldsymbol{V}; \tag{3.60}$$

$$\boldsymbol{\mathcal{S}}_{bG} = \boldsymbol{D}_{b'} \boldsymbol{V}, \tag{3.61}$$

where the differential matrices in explicit form read:

$$\boldsymbol{D}_a = \begin{pmatrix} \partial_x & 0 & 0 & 0 & 0 & 0 & 0 & 0 \\ 0 & \partial_y & 0 & 0 & 0 & 0 & 0 & 0 \\ \partial_y & \partial_x & 0 & 0 & 0 & 0 & 0 & 0 \\ 0 & 0 & 0 & -\partial_x & 0 & 0 & 0 & 0 \\ 0 & 0 & 0 & -\partial_y & 0 & 0 & 0 & 0 \end{pmatrix}; \quad \boldsymbol{D}_b = \begin{pmatrix} 0 & 0 & \partial_z & 0 & 0 & 0 & 0 & 0 \\ \partial_z & 0 & \partial_x & 0 & 0 & 0 & 0 & 0 \\ 0 & \partial_z & \partial_y & 0 & 0 & 0 & 0 & 0 \\ 0 & 0 & 0 & -\partial_z & 0 & 0 & 0 & 0 \end{pmatrix};$$

$$\boldsymbol{D}_{b'} = \begin{pmatrix} 0 & 0 & 0 & 0 & 1 & 0 & 0 & 0 \\ 0 & 0 & 0 & 0 & 0 & 1 & 0 & 0 \\ 0 & 0 & 0 & 0 & 0 & 0 & 1 & 0 \\ 0 & 0 & 0 & 0 & 0 & 0 & 0 & -1 \end{pmatrix}.$$

The physical constitutive matrix $\boldsymbol{H}$ can be partitioned by dividing cells related to modeled and not modeled quantitiesas in the following:

$$\boldsymbol{H}_{aa} = \begin{pmatrix} C_{11} & C_{12} & C_{16} & 0 & 0 & C_{13} & 0 & 0 \\ C_{12} & C_{22} & C_{26} & 0 & 0 & C_{23} & 0 & 0 \\ C_{16} & C_{26} & C_{66} & 0 & 0 & C_{36} & 0 & 0 \\ 0 & 0 & 0 & -\varepsilon_{11} & -\varepsilon_{12} & 0 & 0 & 0 \\ 0 & 0 & 0 & -\varepsilon_{12} & -\varepsilon_{22} & 0 & 0 & 0 \\ C_{13} & C_{23} & C_{36} & 0 & 0 & C_{33} & 0 & 0 \\ 0 & 0 & 0 & 0 & 0 & 0 & C_{55} & C_{45} \\ 0 & 0 & 0 & 0 & 0 & 0 & C_{45} & C_{44} \end{pmatrix}; \quad \boldsymbol{H}_{ab} = \begin{pmatrix} -e_{31} \\ -e_{32} \\ -e_{36} \\ 0 \\ 0 \\ -e_{33} \\ 0 \\ 0 \end{pmatrix};$$

$$\boldsymbol{H}_{ba} = \begin{pmatrix} -e_{31} & -e_{32} & -e_{36} & 0 & 0 & -e_{33} & 0 & 0 \end{pmatrix}; \quad \boldsymbol{H}_{bb} = \begin{pmatrix} -\varepsilon_{33} \end{pmatrix}.$$

After calculations, matrix $\widetilde{\boldsymbol{H}}$ of becomes:

$$\widetilde{\boldsymbol{H}} = \left\{ \begin{array}{cc} \widetilde{\boldsymbol{H}}_{aa} & \widetilde{\boldsymbol{H}}_{ab} \\ \widetilde{\boldsymbol{H}}_{ba} & \widetilde{\boldsymbol{H}}_{bb} \end{array} \right\}, \tag{3.62}$$

with:

$$\widetilde{\boldsymbol{H}}_{aa}(1,1) = C_{11} + \frac{C_{33}e_{31}^2 - C_{13}\left(2e_{31}e_{33} + C_{13}\varepsilon_{33}\right)}{e_{33}^2 + C_{33}\varepsilon_{33}}$$

$$\widetilde{\boldsymbol{H}}_{aa}(1,2) = \frac{e_{33}\left(-C_{13}e_{32} + C_{12}e_{33}\right) + C_{33}\left(e_{31}e_{32} + C_{12}\varepsilon_{33}\right) - C_{23}\left(e_{31}e_{33} + C_{13}\varepsilon_{33}\right)}{e_{33}^2 + C_{33}\varepsilon_{33}}$$

$$\widetilde{\boldsymbol{H}}_{aa}(1,3) = C_{16} + \frac{\left(C_{33}e_{31} - C_{13}e_{33}\right)e_{36} - C_{36}\left(e_{31}e_{33} + C_{13}\varepsilon_{33}\right)}{e_{33}^2 + C_{33}\varepsilon_{33}}$$

$$\widetilde{\boldsymbol{H}}_{aa}(1,4) = 0$$

$$\widetilde{\boldsymbol{H}}_{aa}(1,5) = 0$$

$$\widetilde{\boldsymbol{H}}_{aa}(2,1) = \frac{e_{33}\left(-C_{13}e_{32} + C_{12}e_{33}\right) + C_{33}\left(e_{31}e_{32} + C_{12}\varepsilon_{33}\right) - C_{23}\left(e_{31}e_{33} + C_{13}\varepsilon_{33}\right)}{e_{33}^2 + C_{33}\varepsilon_{33}}$$

$$\widetilde{\boldsymbol{H}}_{aa}(2,2) = C_{22} + \frac{C_{33}e_{32}^2 - C_{23}\left(2e_{32}e_{33} + C_{23}\varepsilon_{33}\right)}{e_{33}^2 + C_{33}\varepsilon_{33}}$$

$$\widetilde{\boldsymbol{H}}_{aa}(2,3) = C_{26} + \frac{\left(C_{33}e_{32} - C_{23}e_{33}\right)e_{36} - C_{36}\left(e_{32}e_{33} + C_{23}\varepsilon_{33}\right)}{e_{33}^2 + C_{33}\varepsilon_{33}}$$

$$\widetilde{\boldsymbol{H}}_{aa}(2,4) = 0$$

$$\widetilde{\boldsymbol{H}}_{aa}(2,5) = 0$$

$$\widetilde{\boldsymbol{H}}_{aa}(3,1) = C_{16} + \frac{\left(C_{33}e_{31} - C_{13}e_{33}\right)e_{36} - C_{36}\left(e_{31}e_{33} + C_{13}\varepsilon_{33}\right)}{e_{33}^2 + C_{33}\varepsilon_{33}}$$

$$\widetilde{\boldsymbol{H}}_{aa}(3,2) = C_{26} + \frac{\left(C_{33}e_{32} - C_{23}e_{33}\right)e_{36} - C_{36}\left(e_{32}e_{33} + C_{23}\varepsilon_{33}\right)}{e_{33}^2 + C_{33}\varepsilon_{33}}$$

$$\widetilde{\boldsymbol{H}}_{aa}(3,3) = C_{66} + \frac{-2C_{36}e_{33}e_{36} + C_{33}e_{36}^2 - C_{36}^2\varepsilon_{33}}{e_{33}^2 + C_{33}\varepsilon_{33}}$$

$$\widetilde{\boldsymbol{H}}_{aa}(3,4) = 0$$

$$\widetilde{\boldsymbol{H}}_{aa}(3,5) = 0$$

$$\widetilde{\boldsymbol{H}}_{aa}(4,1) = 0$$

$$\widetilde{\boldsymbol{H}}_{aa}(4,2) = 0$$

$$\widetilde{\boldsymbol{H}}_{aa}(4,3) = 0$$

$$\widetilde{\boldsymbol{H}}_{aa}(4,4) = \frac{C_{55}e_{14}^2 - 2C_{45}e_{14}e_{15} + C_{44}e_{15}^2}{C_{45}^2 - C_{44}C_{55}} - \varepsilon_{11}$$

$$\widetilde{\boldsymbol{H}}_{aa}(4,5) = \frac{C_{55}e_{14}e_{24} + C_{44}e_{15}e_{25} - C_{45}\left(e_{15}e_{24} + e_{14}e_{25}\right)}{C_{45}^2 - C_{44}C_{55}} - \varepsilon_{12}$$

$$\widetilde{\boldsymbol{H}}_{aa}(5,1) = 0$$

$$\widetilde{\boldsymbol{H}}_{aa}(5,2) = 0$$

$$\widetilde{\boldsymbol{H}}_{aa}(5,3) = 0$$

$$\widetilde{\boldsymbol{H}}_{aa}(5,4) = \frac{C_{55}e_{14}e_{24} + C_{44}e_{15}e_{25} - C_{45}\left(e_{15}e_{24} + e_{14}e_{25}\right)}{C_{45}^2 - C_{44}C_{55}} - \varepsilon_{12}$$

$$\widetilde{\boldsymbol{H}}_{aa}(5,5) = \frac{C_{55}e_{24}^2 - 2C_{45}e_{24}e_{25} + C_{44}e_{25}^2}{C_{45}^2 - C_{44}C_{55}} - \varepsilon_{22}$$

$$\widetilde{\boldsymbol{H}}_{ab}^T = \begin{bmatrix} \frac{e_{31}e_{33}+C_{13}\varepsilon_{33}}{e_{33}^2+C_{33}\varepsilon_{33}} & 0 & 0 & \frac{C_{33}e_{31}-C_{13}e_{33}}{e_{33}^2+C_{33}\varepsilon_{33}} \\ \frac{e_{32}e_{33}+C_{23}\varepsilon_{33}}{e_{33}^2+C_{33}\varepsilon_{33}} & 0 & 0 & \frac{C_{33}e_{32}-C_{23}e_{33}}{e_{33}^2+C_{33}\varepsilon_{33}} \\ \frac{e_{33}e_{36}+C_{36}\varepsilon_{33}}{e_{33}^2+C_{33}\varepsilon_{33}} & 0 & 0 & \frac{-C_{36}e_{33}+C_{33}e_{36}}{e_{33}^2+C_{33}\varepsilon_{33}} \\ 0 & \frac{-C_{45}e_{14}+C_{44}e_{15}}{C_{45}^2-C_{44}C_{55}} & \frac{C_{55}e_{14}-C_{45}e_{15}}{C_{45}^2-C_{44}C_{55}} & 0 \\ 0 & \frac{-C_{45}e_{24}+C_{44}e_{25}}{C_{45}^2-C_{44}C_{55}} & \frac{C_{55}e_{24}-C_{45}e_{25}}{C_{45}^2-C_{44}C_{55}} & 0 \end{bmatrix};$$

$$\widetilde{\boldsymbol{H}}_{ba} = \begin{bmatrix} -\frac{e_{31}e_{33}+C_{13}\varepsilon_{33}}{e_{33}^2+C_{33}\varepsilon_{33}} & -\frac{e_{32}e_{33}+C_{23}\varepsilon_{33}}{e_{33}^2+C_{33}\varepsilon_{33}} & -\frac{e_{33}e_{36}+C_{36}\varepsilon_{33}}{e_{33}^2+C_{33}\varepsilon_{33}} & 0 & 0 \\ 0 & 0 & 0 & \frac{C_{45}e_{14}-C_{44}e_{15}}{C_{45}^2-C_{44}C_{55}} & \frac{C_{45}e_{24}-C_{44}e_{25}}{C_{45}^2-C_{44}C_{55}} \\ 0 & 0 & 0 & \frac{-C_{55}e_{14}+C_{45}e_{15}}{C_{45}^2-C_{44}C_{55}} & \frac{-C_{55}e_{24}+C_{45}e_{25}}{C_{45}^2-C_{44}C_{55}} \\ \frac{-C_{33}e_{31}+C_{13}e_{33}}{e_{33}^2+C_{33}\varepsilon_{33}} & \frac{-C_{33}e_{32}+C_{23}e_{33}}{e_{33}^2+C_{33}\varepsilon_{33}} & \frac{C_{36}e_{33}-C_{33}e_{36}}{e_{33}^2+C_{33}\varepsilon_{33}} & 0 & 0 \end{bmatrix}.$$

$$\widetilde{\boldsymbol{H}}_{bb} = \begin{bmatrix} \frac{1}{C_{33}+e_{33}^2/\varepsilon_{33}} & 0 & 0 & -\frac{e_{33}}{e_{33}^2+C_{33}\varepsilon_{33}} \\ 0 & \frac{1}{-C_{45}^2/C_{44}+C_{55}} & \frac{C_{45}}{C_{45}^2-C_{44}C_{55}} & 0 \\ 0 & \frac{C_{45}}{C_{45}^2-C_{44}C_{55}} & \frac{1}{C_{44}-C_{45}^2/C_{55}} & 0 \\ -\frac{e_{33}}{e_{33}^2+C_{33}\varepsilon_{33}} & 0 & 0 & -\frac{1}{e_{33}^2/C_{33}+\varepsilon_{33}} \end{bmatrix}.$$

3.5 Through-the-thickness assumptions of primary variables - CUF

3.5.1 PVD case

As discussed in Sec. 2, the behavior of primary unknowns $\boldsymbol{U}^k$ is postulated in the thickness plate z-directions according to a given expansion,

$$\boldsymbol{U}^k(x,y,z) = F_\tau(z)\,\boldsymbol{U}_\tau^k(x,y) \quad \tau = 0,1,...,N, \tag{3.63}$$

while for virtual variations:

$$\delta \boldsymbol{U}^k(x,y,z) = F_s(z)\ \delta \boldsymbol{U}^k_s(x,y) \quad s = 0,1,...,N. \tag{3.64}$$

The repeated indexes are summed over their ranges. The polynomials $F_\tau(z)$ constitute a set of independent functions. Such a base are arbitrarily chosen: power of z and Lagrange polynomials can be considered for ESL and LW modeling respectively. N denotes the order of the introduced expansion. Note that the variables concerning displacements, electrical potential, magnetic potential and temperature are included in vector $\boldsymbol{U}^k$. The above expansion is made according to the Carrera's Unified Formulation CUF [12], which permits to write in a unified form a large variety of plate theories.

3.5.2 RMVT case

The behavior of unknowns $\boldsymbol{V}^k$ is postulated in the thickness plate z-directions according to the expansion described in the PVD case.

3.5.3 Acronyms for the employed plate modeling

Appropriate acronyms are introduced in order to indicate the use of a particular plate modeling theory. Fig. 3.2 shows how the acronyms are built: the first field can be "E" or "L", according to the ESL or LW description, respectively; the second field can be "D" or "M", according to the PVD or RMVT application, respectively; the last field can assume the numbers 1-4, according to the order of the adopted expansion in the thickness direction.

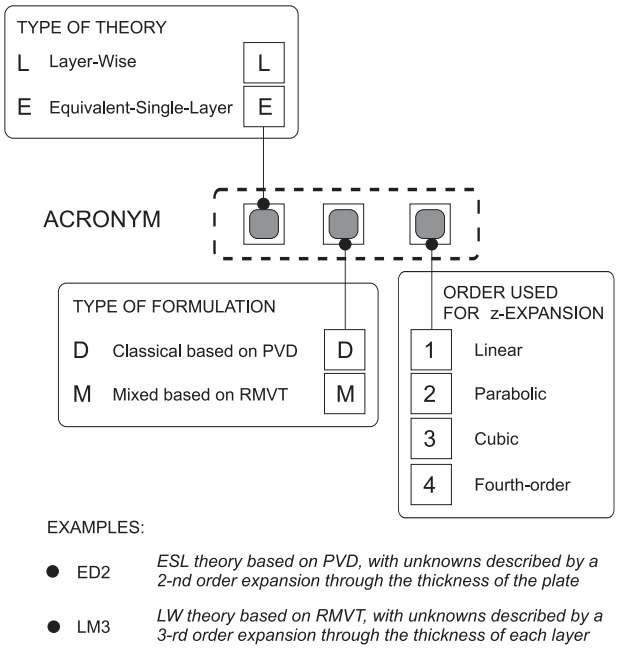

Figure 3.2. Meanings of the introduced Acronyms

Chapter 4

FE matrices for static and dynamic multifield problems

4.1 FEM discretization

4.1.1 PVD case

In case of FEM implementation, unknowns can be expressed in terms of their nodal values, via the shape functions N_i:

$$\boldsymbol{U}^k_\tau(x,y) = N_i(x,y)\boldsymbol{Q}^k_{\tau i} \quad i = 1,2,...,N_n; \tag{4.1}$$

for virtual variations:

$$\delta\boldsymbol{U}^k_s(x,y) = N_j(x,y)\delta\boldsymbol{Q}^k_{sj} \quad j = 1,2,...,N_n, \tag{4.2}$$

where N_n denotes the number of nodes of the considered finite element and $\boldsymbol{Q}^k_{\tau i}$ is the vector of the nodal values of the primary unknowns:

$$\boldsymbol{Q}^{kT}_{\tau i} = \left\{ \begin{array}{ccccccc} Q^k_{u_x\tau i} & Q^k_{u_y\tau i} & Q^k_{u_z\tau i} & Q^k_{\phi\tau i} & Q^k_{\varphi\tau i} & Q^k_{\theta\tau i} \end{array} \right\}. \tag{4.3}$$

Substituting Eq. 4.1 in Eq. 3.63, the final expression of primary unknowns is obtained:

$$\boldsymbol{U}^k(x,y,z) = F_\tau N_i \boldsymbol{Q}^k_{\tau i}. \tag{4.4}$$

Fundamental Nucleus

Substituting Eqs. 1.17,1.33,3.63 and 4.1 in the variational statement of Eq. 3.9 leads to a set of equilibrium equations which can be formally put in the following compact form:

$$\delta\boldsymbol{Q}^k_{sj}: \quad \boldsymbol{M}^{k\tau sij}\,\ddot{\boldsymbol{Q}}^k_{\tau i} + \boldsymbol{K}^{k\tau sij}\,\boldsymbol{Q}^k_{\tau i} \;=\; \boldsymbol{P}^k_{\tau i}, \tag{4.5}$$

where $\boldsymbol{P}^k$ is the vector of external loads. The related boundary conditions can be expressed by $\overline{\boldsymbol{Q}}^k$.
The number of obtained equations coincides with the number of introduced variables: τ and s vary from 0 to N, i and j vary from 1 to N_n and k ranges from 1 to N_l. Matrix $\boldsymbol{K}^{k\tau sij}$ is the so-called stiffness fundamental nucleus. In this case it is a 6×6 array and it provides the information to build the stiffness matrix, while matrix $\boldsymbol{M}^{k\tau sij}$ is the fundamental nucleus related to the mass matrix. Fundamental nuclei related to other particular cases of PVD applications can be obtained as particular cases. See Appendix A for more details.

4.1.2 RMVT case

In case of FEM implementation, unknowns can be expressed in terms of their nodal values, via the shape functions N_i, as done for the PVD case:

$$\boldsymbol{V}^k_\tau(x,y) = N_i(x,y)\boldsymbol{R}^k_{\tau i} \quad i = 1,2,...,N_n, \tag{4.6}$$

while for the virtual variations:

$$\delta\boldsymbol{V}^k_s(x,y) = N_j(x,y)\delta\boldsymbol{R}^k_{sj} \quad j = 1,2,...,N_n, \tag{4.7}$$

where N_n denotes the number of nodes concerning the considered finite element and $\boldsymbol{R}^k_{\tau i}$ is the vector containing nodal values of unknowns:

$$\boldsymbol{R}^{kT}_{\tau i} = \left\{ \begin{array}{ccccccccccc} R^k_{u_x\tau i} & R^k_{u_y\tau i} & R^k_{u_z\tau i} & R^k_{\phi\tau i} & R^k_{\varphi\tau i} & R^k_{\theta\tau i} & R^k_{\sigma_{zz}\tau i} & R^k_{\sigma_{xz}\tau i} & R^k_{\sigma_{yz}\tau i} & R^k_{D_z\tau i} & R^k_{B_z\tau i} \end{array} \right\}. \tag{4.8}$$

The final expression of the primary unknowns is:

$$\boldsymbol{V}^k(x,y,z) = F_\tau N_i \boldsymbol{R}^k_{\tau i}. \tag{4.9}$$

Fundamental Nucleus

Substituting Eqs. 3.37,3.38,3.39,3.51 and 4.9 in the variational statement in Eq. 3.20 leads to a set of equilibrium equations which can be formally put in the following compact form:

$$\delta\boldsymbol{R}^k_{sj}: \quad \boldsymbol{M}^{k\tau sij}\,\ddot{\boldsymbol{R}}^k_{\tau i} + \boldsymbol{K}^{k\tau sij}\,\boldsymbol{R}^k_{\tau i} \;=\; \boldsymbol{P}'^k_{\tau i}, \tag{4.10}$$

where $\boldsymbol{P}'^k$ is the vector in analogy with $\boldsymbol{P}^k$ (Sec. 4.1.1) and the related boundary conditions are $\overline{\boldsymbol{R}}^k$.
The number of obtained equations coincides with the number of introduced variables: τ and s vary from 0 to N, i and j vary from 1 to N_n and k ranges from 1 to N_l.
Matrix $\boldsymbol{K}^{k\tau sij}$ is the stiffness fundamental nucleus and, in this case, it is an 11×11 matrix. Matrix $\boldsymbol{M}^{k\tau sij}$ represents the fundamental nucleus related to the mass matrix. Fundamental nuclei related to other particular cases of RMVT applications can be obtained as particular cases. See Appendix B) for more details.

4.2 The assembly of fundamental nuclei to obtain the FE stiffness matrix

Through an example, in Fig. 4.1 is summarized how to assembly the stiffness fundamental nucleus in order to obtain the stiffness matrix of the generic FE. The procedure is the same in case of multifield/mixed formulation, being the only difference in the dimension of the considered fundamental nucleus. Once the FE stiffness matrix is obtained, the further standard assembly procedure leads to the structure stiffness matrix. The same procedure can be applied to obtain the mass matrix.

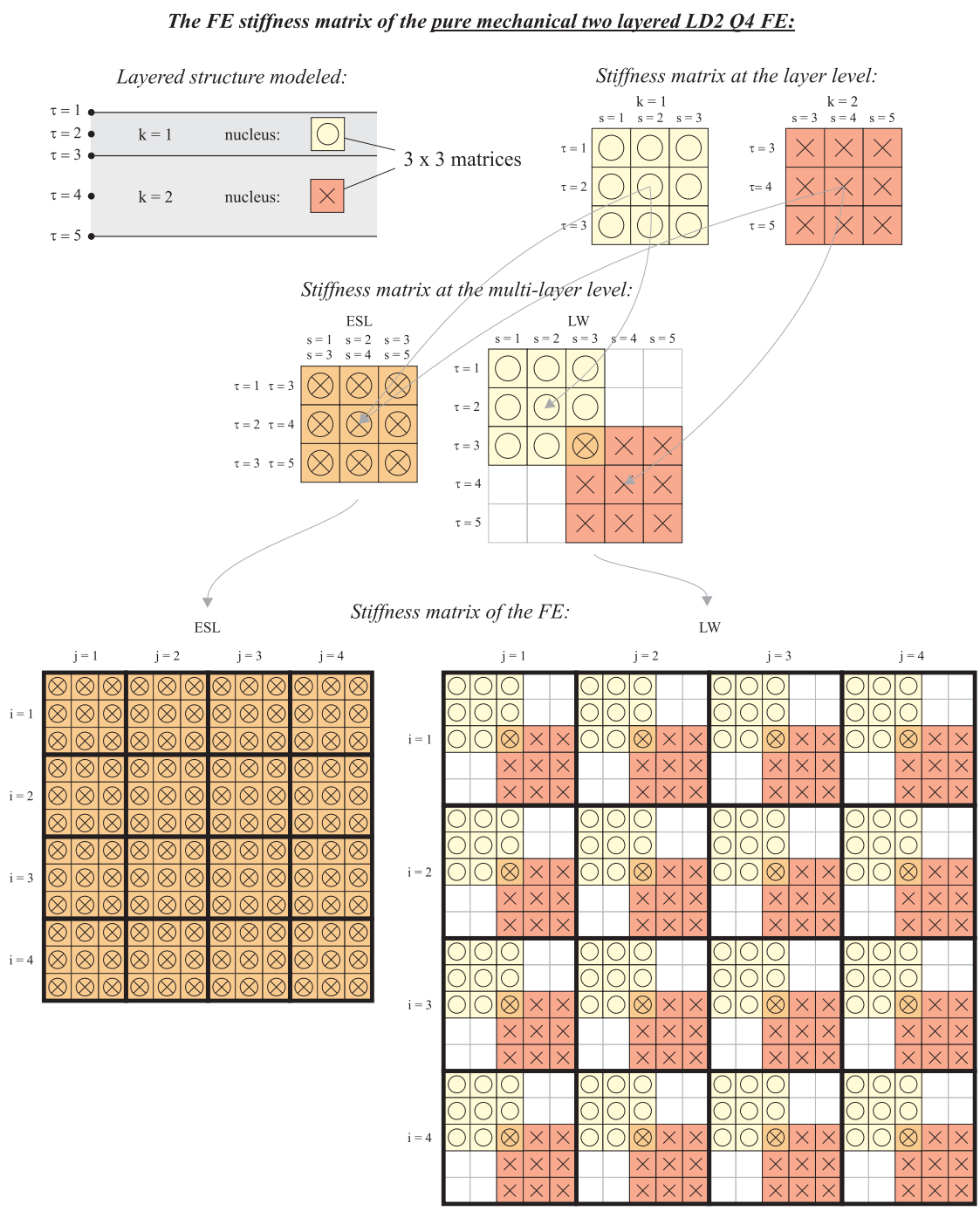

Figure 4.1. Assembly-scheme explaining how the FE stiffness matrix is obtained from the stiffness fundamental nucleus - Two layered LD2 Q4 FE - PVD-u_x,u_y,u_z

4.3 Several examples of fundamental nuclei

4.3.1 Fundamental nuclei for PVD-u_x,u_y,u_z

The stiffness fundamental nucleus $\boldsymbol{K}^{k\tau sij}$ related to the PVD mechanical application PVD-u_x,u_y,u_z is listed below. In the following, the layer-superscript k is always implied to simplify equations.
The stiffness fundamental nucleus is:

$$\boldsymbol{K}^{\tau sij} = \begin{bmatrix} K_{11} & K_{12} & K_{13} \\ K_{21} & K_{22} & K_{23} \\ K_{31} & K_{32} & K_{33} \end{bmatrix}. \tag{4.11}$$

Its elements are:

$$\begin{aligned}
K_{11} &= C_{55} \lhd N_i N_j \rhd_{\Omega_e} \lessdot F_{\tau,z} F_{s,z} \gtrdot_{z_e^k} + C_{11} \lhd N_{i,x} N_{j,x} \rhd_{\Omega_e} \lessdot F_\tau F_s \gtrdot_{z_e^k} + C_{16} \lhd N_{i,y} N_{j,x} \rhd_{\Omega_e} \lessdot F_\tau F_s \gtrdot_{z_e^k} + \\
&\quad + C_{16} \lhd N_{i,x} N_{j,y} \rhd_{\Omega_e} \lessdot F_\tau F_s \gtrdot_{z_e^k} + C_{66} \lhd N_{i,y} N_{j,y} \rhd_{\Omega_e} \lessdot F_\tau F_s \gtrdot_{z_e^k}; \\
K_{21} &= C_{45} \lhd N_i N_j \rhd_{\Omega_e} \lessdot F_{\tau,z} F_{s,z} \gtrdot_{z_e^k} + C_{16} \lhd N_{i,x} N_{j,x} \rhd_{\Omega_e} \lessdot F_\tau F_s \gtrdot_{z_e^k} + C_{12} \lhd N_{i,y} N_{j,x} \rhd_{\Omega_e} \lessdot F_\tau F_s \gtrdot_{z_e^k} + \\
&\quad + C_{66} \lhd N_{i,x} N_{j,y} \rhd_{\Omega_e} \lessdot F_\tau F_s \gtrdot_{z_e^k} + C_{26} \lhd N_{i,y} N_{j,y} \rhd_{\Omega_e} \lessdot F_\tau F_s \gtrdot_{z_e^k}; \\
K_{31} &= C_{55} \lhd N_{i,x} N_j \rhd_{\Omega_e} \lessdot F_\tau F_{s,z} \gtrdot_{z_e^k} + C_{45} \lhd N_{i,y} N_j \rhd_{\Omega_e} \lessdot F_\tau F_{s,z} \gtrdot_{z_e^k} + C_{13} \lhd N_i N_{j,x} \rhd_{\Omega_e} \lessdot F_{\tau,z} F_s \gtrdot_{z_e^k} + \\
&\quad + C_{36} \lhd N_i N_{j,y} \rhd_{\Omega_e} \lessdot F_{\tau,z} F_s \gtrdot_{z_e^k}; \\
K_{12} &= C_{45} \lhd N_i N_j \rhd_{\Omega_e} \lessdot F_{\tau,z} F_{s,x} \gtrdot_{z_e^k} + C_{16} \lhd N_{i,x} N_{j,x} \rhd_{\Omega_e} \lessdot F_\tau F_s \gtrdot_{z_e^k} + C_{66} \lhd N_{i,y} N_{j,x} \rhd_{\Omega_e} \lessdot F_\tau F_s \gtrdot_{z_e^k} + \\
&\quad + C_{12} \lhd N_{i,x} N_{j,y} \rhd_{\Omega_e} \lessdot F_\tau F_s \gtrdot_{z_e^k} + C_{26} \lhd N_{i,y} N_{j,y} \rhd_{\Omega_e} \lessdot F_\tau F_s \gtrdot_{z_e^k}; \\
K_{22} &= C_{44} \lhd N_i N_j \rhd_{\Omega_e} \lessdot F_{\tau,z} F_{s,z} \gtrdot_{z_e^k} + C_{66} \lhd N_{i,x} N_{j,x} \rhd_{\Omega_e} \lessdot F_\tau F_s \gtrdot_{z_e^k} + C_{26} \lhd N_{i,y} N_{j,x} \rhd_{\Omega_e} \lessdot F_\tau F_s \gtrdot_{z_e^k} + \\
&\quad + C_{26} \lhd N_{i,x} N_{j,y} \rhd_{\Omega_e} \lessdot F_\tau F_s \gtrdot_{z_e^k} + C_{22} \lhd N_{i,y} N_{j,y} \rhd_{\Omega_e} \lessdot F_\tau F_s \gtrdot_{z_e^k}; \\
K_{32} &= C_{45} \lhd N_{i,x} N_j \rhd_{\Omega_e} \lessdot F_\tau F_{s,z} \gtrdot_{z_e^k} + C_{44} \lhd N_{i,y} N_j \rhd_{\Omega_e} \lessdot F_\tau F_{s,z} \gtrdot_{z_e^k} + C_{36} \lhd N_i N_{j,x} \rhd_{\Omega_e} \lessdot F_{\tau,z} F_s \gtrdot_{z_e^k} + \\
&\quad + C_{23} \lhd N_i N_{j,y} \rhd_{\Omega_e} \lessdot F_{\tau,z} F_s \gtrdot_{z_e^k}; \\
K_{13} &= C_{13} \lhd N_{i,x} N_j \rhd_{\Omega_e} \lessdot F_\tau F_{s,z} \gtrdot_{z_e^k} + C_{36} \lhd N_{i,y} N_j \rhd_{\Omega_e} \lessdot F_\tau F_{s,z} \gtrdot_{z_e^k} + C_{55} \lhd N_i N_{j,x} \rhd_{\Omega_e} \lessdot F_{\tau,z} F_s \gtrdot_{z_e^k} + \\
&\quad + C_{45} \lhd N_i N_{j,y} \rhd_{\Omega_e} \lessdot F_{\tau,z} F_s \gtrdot_{z_e^k}; \\
K_{23} &= C_{36} \lhd N_{i,x} N_j \rhd_{\Omega_e} \lessdot F_\tau F_{s,z} \gtrdot_{z_e^k} + C_{23} \lhd N_{i,y} N_j \rhd_{\Omega_e} \lessdot F_\tau F_{s,z} \gtrdot_{z_e^k} + C_{45} \lhd N_i N_{j,x} \rhd_{\Omega_e} \lessdot F_{\tau,z} F_s \gtrdot_{z_e^k} + \\
&\quad + C_{44} \lhd N_i N_{j,y} \rhd_{\Omega_e} \lessdot F_{\tau,z} F_s \gtrdot_{z_e^k}; \\
K_{33} &= C_{33} \lhd N_i N_j \rhd_{\Omega_e} \lessdot F_{\tau,z} F_{s,z} \gtrdot_{z_e^k} + C_{55} \lhd N_{i,x} N_{j,x} \rhd_{\Omega_e} \lessdot F_\tau F_s \gtrdot_{z_e^k} + C_{45} \lhd N_{i,y} N_{j,x} \rhd_{\Omega_e} \lessdot F_\tau F_s \gtrdot_{z_e^k} + \\
&\quad + C_{45} \lhd N_{i,x} N_{j,y} \rhd_{\Omega_e} \lessdot F_\tau F_s \gtrdot_{z_e^k} + C_{44} \lhd N_{i,y} N_{j,y} \rhd_{\Omega_e} \lessdot F_\tau F_s \gtrdot_{z_e^k};
\end{aligned}$$

Subscripts after a comma indicate derivatives,

$$\lhd ... \rhd_{\Omega_e} = \int_{\Omega_{element}} (...)\, d\Omega_{element} \qquad \text{and} \qquad \lessdot ... \gtrdot_{z_e^k} = \int_{k^{th\,layer}} (...) dz_{k^{th\,layer}}.$$

Non-zero elements of the mass fundamental nucleus $\boldsymbol{M}^{\tau sij}$ are:

$$M_{11} = M_{22} = M_{33} = \rho \lhd N_i N_j \rhd_{\Omega_e} \lessdot F_\tau F_s \gtrdot_{z_e^k}.$$

4.3.2 Fundamental nuclei for PVD-u_x,u_y,u_z,θ

The stiffness fundamental nucleus $\boldsymbol{K}^{k\tau sij}$ related to the PVD thermo-mechanical application PVD-u_x,u_y,u_z,θ is listed below. In the following, the layer-superscript k is always implied to simplify equations.
The stiffness fundamental nucleus is:

$$\boldsymbol{K}^{\tau sij} = \begin{bmatrix} K_{11} & K_{12} & K_{13} & K_{14} \\ K_{21} & K_{22} & K_{23} & K_{24} \\ K_{31} & K_{32} & K_{33} & K_{34} \\ K_{41} & K_{42} & K_{43} & K_{44} \end{bmatrix}. \tag{4.12}$$

Its elements are:

$$\begin{aligned}
K_{11} &= C_{55} \lhd N_i N_j \rhd_{\Omega_e} \lessdot F_{\tau,z} F_{s,z} \gtrdot_{z_e^k} + C_{11} \lhd N_{i,x} N_{j,x} \rhd_{\Omega_e} \lessdot F_\tau F_s \gtrdot_{z_e^k} + C_{16} \lhd N_{i,y} N_{j,x} \rhd_{\Omega_e} \lessdot F_\tau F_s \gtrdot_{z_e^k} + \\
&\quad + C_{16} \lhd N_{i,x} N_{j,y} \rhd_{\Omega_e} \lessdot F_\tau F_s \gtrdot_{z_e^k} + C_{66} \lhd N_{i,y} N_{j,y} \rhd_{\Omega_e} \lessdot F_\tau F_s \gtrdot_{z_e^k}; \\
K_{21} &= C_{45} \lhd N_i N_j \rhd_{\Omega_e} \lessdot F_{\tau,z} F_{s,z} \gtrdot_{z_e^k} + C_{16} \lhd N_{i,x} N_{j,x} \rhd_{\Omega_e} \lessdot F_\tau F_s \gtrdot_{z_e^k} + C_{12} \lhd N_{i,y} N_{j,x} \rhd_{\Omega_e} \lessdot F_\tau F_s \gtrdot_{z_e^k} + \\
&\quad + C_{66} \lhd N_{i,x} N_{j,y} \rhd_{\Omega_e} \lessdot F_\tau F_s \gtrdot_{z_e^k} + C_{26} \lhd N_{i,y} N_{j,y} \rhd_{\Omega_e} \lessdot F_\tau F_s \gtrdot_{z_e^k}; \\
K_{31} &= C_{55} \lhd N_{i,x} N_j \rhd_{\Omega_e} \lessdot F_\tau F_{s,z} \gtrdot_{z_e^k} + C_{45} \lhd N_{i,y} N_j \rhd_{\Omega_e} \lessdot F_\tau F_{s,z} \gtrdot_{z_e^k} + C_{13} \lhd N_i N_{j,x} \rhd_{\Omega_e} \lessdot F_{\tau,z} F_s \gtrdot_{z_e^k} + \\
&\quad + C_{36} \lhd N_i N_{j,y} \rhd_{\Omega_e} \lessdot F_{\tau,z} F_s \gtrdot_{z_e^k}; \\
K_{41} &= -\lambda_1 \lhd N_i N_{j,x} \rhd_{\Omega_e} \lessdot F_\tau F_s \gtrdot_{z_e^k} - \lambda_6 \lhd N_i N_{j,y} \rhd_{\Omega_e} \lessdot F_\tau F_s \gtrdot_{z_e^k}; \\
K_{12} &= C_{45} \lhd N_i N_j \rhd_{\Omega_e} \lessdot F_{\tau,z} F_{s,x} \gtrdot_{z_e^k} + C_{16} \lhd N_{i,x} N_{j,x} \rhd_{\Omega_e} \lessdot F_\tau F_s \gtrdot_{z_e^k} + C_{66} \lhd N_{i,y} N_{j,x} \rhd_{\Omega_e} \lessdot F_\tau F_s \gtrdot_{z_e^k} + \\
&\quad + C_{12} \lhd N_{i,x} N_{j,y} \rhd_{\Omega_e} \lessdot F_\tau F_s \gtrdot_{z_e^k} + C_{26} \lhd N_{i,y} N_{j,y} \rhd_{\Omega_e} \lessdot F_\tau F_s \gtrdot_{z_e^k}; \\
K_{22} &= C_{44} \lhd N_i N_j \rhd_{\Omega_e} \lessdot F_{\tau,z} F_{s,z} \gtrdot_{z_e^k} + C_{66} \lhd N_{i,x} N_{j,x} \rhd_{\Omega_e} \lessdot F_\tau F_s \gtrdot_{z_e^k} + C_{26} \lhd N_{i,y} N_{j,x} \rhd_{\Omega_e} \lessdot F_\tau F_s \gtrdot_{z_e^k} + \\
&\quad + C_{26} \lhd N_{i,x} N_{j,y} \rhd_{\Omega_e} \lessdot F_\tau F_s \gtrdot_{z_e^k} + C_{22} \lhd N_{i,y} N_{j,y} \rhd_{\Omega_e} \lessdot F_\tau F_s \gtrdot_{z_e^k}; \\
K_{32} &= C_{45} \lhd N_{i,x} N_j \rhd_{\Omega_e} \lessdot F_\tau F_{s,z} \gtrdot_{z_e^k} + C_{44} \lhd N_{i,y} N_j \rhd_{\Omega_e} \lessdot F_\tau F_{s,z} \gtrdot_{z_e^k} + C_{36} \lhd N_i N_{j,x} \rhd_{\Omega_e} \lessdot F_{\tau,z} F_s \gtrdot_{z_e^k} + \\
&\quad + C_{23} \lhd N_i N_{j,y} \rhd_{\Omega_e} \lessdot F_{\tau,z} F_s \gtrdot_{z_e^k}; \\
K_{42} &= -\lambda_6 \lhd N_i N_{j,x} \rhd_{\Omega_e} \lessdot F_\tau F_s \gtrdot_{z_e^k} - \lambda_2 \lhd N_i N_{j,y} \rhd_{\Omega_e} \lessdot F_\tau F_s \gtrdot_{z_e^k}; \\
K_{13} &= C_{13} \lhd N_{i,x} N_j \rhd_{\Omega_e} \lessdot F_\tau F_{s,z} \gtrdot_{z_e^k} + C_{36} \lhd N_{i,y} N_j \rhd_{\Omega_e} \lessdot F_\tau F_{s,z} \gtrdot_{z_e^k} + C_{55} \lhd N_i N_{j,x} \rhd_{\Omega_e} \lessdot F_{\tau,z} F_s \gtrdot_{z_e^k} + \\
&\quad + C_{45} \lhd N_i N_{j,y} \rhd_{\Omega_e} \lessdot F_{\tau,z} F_s \gtrdot_{z_e^k}; \\
K_{23} &= C_{36} \lhd N_{i,x} N_j \rhd_{\Omega_e} \lessdot F_\tau F_{s,z} \gtrdot_{z_e^k} + C_{23} \lhd N_{i,y} N_j \rhd_{\Omega_e} \lessdot F_\tau F_{s,z} \gtrdot_{z_e^k} + C_{45} \lhd N_i N_{j,x} \rhd_{\Omega_e} \lessdot F_{\tau,z} F_s \gtrdot_{z_e^k} + \\
&\quad + C_{44} \lhd N_i N_{j,y} \rhd_{\Omega_e} \lessdot F_{\tau,z} F_s \gtrdot_{z_e^k}; \\
K_{33} &= C_{33} \lhd N_i N_j \rhd_{\Omega_e} \lessdot F_{\tau,z} F_{s,z} \gtrdot_{z_e^k} + C_{55} \lhd N_{i,x} N_{j,x} \rhd_{\Omega_e} \lessdot F_\tau F_s \gtrdot_{z_e^k} + C_{45} \lhd N_{i,y} N_{j,x} \rhd_{\Omega_e} \lessdot F_\tau F_s \gtrdot_{z_e^k} + \\
&\quad + C_{45} \lhd N_{i,x} N_{j,y} \rhd_{\Omega_e} \lessdot F_\tau F_s \gtrdot_{z_e^k} + C_{44} \lhd N_{i,y} N_{j,y} \rhd_{\Omega_e} \lessdot F_\tau F_s \gtrdot_{z_e^k}; \\
K_{43} &= -\lambda_3 \lhd N_i N_j \rhd_{\Omega_e} \lessdot F_\tau F_{s,z} \gtrdot_{z_e^k}; \\
K_{14} &= -\lambda_1 \lhd N_{i,x} N_j \rhd_{\Omega_e} \lessdot F_\tau F_s \gtrdot_{z_e^k} - \lambda_6 \lhd N_{i,y} N_j \rhd_{\Omega_e} \lessdot F_\tau F_s \gtrdot_{z_e^k}; \\
K_{24} &= -\lambda_6 \lhd N_{i,x} N_j \rhd_{\Omega_e} \lessdot F_\tau F_s \gtrdot_{z_e^k} - \lambda_2 \lhd N_{i,y} N_j \rhd_{\Omega_e} \lessdot F_\tau F_s \gtrdot_{z_e^k}; \\
K_{34} &= -\lambda_3 \lhd N_i N_j \rhd_{\Omega_e} \lessdot F_{\tau,z} F_s \gtrdot_{z_e^k};
\end{aligned}$$

$$K_{44} = -\frac{\rho C \lhd N_i N_j \rhd_{\Omega_e} \lessdot F_\tau F_s \gtrdot_{z_e^k}}{\theta_{ref}}.$$

Non-zero elements of the mass fundamental nucleus $\boldsymbol{M}^{\tau sij}$ are:

$$M_{11} = M_{22} = M_{33} = \rho \lhd N_i N_j \rhd_{\Omega_e} \lessdot F_\tau F_s \gtrdot_{z_e^k}.$$

The fundamental nuclei showed above permits to calculate the instantaneous mechanical deformation and the temperature profile in the plate, when a mechanical/thermal loading is applied. The stiffness variation due to the thermo-mechanical coupling interactions is considered, while heat conduction and transient effects are not taken into account. In other word, the solution is the one valid at the initial time $t = 0$.
If a thermal loading is considered and the steady-state temperature profile is required, the cell K_{44} of $\boldsymbol{K}^{\tau sij}$ should be modified as in the following:

$$K_{44} = -k_{33} \lhd N_i N_j \rhd_{\Omega_e} \lessdot F_{\tau,z} F_{s,z} \gtrdot_{z_e^k} - k_{22} \lhd N_{i,y} N_{j,y} \rhd_{\Omega_e} \lessdot F_\tau F_s \gtrdot_{z_e^k} - k_{11} \lhd N_{i,x} N_{j,x} \rhd_{\Omega_e} \lessdot F_\tau F_s \gtrdot_{z_e^k}.$$

4.3.3 Fundamental nuclei for RMVT-u_x,u_y,u_z,$\phi(D_z)$

The stiffness fundamental nucleus $\boldsymbol{K}^{k\tau sij}$ related to the RMVT-u_x,u_y,u_z,$\phi(D_z)$ application is listed below. The explicit form of constitutive coefficients can be found in Sec. 3.4.1. In the following, the layer-superscript k is always implied to simplify equations.
The stiffness fundamental nucleus is:

$$\boldsymbol{K}^{\tau sij} = \begin{bmatrix} K_{11} & K_{12} & K_{13} & K_{14} & K_{15} \\ K_{21} & K_{22} & K_{23} & K_{24} & K_{25} \\ K_{31} & K_{32} & K_{33} & K_{34} & K_{35} \\ K_{41} & K_{42} & K_{43} & K_{44} & K_{45} \\ K_{51} & K_{52} & K_{53} & K_{54} & K_{55} \end{bmatrix}. \tag{4.13}$$

Its elements are:

$$\begin{aligned}
K_{11} &= \widetilde{\boldsymbol{H}}_{aa}(7,7) \triangleleft N_i N_j \triangleright_{\Omega_e} \lessdot F_{\tau,z} F_{s,z} \gtrdot_{z_e^k} + \widetilde{\boldsymbol{H}}_{aa}(1,1) \triangleleft N_{i,x} N_{j,x} \triangleright_{\Omega_e} \lessdot F_\tau F_s \gtrdot_{z_e^k} + \\
&+ \widetilde{\boldsymbol{H}}_{aa}(3,1) \triangleleft N_{i,y} N_{j,x} \triangleright_{\Omega_e} \lessdot F_\tau F_s \gtrdot_{z_e^k} + \widetilde{\boldsymbol{H}}_{aa}(1,3) \triangleleft N_{i,x} N_{j,y} \triangleright_{\Omega_e} \lessdot F_\tau F_s \gtrdot_{z_e^k} + \\
&+ \widetilde{\boldsymbol{H}}_{aa}(3,3) \triangleleft N_{i,y} N_{j,y} \triangleright_{\Omega_e} \lessdot F_\tau F_s \gtrdot_{z_e^k}; \\
K_{21} &= \widetilde{\boldsymbol{H}}_{aa}(8,7) \triangleleft N_i N_j \triangleright_{\Omega_e} \lessdot F_{\tau,z} F_{s,z} \gtrdot_{z_e^k} + \widetilde{\boldsymbol{H}}_{aa}(3,1) \triangleleft N_{i,x} N_{j,x} \triangleright_{\Omega_e} \lessdot F_\tau F_s \gtrdot_{z_e^k} + \\
&+ \widetilde{\boldsymbol{H}}_{aa}(2,1) \triangleleft N_{i,y} N_{j,x} \triangleright_{\Omega_e} \lessdot F_\tau F_s \gtrdot_{z_e^k} + \widetilde{\boldsymbol{H}}_{aa}(3,3) \triangleleft N_{i,x} N_{j,y} \triangleright_{\Omega_e} \lessdot F_\tau F_s \gtrdot_{z_e^k} + \\
&+ \widetilde{\boldsymbol{H}}_{aa}(2,3) \triangleleft N_{i,y} N_{j,y} \triangleright_{\Omega_e} \lessdot F_\tau F_s \gtrdot_{z_e^k}; \\
K_{31} &= \widetilde{\boldsymbol{H}}_{aa}(7,7) \triangleleft N_{i,x} N_j \triangleright_{\Omega_e} \lessdot F_\tau F_{s,z} \gtrdot_{z_e^k} + \widetilde{\boldsymbol{H}}_{aa}(8,7) \triangleleft N_{i,y} N_j \triangleright_{\Omega_e} \lessdot F_\tau F_{s,z} \gtrdot_{z_e^k} + \\
&+ \widetilde{\boldsymbol{H}}_{aa}(6,1) \triangleleft N_i N_{j,x} \triangleright_{\Omega_e} \lessdot F_{\tau,z} F_s \gtrdot_{z_e^k} + \widetilde{\boldsymbol{H}}_{aa}(6,3) \triangleleft N_i N_{j,y} \triangleright_{\Omega_e} \lessdot F_{\tau,z} F_s \gtrdot_{z_e^k}; \\
K_{41} &= -\widetilde{\boldsymbol{H}}_{aa}(4,7) \triangleleft N_{i,x} N_j \triangleright_{\Omega_e} \lessdot F_\tau F_{s,z} \gtrdot_{z_e^k} - \widetilde{\boldsymbol{H}}_{aa}(5,7) \triangleleft N_{i,y} N_j \triangleright_{\Omega_e} \lessdot F_\tau F_{s,z} \gtrdot_{z_e^k}; \\
K_{51} &= \widetilde{\boldsymbol{H}}_{ba}(1,1) \triangleleft N_i N_{j,x} \triangleright_{\Omega_e} \lessdot F_\tau F_s \gtrdot_{z_e^k} + \widetilde{\boldsymbol{H}}_{ba}(1,3) \triangleleft N_i N_{j,y} \triangleright_{\Omega_e} \lessdot F_\tau F_s \gtrdot_{z_e^k}; \\
K_{12} &= \widetilde{\boldsymbol{H}}_{aa}(7,8) \triangleleft N_i N_j \triangleright_{\Omega_e} \lessdot F_{\tau,z} F_{s,z} \gtrdot_{z_e^k} + \widetilde{\boldsymbol{H}}_{aa}(1,3) \triangleleft N_{i,x} N_{j,x} \triangleright_{\Omega_e} \lessdot F_\tau F_s \gtrdot_{z_e^k} + \\
&+ \widetilde{\boldsymbol{H}}_{aa}(3,3) \triangleleft N_{i,y} N_{j,x} \triangleright_{\Omega_e} \lessdot F_\tau F_s \gtrdot_{z_e^k} + \widetilde{\boldsymbol{H}}_{aa}(1,2) \triangleleft N_{i,x} N_{j,y} \triangleright_{\Omega_e} \lessdot F_\tau F_s \gtrdot_{z_e^k} + \\
&+ \widetilde{\boldsymbol{H}}_{aa}(3,2) \triangleleft N_{i,y} N_{j,y} \triangleright_{\Omega_e} \lessdot F_\tau F_s \gtrdot_{z_e^k}; \\
K_{22} &= \widetilde{\boldsymbol{H}}_{aa}(8,8) \triangleleft N_i N_j \triangleright_{\Omega_e} \lessdot F_{\tau,z} F_{s,z} \gtrdot_{z_e^k} + \widetilde{\boldsymbol{H}}_{aa}(3,3) \triangleleft N_{i,x} N_{j,x} \triangleright_{\Omega_e} \lessdot F_\tau F_s \gtrdot_{z_e^k} + \\
&+ \widetilde{\boldsymbol{H}}_{aa}(2,3) \triangleleft N_{i,y} N_{j,x} \triangleright_{\Omega_e} \lessdot F_\tau F_s \gtrdot_{z_e^k} + \widetilde{\boldsymbol{H}}_{aa}(3,2) \triangleleft N_{i,x} N_{j,y} \triangleright_{\Omega_e} \lessdot F_\tau F_s \gtrdot_{z_e^k} + \\
&+ \widetilde{\boldsymbol{H}}_{aa}(2,2) \triangleleft N_{i,y} N_{j,y} \triangleright_{\Omega_e} \lessdot F_\tau F_s \gtrdot_{z_e^k}; \\
K_{32} &= \widetilde{\boldsymbol{H}}_{aa}(7,8) \triangleleft N_{i,x} N_j \triangleright_{\Omega_e} \lessdot F_\tau F_{s,z} \gtrdot_{z_e^k} + \widetilde{\boldsymbol{H}}_{aa}(8,8) \triangleleft N_{i,y} N_j \triangleright_{\Omega_e} \lessdot F_\tau F_{s,z} \gtrdot_{z_e^k} + \\
&+ \widetilde{\boldsymbol{H}}_{aa}(6,3) \triangleleft N_i N_{j,x} \triangleright_{\Omega_e} \lessdot F_{\tau,z} F_s \gtrdot_{z_e^k} + \widetilde{\boldsymbol{H}}_{aa}(6,2) \triangleleft N_i N_{j,y} \triangleright_{\Omega_e} \lessdot F_{\tau,z} F_s \gtrdot_{z_e^k}; \\
K_{42} &= -\widetilde{\boldsymbol{H}}_{aa}(4,8) \triangleleft N_{i,x} N_j \triangleright_{\Omega_e} \lessdot F_\tau F_{s,z} \gtrdot_{z_e^k} - \widetilde{\boldsymbol{H}}_{aa}(5,8) \triangleleft N_{i,y} N_j \triangleright_{\Omega_e} \lessdot F_\tau F_{s,z} \gtrdot_{z_e^k}; \\
K_{52} &= \widetilde{\boldsymbol{H}}_{ba}(1,3) \triangleleft N_i N_{j,x} \triangleright_{\Omega_e} \lessdot F_\tau F_s \gtrdot_{z_e^k} + \widetilde{\boldsymbol{H}}_{ba}(1,2) \triangleleft N_i N_{j,y} \triangleright_{\Omega_e} \lessdot F_\tau F_s \gtrdot_{z_e^k}; \\
K_{13} &= \widetilde{\boldsymbol{H}}_{aa}(1,6) \triangleleft N_{i,x} N_j \triangleright_{\Omega_e} \lessdot F_\tau F_{s,z} \gtrdot_{z_e^k} + \widetilde{\boldsymbol{H}}_{aa}(3,6) \triangleleft N_{i,y} N_j \triangleright_{\Omega_e} \lessdot F_\tau F_{s,z} \gtrdot_{z_e^k} + \\
&+ \widetilde{\boldsymbol{H}}_{aa}(7,7) \triangleleft N_i N_{j,x} \triangleright_{\Omega_e} \lessdot F_{\tau,z} F_s \gtrdot_{z_e^k} + \widetilde{\boldsymbol{H}}_{aa}(7,8) \triangleleft N_i N_{j,y} \triangleright_{\Omega_e} \lessdot F_{\tau,z} F_s \gtrdot_{z_e^k};
\end{aligned}$$

$$K_{23} = \widetilde{\boldsymbol{H}}_{aa}(3,6) \lhd N_{i,x}N_j \rhd_{\Omega_e} \lessdot F_\tau F_{s,z} \gtrdot_{z_e^k} + \widetilde{\boldsymbol{H}}_{aa}(2,6) \lhd N_{i,y}N_j \rhd_{\Omega_e} \lessdot F_\tau F_{s,z} \gtrdot_{z_e^k} +$$
$$+ \widetilde{\boldsymbol{H}}_{aa}(8,7) \lhd N_i N_{j,x} \rhd_{\Omega_e} \lessdot F_{\tau,z} F_s \gtrdot_{z_e^k} + \widetilde{\boldsymbol{H}}_{aa}(8,8) \lhd N_i N_{j,y} \rhd_{\Omega_e} \lessdot F_{\tau,z} F_s \gtrdot_{z_e^k};$$

$$K_{33} = \widetilde{\boldsymbol{H}}_{aa}(6,6) \lhd N_i N_j \rhd_{\Omega_e} \lessdot F_{\tau,z} F_{s,z} \gtrdot_{z_e^k} + \widetilde{\boldsymbol{H}}_{aa}(7,7) \lhd N_{i,x}N_{j,x} \rhd_{\Omega_e} \lessdot F_\tau F_s \gtrdot_{z_e^k} +$$
$$+ \widetilde{\boldsymbol{H}}_{aa}(8,7) \lhd N_{i,y}N_{j,x} \rhd_{\Omega_e} F_\tau F_s + \widetilde{\boldsymbol{H}}_{aa}(7,8) \lhd N_{i,x}N_{j,y} \rhd_{\Omega_e} \lessdot F_\tau F_s \gtrdot_{z_e^k} +$$
$$+ \widetilde{\boldsymbol{H}}_{aa}(8,8) \lhd N_{i,y}N_{j,y} \rhd_{\Omega_e} \lessdot F_\tau F_s \gtrdot_{z_e^k};$$

$$K_{43} = -\widetilde{\boldsymbol{H}}_{aa}(4,7) \lhd N_{i,x}N_{j,x} \rhd_{\Omega_e} \lessdot F_\tau F_s \gtrdot_{z_e^k} - \widetilde{\boldsymbol{H}}_{aa}(5,7) \lhd N_{i,y}N_{j,x} \rhd_{\Omega_e} \lessdot F_\tau F_s \gtrdot_{z_e^k} +$$
$$- \widetilde{\boldsymbol{H}}_{aa}(4,8) \lhd N_{i,x}N_{j,y} \rhd_{\Omega_e} \lessdot F_\tau F_s \gtrdot_{z_e^k} - \widetilde{\boldsymbol{H}}_{aa}(5,8) \lhd N_{i,y}N_{j,y} \rhd_{\Omega_e} \lessdot F_\tau F_s \gtrdot_{z_e^k};$$

$$K_{53} = \widetilde{\boldsymbol{H}}_{ba}(1,6) \lhd N_i N_j \rhd_{\Omega_e} \lessdot F_\tau F_{s,z} \gtrdot_{z_e^k};$$

$$K_{14} = -\widetilde{\boldsymbol{H}}_{aa}(7,4) \lhd N_i N_{j,x} \rhd_{\Omega_e} \lessdot F_{\tau,z} F_s \gtrdot_{z_e^k} - \widetilde{\boldsymbol{H}}_{aa}(7,5) \lhd N_i N_{j,y} \rhd_{\Omega_e} \lessdot F_{\tau,z} F_s \gtrdot_{z_e^k};$$

$$K_{24} = -\widetilde{\boldsymbol{H}}_{aa}(8,4) \lhd N_i N_{j,x} \rhd_{\Omega_e} \lessdot F_{\tau,z} F_s \gtrdot_{z_e^k} - \widetilde{\boldsymbol{H}}_{aa}(8,5) \lhd N_i N_{j,y} \rhd_{\Omega_e} \lessdot F_{\tau,z} F_s \gtrdot_{z_e^k};$$

$$K_{34} = -\widetilde{\boldsymbol{H}}_{aa}(7,4) \lhd N_{i,x}N_{j,x} \rhd_{\Omega_e} \lessdot F_\tau F_s \gtrdot_{z_e^k} - \widetilde{\boldsymbol{H}}_{aa}(8,4) \lhd N_{i,y}N_{j,x} \rhd_{\Omega_e} \lessdot F_\tau F_s \gtrdot_{z_e^k} +$$
$$- \widetilde{\boldsymbol{H}}_{aa}(7,5) \lhd N_{i,x}N_{j,y} \rhd_{\Omega_e} \lessdot F_\tau F_s \gtrdot_{z_e^k} - \widetilde{\boldsymbol{H}}_{aa}(8,5) \lhd N_{i,y}N_{j,y} \rhd_{\Omega_e} \lessdot F_\tau F_s \gtrdot_{z_e^k};$$

$$K_{44} = \widetilde{\boldsymbol{H}}_{aa}(4,4) \lhd N_{i,x}N_{j,x} \rhd_{\Omega_e} \lessdot F_\tau F_s \gtrdot_{z_e^k} + \widetilde{\boldsymbol{H}}_{aa}(5,4) \lhd N_{i,y}N_{j,x} \rhd_{\Omega_e} \lessdot F_\tau F_s \gtrdot_{z_e^k} +$$
$$+ \widetilde{\boldsymbol{H}}_{aa}(4,5) \lhd N_{i,x}N_{j,y} \rhd_{\Omega_e} \lessdot F_\tau F_s \gtrdot_{z_e^k} + \widetilde{\boldsymbol{H}}_{aa}(5,5) \lhd N_{i,y}N_{j,y} \rhd_{\Omega_e} \lessdot F_\tau F_s \gtrdot_{z_e^k};$$

$$K_{54} = \lhd N_i N_j \rhd_{\Omega_e} \lessdot F_\tau F_{s,z} \gtrdot_{z_e^k};$$

$$K_{15} = -\widetilde{\boldsymbol{H}}_{ab}(1,1) \lhd N_{i,x}N_j \rhd_{\Omega_e} \lessdot F_\tau F_s \gtrdot_{z_e^k} - \widetilde{\boldsymbol{H}}_{ab}(3,1) \lhd N_{i,y}N_j \rhd_{\Omega_e} \lessdot F_\tau F_s \gtrdot_{z_e^k};$$

$$K_{25} = -\widetilde{\boldsymbol{H}}_{ab}(3,1) \lhd N_{i,x}N_j \rhd_{\Omega_e} \lessdot F_\tau F_s \gtrdot_{z_e^k} - \widetilde{\boldsymbol{H}}_{ab}(2,1) \lhd N_{i,y}N_j \rhd_{\Omega_e} \lessdot F_\tau F_s \gtrdot_{z_e^k};$$

$$K_{35} = -\widetilde{\boldsymbol{H}}_{ab}(6,1) \lhd N_i N_j \rhd_{\Omega_e} \lessdot F_{\tau,z} F_s \gtrdot_{z_e^k};$$

$$K_{45} = \lhd N_i N_j \rhd_{\Omega_e} \lessdot F_{\tau,z} F_s \gtrdot_{z_e^k};$$

$$K_{55} = -\widetilde{\boldsymbol{H}}_{bb}(1,1) \lhd N_i N_j \rhd_{\Omega_e} \lessdot F_\tau F_s \gtrdot_{z_e^k}.$$

Non-zero elements of the mass fundamental nucleus $\boldsymbol{M}^{\tau sij}$ are:

$$M_{11} = M_{22} = M_{33} = \rho \lhd N_i N_j \rhd_{\Omega_e} \lessdot F_\tau F_s \gtrdot_{z_e^k}.$$

4.3.4 Fundamental nuclei for RMVT-u_x,u_y,u_z,$\phi(\sigma_{zz},\sigma_{xz},\sigma_{yz},D_z)$

The stiffness fundamental nucleus $\boldsymbol{K}^{k\tau sij}$ related to the RMVT-u_x,u_y,u_z,$\phi(\sigma_{zz},\sigma_{xz},\sigma_{yz},D_z)$ application is listed below. The explicit form of constitutive coefficients can be found in Sec. 3.4.2. In the following, the layer-superscript k is always implied to simplify equations.
The stiffness fundamental nucleus is:

$$\boldsymbol{K}^{\tau sij} = \begin{bmatrix} K_{11} & K_{12} & K_{13} & K_{14} & K_{15} & K_{16} & K_{17} & K_{18} \\ K_{21} & K_{22} & K_{23} & K_{24} & K_{25} & K_{26} & K_{27} & K_{28} \\ K_{31} & K_{32} & K_{33} & K_{34} & K_{35} & K_{36} & K_{37} & K_{38} \\ K_{41} & K_{42} & K_{43} & K_{44} & K_{45} & K_{46} & K_{47} & K_{48} \\ K_{51} & K_{52} & K_{53} & K_{54} & K_{55} & K_{56} & K_{57} & K_{58} \\ K_{61} & K_{62} & K_{63} & K_{64} & K_{65} & K_{66} & K_{67} & K_{68} \\ K_{71} & K_{72} & K_{73} & K_{74} & K_{75} & K_{76} & K_{77} & K_{78} \\ K_{81} & K_{82} & K_{83} & K_{84} & K_{85} & K_{86} & K_{87} & K_{88} \end{bmatrix}. \tag{4.14}$$

Its elements are:

$$\begin{aligned} K_{11} &= \ll F_s F_\tau \gg_{z_e^k} \widetilde{\boldsymbol{H}}_{\mathrm{aa}11} \lhd N_{i,x} N_{j,x} \rhd_{\Omega_e} + \ll F_s F_\tau \gg_{z_e^k} \widetilde{\boldsymbol{H}}_{\mathrm{aa}31} \lhd N_{i,y} N_{j,x} \rhd_{\Omega_e} + \\ &+ \ll F_s F_\tau \gg_{z_e^k} \widetilde{\boldsymbol{H}}_{\mathrm{aa}13} \lhd N_{i,x} N_{j,y} \rhd_{\Omega_e} + \ll F_s F_\tau \gg_{z_e^k} \widetilde{\boldsymbol{H}}_{\mathrm{aa}33} \lhd N_{i,y} N_{j,y} \rhd_{\Omega_e}; \\ K_{21} &= \ll F_s F_\tau \gg_{z_e^k} \widetilde{\boldsymbol{H}}_{\mathrm{aa}31} \lhd N_{i,x} N_{j,x} \rhd_{\Omega_e} + \ll F_s F_\tau \gg_{z_e^k} \widetilde{\boldsymbol{H}}_{\mathrm{aa}21} \lhd N_{i,y} N_{j,x} \rhd_{\Omega_e} + \\ &+ \ll F_s F_\tau \gg_{z_e^k} \widetilde{\boldsymbol{H}}_{\mathrm{aa}33} \lhd N_{i,x} N_{j,y} \rhd_{\Omega_e} + \ll F_s F_\tau \gg_{z_e^k} \widetilde{\boldsymbol{H}}_{\mathrm{aa}23} \lhd N_{i,y} N_{j,y} \rhd_{\Omega_e}; \\ K_{31} &= 0; \\ K_{41} &= 0; \\ K_{51} &= - \ll F_s F_\tau \gg_{z_e^k} \lhd N_i N_{j,x} \rhd_{\Omega_e} \widetilde{\boldsymbol{H}}_{\mathrm{ba}11} - \ll F_s F_\tau \gg_{z_e^k} \lhd N_i N_{j,y} \rhd_{\Omega_e} \widetilde{\boldsymbol{H}}_{\mathrm{ba}13}; \\ K_{61} &= \ll F_\tau F_{s,z} \gg_{z_e^k} \lhd N_i N_j \rhd_{\Omega_e}; \\ K_{71} &= 0 \\ K_{81} &= \ll F_s F_\tau \gg_{z_e^k} \lhd N_i N_{j,x} \rhd_{\Omega_e} \widetilde{\boldsymbol{H}}_{\mathrm{ba}41} + \ll F_s F_\tau \gg_{z_e^k} \lhd N_i N_{j,y} \rhd_{\Omega_e} \widetilde{\boldsymbol{H}}_{\mathrm{ba}43}; \\ K_{12} &= \ll F_s F_\tau \gg_{z_e^k} \widetilde{\boldsymbol{H}}_{\mathrm{aa}13} \lhd N_{i,x} N_{j,x} \rhd_{\Omega_e} + \ll F_s F_\tau \gg_{z_e^k} \widetilde{\boldsymbol{H}}_{\mathrm{aa}33} \lhd N_{i,y} N_{j,x} \rhd_{\Omega_e} + \\ &+ \ll F_s F_\tau \gg_{z_e^k} \widetilde{\boldsymbol{H}}_{\mathrm{aa}12} \lhd N_{i,x} N_{j,y} \rhd_{\Omega_e} + \ll F_s F_\tau \gg_{z_e^k} \widetilde{\boldsymbol{H}}_{\mathrm{aa}32} \lhd N_{i,y} N_{j,y} \rhd_{\Omega_e}; \\ K_{22} &= \ll F_s F_\tau \gg_{z_e^k} \widetilde{\boldsymbol{H}}_{\mathrm{aa}33} \lhd N_{i,x} N_{j,x} \rhd_{\Omega_e} + \ll F_s F_\tau \gg_{z_e^k} \widetilde{\boldsymbol{H}}_{\mathrm{aa}23} \lhd N_{i,y} N_{j,x} \rhd_{\Omega_e} + \\ &+ \ll F_s F_\tau \gg_{z_e^k} \widetilde{\boldsymbol{H}}_{\mathrm{aa}32} \lhd N_{i,x} N_{j,y} \rhd_{\Omega_e} + \ll F_s F_\tau \gg_{z_e^k} \widetilde{\boldsymbol{H}}_{\mathrm{aa}22} \lhd N_{i,y} N_{j,y} \rhd_{\Omega_e}; \\ K_{32} &= 0; \\ K_{42} &= 0; \\ K_{52} &= - \ll F_s F_\tau \gg_{z_e^k} \lhd N_i N_{j,x} \rhd_{\Omega_e} \widetilde{\boldsymbol{H}}_{\mathrm{ba}13} - \ll F_s F_\tau \gg_{z_e^k} \lhd N_i N_{j,y} \rhd_{\Omega_e} \widetilde{\boldsymbol{H}}_{\mathrm{ba}12}; \\ K_{62} &= 0; \\ K_{72} &= \ll F_\tau F_{s,z} \gg_{z_e^k} \lhd N_i N_j \rhd_{\Omega_e}; \end{aligned}$$

$$K_{82} = \ll F_s F_\tau \gg_{z_e^k} \lhd N_i N_{j,x} \rhd_{\Omega_e} \widetilde{\boldsymbol{H}}_{\mathrm{ba43}} + \ll F_s F_\tau \gg_{z_e^k} \lhd N_i N_{j,y} \rhd_{\Omega_e} \widetilde{\boldsymbol{H}}_{\mathrm{ba42}};$$

$$K_{13} = 0;$$

$$K_{23} = 0;$$

$$K_{33} = 0;$$

$$K_{43} = 0;$$

$$K_{53} = \ll F_{s,z} F_\tau \gg_{z_e^k} \lhd N_i N_j \rhd_{\Omega_e};$$

$$K_{63} = \ll F_s F_\tau \gg_{z_e^k} \lhd N_i N_{j,x} \rhd_{\Omega_e};$$

$$K_{73} = \ll F_s F_\tau \gg_{z_e^k} \lhd N_i N_{j,y} \rhd_{\Omega_e};$$

$$K_{83} = 0;$$

$$K_{14} = 0;$$

$$K_{24} = 0;$$

$$K_{34} = 0;$$

$$K_{44} = \ll F_s F_\tau \gg_{z_e^k} \widetilde{\boldsymbol{H}}_{\mathrm{aa44}} \lhd N_{i,x} N_{j,x} \rhd_{\Omega_e} + \ll F_s F_\tau \gg_{z_e^k} \widetilde{\boldsymbol{H}}_{\mathrm{aa54}} \lhd N_{i,y} N_{j,x} \rhd_{\Omega_e} + \\ + \ll F_s F_\tau \gg_{z_e^k} \widetilde{\boldsymbol{H}}_{\mathrm{aa45}} \lhd N_{i,x} N_{j,y} \rhd_{\Omega_e} + \ll F_s F_\tau \gg_{z_e^k} \widetilde{\boldsymbol{H}}_{\mathrm{aa55}} \lhd N_{i,y} N_{j,y} \rhd_{\Omega_e};$$

$$K_{54} = 0;$$

$$K_{64} = \ll F_s F_\tau \gg_{z_e^k} \lhd N_i N_{j,x} \rhd_{\Omega_e} \widetilde{\boldsymbol{H}}_{\mathrm{ba24}} + \ll F_s F_\tau \gg_{z_e^k} \lhd N_i N_{j,y} \rhd_{\Omega_e} \widetilde{\boldsymbol{H}}_{\mathrm{ba25}};$$

$$K_{74} = \ll F_s F_\tau \gg_{z_e^k} \lhd N_i N_{j,x} \rhd_{\Omega_e} \widetilde{\boldsymbol{H}}_{\mathrm{ba34}} + \ll F_s F_\tau \gg_{z_e^k} \lhd N_i N_{j,y} \rhd_{\Omega_e} \widetilde{\boldsymbol{H}}_{\mathrm{ba35}};$$

$$K_{84} = \ll F_{s,z} F_\tau \gg_{z_e^k} \lhd N_i N_j \rhd_{\Omega_e};$$

$$K_{15} = \ll F_s F_\tau \gg_{z_e^k} \lhd N_j N_{i,x} \rhd_{\Omega_e} \widetilde{\boldsymbol{H}}_{\mathrm{ab11}} + \ll F_s F_\tau \gg_{z_e^k} \lhd N_j N_{i,y} \rhd_{\Omega_e} \widetilde{\boldsymbol{H}}_{\mathrm{ab31}};$$

$$K_{25} = \ll F_s F_\tau \gg_{z_e^k} \lhd N_j N_{i,x} \rhd_{\Omega_e} \widetilde{\boldsymbol{H}}_{\mathrm{ab31}} + \ll F_s F_\tau \gg_{z_e^k} \lhd N_j N_{i,y} \rhd_{\Omega_e} \widetilde{\boldsymbol{H}}_{\mathrm{ab21}};$$

$$K_{35} = \ll F_s F_{\tau,z} \gg_{z_e^k} \lhd N_i N_j \rhd_{\Omega_e};$$

$$K_{45} = 0;$$

$$K_{55} = - \ll F_s F_\tau \gg_{z_e^k} \lhd N_i N_j \rhd_{\Omega_e} \widetilde{\boldsymbol{H}}_{\mathrm{bb11}};$$

$$K_{65} = 0;$$

$$K_{75} = 0;$$

$$K_{85} = \ll F_s F_\tau \gg_{z_e^k} \lhd N_i N_j \rhd_{\Omega_e} \widetilde{\boldsymbol{H}}_{\mathrm{bb41}};$$

$$K_{16} = \ll F_s F_{\tau,z} \gg_{z_e^k} \lhd N_i N_j \rhd_{\Omega_e};$$

$$K_{26} = 0;$$

$$K_{36} = \ll F_s F_\tau \gg_{z_e^k} \lhd N_j N_{i,x} \rhd_{\Omega_e};$$

$$K_{46} = - \lessdot F_s F_\tau \gtrdot_{z_e^k} \lhd N_j N_{i,x} \rhd_{\Omega_e} \widetilde{\boldsymbol{H}}_{\mathrm{ab42}} - \lessdot F_s F_\tau \gtrdot_{z_e^k} \lhd N_j N_{i,y} \rhd_{\Omega_e} \widetilde{\boldsymbol{H}}_{\mathrm{ab52}};$$

$$K_{56} = 0;$$

$$K_{66} = - \lessdot F_s F_\tau \gtrdot_{z_e^k} \lhd N_i N_j \rhd_{\Omega_e} \widetilde{\boldsymbol{H}}_{\mathrm{bb22}};$$

$$K_{76} = - \lessdot F_s F_\tau \gtrdot_{z_e^k} \lhd N_i N_j \rhd_{\Omega_e} \widetilde{\boldsymbol{H}}_{\mathrm{bb32}};$$

$$K_{86} = 0;$$

$$K_{17} = 0;$$

$$K_{27} = \lessdot F_s F_{\tau,z} \gtrdot_{z_e^k} \lhd N_i N_j \rhd_{\Omega_e};$$

$$K_{37} = \lessdot F_s F_\tau \gtrdot_{z_e^k} \lhd N_j N_{i,y} \rhd_{\Omega_e};$$

$$K_{47} = - \lessdot F_s F_\tau \gtrdot_{z_e^k} \lhd N_j N_{i,x} \rhd_{\Omega_e} \widetilde{\boldsymbol{H}}_{\mathrm{ab43}} - \lessdot F_s F_\tau \gtrdot_{z_e^k} \lhd N_j N_{i,y} \rhd_{\Omega_e} \widetilde{\boldsymbol{H}}_{\mathrm{ab53}};$$

$$K_{57} = 0;$$

$$K_{67} = - \lessdot F_s F_\tau \gtrdot_{z_e^k} \lhd N_i N_j \rhd_{\Omega_e} \widetilde{\boldsymbol{H}}_{\mathrm{bb23}};$$

$$K_{77} = - \lessdot F_s F_\tau \gtrdot_{z_e^k} \lhd N_i N_j \rhd_{\Omega_e} \widetilde{\boldsymbol{H}}_{\mathrm{bb33}};$$

$$K_{87} = 0;$$

$$K_{18} = - \lessdot F_s F_\tau \gtrdot_{z_e^k} \lhd N_j N_{i,x} \rhd_{\Omega_e} \widetilde{\boldsymbol{H}}_{\mathrm{ab14}} - \lessdot F_s F_\tau \gtrdot_{z_e^k} \lhd N_j N_{i,y} \rhd_{\Omega_e} \widetilde{\boldsymbol{H}}_{\mathrm{ab34}};$$

$$K_{28} = - \lessdot F_s F_\tau \gtrdot_{z_e^k} \lhd N_j N_{i,x} \rhd_{\Omega_e} \widetilde{\boldsymbol{H}}_{\mathrm{ab34}} - \lessdot F_s F_\tau \gtrdot_{z_e^k} \lhd N_j N_{i,y} \rhd_{\Omega_e} \widetilde{\boldsymbol{H}}_{\mathrm{ab24}};$$

$$K_{38} = 0;$$

$$K_{48} = \lessdot F_s F_{\tau,z} \gtrdot_{z_e^k} \lhd N_i N_j \rhd_{\Omega_e};$$

$$K_{58} = \lessdot F_s F_\tau \gtrdot_{z_e^k} \lhd N_i N_j \rhd_{\Omega_e} \widetilde{\boldsymbol{H}}_{\mathrm{bb14}};$$

$$K_{68} = 0;$$

$$K_{78} = 0;$$

$$K_{88} = - \lessdot F_s F_\tau \gtrdot_{z_e^k} \lhd N_i N_j \rhd_{\Omega_e} \widetilde{\boldsymbol{H}}_{\mathrm{bb44}}.$$

4.4 The buckling fundamental nucleus

Dealing with plates, buckling analysis requires to consider the out-of-plane component of the internal forces parallel to the plate middle surface. Such components, which are different from zero only when the plate middle surface stays in bending configuration, can be imposed in the analysis by introducing the buckling fundamental nucleus $\boldsymbol{K_G}^{k\tau sij}$. Only its third diagonal component $\boldsymbol{K_G}_{33}^{k\tau sij}$ is different from zero:

$$\begin{aligned}\boldsymbol{K_G}_{33}^{k\tau sij} =& \sigma_{xx} \lessdot F_\tau F_s \gtrdot_{z_e^k} \lhd N_{i,x} N_{j,x} \rhd_{\Omega_e} + \sigma_{yy} \lessdot F_\tau F_s \gtrdot_{z_e^k} \lhd N_{i,y} N_{j,y} \rhd_{\Omega_e} + \\ &+ \sigma_{xy} \lessdot F_\tau F_s \gtrdot_{z_e^k} \lhd N_{i,x} N_{j,y} \rhd_{\Omega_e} + \sigma_{yx} \lessdot F_\tau F_s \gtrdot_{z_e^k} \lhd N_{i,y} N_{j,x} \rhd_{\Omega_e} .\end{aligned} \tag{4.15}$$

σ_{xx}, σ_{yy}, and σ_{xy} are the in-plane internal stress. $\boldsymbol{K_G}_{33}^{k\tau sij}$ concerns the out-of-plane buckling of the plate, which occurs largely before the here neglected in-plane buckling. The physical meaning of the right member in Eq. 4.15 is:

$$\lhd \sigma_{yy} u_{z,yy} + \sigma_{xy} u_{z,xy} + \sigma_{yx} u_{z,yx} \rhd_{\Omega_e} , \tag{4.16}$$

This contribution can be obtained writing the equation of equilibrium to the translation along the plate-thickness direction of an infinitesimal rectangular portion of plate in deformed configuration: Fig. 4.2. Note that there is not out-of-plain loading. Without buckling the plate

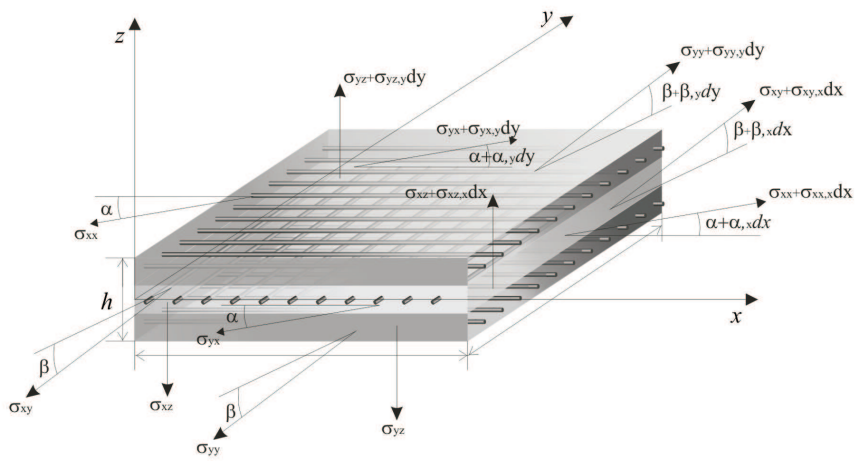

Figure 4.2. Infinitesimal rectangular portion of plate in out-of-plane deformed configuration: internal stresses relevant to write the equilibrium to the translation along the plate-thickness direction

stays in the in-plane configuration ($\alpha = \beta = 0$) and the indefinite equation of equilibrium to the translation along the z-axis is:

$$\sigma_{xz,x} + \sigma_{yz,y} = 0. \tag{4.17}$$

More in general, if α and β are different from zero (out-of-plane deformed configuration), all the z-axis projections of σ_{xx}, σ_{yy}, σ_{xy}, σ_{yx} and of their respective increments $\sigma_{xx,x}dx$, $\sigma_{yy,y}dy$, $\sigma_{xy,x}dy$ and $\sigma_{yx,y}dx$ have to be considered. Consequently, Eq. 4.17 becomes:

$$\begin{aligned}\sigma_{xz,x} + \sigma_{yz,y} =& -\sigma_{xx} u_{z,xx} dx - \sigma_{yy} u_{z,yy} dy - (\sigma_{xx,x} u_{z,x} dx + \sigma_{xy,y} u_{z,x} dy) + \\ &- (\sigma_{yy,y} u_{z,y} dy + \sigma_{xy,x} u_{z,y} dx) - \sigma_{xy} u_{z,xy} dy + \sigma_{yx} u_{z,yx} dx,\end{aligned} \tag{4.18}$$

where the assumptions of $sin(\alpha) \simeq \alpha \simeq u_{z,x}$ and $sin(\beta) \simeq \beta \simeq u_{z,y}$ are made and higher order terms are neglected. The two brackets in Eq. 4.18 are equal to zero since they describe the translational equilibrium along the x-axis and y-axis, respectively. Thus the indefinite equation of equilibrium to the translation along the z-axis in deformed configuration is:

$$\sigma_{xz,x} + \sigma_{yz,y} = -\sigma_{xx}u_{z,xx}dx - \sigma_{yy}u_{z,yy}dy - \sigma_{xy}u_{z,xx}dy - \sigma_{xy}u_{z,xy}dx - \sigma_{yx}u_{z,yx}dx. \quad (4.19)$$

It can be demonstrated that the left member of Eq. 4.18 is related to the fourth order derivatives of u_z on the plate surfaces. The right member of Eq. 4.18 justifies the Eq. 4.15: in Eq. 4.15 the u_z component is implied by the fact that G_{33} corresponds to the third component of the diagonal of $\boldsymbol{K_G}^{k\tau sij}$. Moreover, the second order derivatives in the right member of Eq. 4.18 are expressed through the derivatives of the shape functions in Eq. 4.15. Integrals $\leqslant ... \geqslant_{z_e^k}$ and $\lhd ... \rhd_{\Omega_e}$ are present in Eq. 4.15 in order to impose the equilibrium at the FE level and not punctually as in Eq. 4.18.
In conclusion, through the buckling fundamental nucleus $\boldsymbol{K_G}^{k\tau sij}$, the internal excitations typical of buckling can be directly assigned in the model. With the purpose to analyze the stability of the buckling problem, σ_{xx}, σ_{yy}, σ_{xy} and σ_{yx} can be imposed as inputs defined apart a constant. Such constant is the i-th eigenvalue of the corresponding problem described in Sec. 4.5 at Eq. 4.23. The i-th buckling load is given by the i-th eigenvalue multiplied by the previously assigned σ_{xx}, σ_{yy}, σ_{xy}.

4.5 Static and dynamic FEM problem

Whatever is the considered variational statement, starting from fundamental Nuclei, for a given discretization, mass matrix $\boldsymbol{M}$ and stiffness matrix $\boldsymbol{K}$ can be calculated by numerical integration and the assembly procedure. These two matrices are representative of inertial and Gibbs free energy contribution respectively. It should be emphasized that the stiffness matrix, regardless its name, contains information pertaining to all the considered fields and not only to the mechanical field. On the contrary, the mass matrix only concerns the mechanical field. In fact, mass apart, there are not other physical quantity related to the second time derivative of primary unknowns when defining the kinetic energy.
The stiffness matrix is symmetric due to the symmetric nature of the matrix products that from the variational statement lead to the fundamental nucleus. In addition, $\boldsymbol{K}$ is positive definite in the pure mechanical case, where only non-negative energetic contributions are admitted. One consequence of coupling the non-mechanical fields to the mechanical field is that the stiffness matrix becomes no longer positive defined: the non-mechanical fields imply a negative amount of mechanical energy due to negative coefficients along the diagonal of the constitutive matrix in Eq. 1.18 (such negative coefficients cause negative numbers on the diagonal of $\boldsymbol{K}$). The amount of energy subtracted to the mechanical field results distributed among the coupled fields under the form of thermal, electric or magnetic energy, leaving unchanged the total amount of energy. Consequently, the efficient positive definite matrix solution algorithms used in pure mechanical analysis cannot be adopted in multifield problems. That is a coupled problem is more time consuming to solve than a pure structural problem of the same size.
The undamped dynamic problem can be written in terms of the following ordinary differential equations system:

$$\boldsymbol{M}\ddot{\boldsymbol{Q}} + \boldsymbol{K}\boldsymbol{Q} = \boldsymbol{F}, \quad (4.20)$$

where:
$\boldsymbol{Q}$ is the vector of nodal primary unknowns;

$\ddot{\boldsymbol{Q}}$ is the vector of nodal accelerations;
$\boldsymbol{F}$ is the vector of nodal loads.
Moreover, the i-th natural frequency of the system ω_i can be calculated by solving the generalized eigenvalues problem:

$$(-\omega_i^2 \boldsymbol{M} + \boldsymbol{K})\boldsymbol{a_i} = \boldsymbol{0}, \tag{4.21}$$

where ω_i^2 are the eigenvalues and $\boldsymbol{a_i}$ are the eigenvectors. The system can be solved taking into account the boundary conditions $\overline{\boldsymbol{Q}}^k$ which are related to the various fields addressed to in the analysis.
If a static analysis is required, the system to solve is the following:

$$\boldsymbol{K}\boldsymbol{Q} = \boldsymbol{F}. \tag{4.22}$$

Bucking load constants P_i^{cr} can be calculated introducing the matrix $\boldsymbol{K_G}$, which permits to find the configurations of equilibrium when the structure is deformed according to buckling modes:

$$(P_i^{cr}\boldsymbol{K_G} + \boldsymbol{K})\boldsymbol{a_i} = \boldsymbol{0}. \tag{4.23}$$

Natural frequencies of the system in pre-loaded configuration can be calculated finding the generalized eigenvalues of the following system:

$$(-\omega_i^2 \boldsymbol{M} + \boldsymbol{K}_G + \boldsymbol{K})\boldsymbol{a_i} = \boldsymbol{0}. \tag{4.24}$$

4.6 Analytical investigation about the coupling effect on undamped natural frequencies

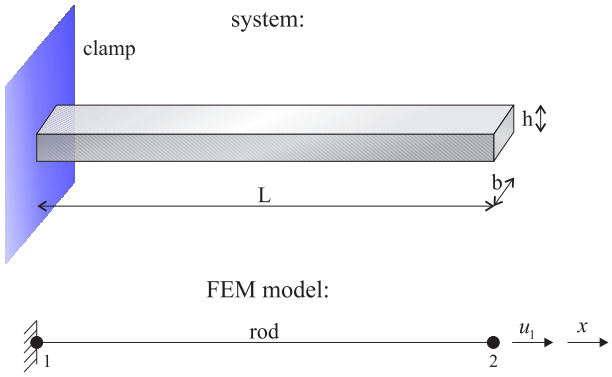

Figure 4.3. System and FEM model

In this section, the effect provided by thermo-mechanical coupling on the undamped natural frequencies will be identified through a single Degree Of Freedom (SDOF) example. In Fig. 4.3 is represented the structural system and the FEM model: a rod clamped at one tip. The clamp is intended also in the thermal sense: no temperature variation at the tip. For sake of simplicity, the structure is modeled by just one rod FE.
Considering just u_x and θ as primary unknowns, the PVD stiffness matrix Fundamental Nucleus for the thermo-mechanical case is the following:

$$\begin{bmatrix} C_{11}N_{2,x}N_{2,x} & -\lambda_1 N_{2,x}N_2 \\ -\lambda_1 N_2 N_{2,x} & -\frac{\rho C}{\theta_{ref}}N_2 N_2 \end{bmatrix}, \tag{4.25}$$

where N_2 is the second linear shape function, x/L, and $N_{2,x}$ is its derivative along the x-axis, $1/L$. Note that, since the problem is one-dimensional, the thickness functions have not been referred to (in principle the thickness function is one and unitary). Moreover, $C_{11} = E_1$.
The Fundamental Nucleus of the mass matrix is the following:

$$\begin{bmatrix} \rho N_2 N_2 & 0 \\ 0 & 0 \end{bmatrix}. \tag{4.26}$$

The mass matrix $[M]$ and the stiffness matrix $[K]$ of the problem can be obtained integrating on the structure's volume the stiffness and the mass fundamental nuclei:

$$[M] = \begin{bmatrix} \frac{1}{3}\rho V & 0 \\ 0 & 0 \end{bmatrix}; \qquad [K] = \begin{bmatrix} E_1 \frac{V}{L^2} & -\frac{1}{2}\lambda_1 \frac{V}{L} \\ -\frac{1}{2}\lambda_1 \frac{V}{L} & -\frac{1}{3}\frac{\rho C}{\theta_{ref}} V \end{bmatrix}, \tag{4.27}$$

where $V = Lbh$.
The following generalized eigenvalue problem can be written in order to find the undamped natural frequencies of the system[1]:

$$\left(-\omega^2 \begin{bmatrix} \frac{1}{3}\rho V & 0 \\ 0 & 0 \end{bmatrix} + \begin{bmatrix} E_1 \frac{V}{L^2} & -\frac{1}{2}\lambda_1 \frac{V}{L} \\ -\frac{1}{2}\lambda_1 \frac{V}{L} & -\frac{1}{3}\frac{\rho C}{\theta_{ref}} V \end{bmatrix} \right) \begin{Bmatrix} \widehat{u}_1 \\ \widehat{\theta} \end{Bmatrix} = \begin{Bmatrix} 0 \\ 0 \end{Bmatrix}. \tag{4.28}$$

[1]Since the mathematical model is represented by just one FE, the assembly procedure is not necessary.

ω is the undamped natural frequency in $[rad]$, while $\widehat{u}_1$ and $\widehat{\theta}_2$ are the two component of the eigenvector.
From Eq. 4.28 it is clear that the system has only one natural frequency and this is because the mass matrix has only one element along the diagonal: even if the primary unknowns of the FEM problems are two, the number of DOFs is one.
Moreover, since the matrix coefficients are all negatives, the second row of Eq. 4.28 is true only if the temperature variation $\widehat{\theta}$ is of opposite sign respect to the displacement variation. This confirm the perfect gas analogy according to which an expanded material becomes colder and viceversa.
Solving Eq. 4.28 respect to $\widehat{\theta}$, it is that:

$$\widehat{\theta} = -\frac{\frac{1}{2}\lambda_1 \frac{V}{L}}{\frac{1}{3}\frac{\rho C}{\theta_{ref}} V}\widehat{u}_1 = -Z\widehat{u}_1\,, \tag{4.29}$$

where Z is a positive quantity.
Substituting Eq. 4.29 into the first row of Eq. 4.28, Eq. 4.30 can be written:

$$\left(-\omega^2 \frac{1}{3}\rho V + \left(E_1 \frac{V}{L^2} + \frac{1}{2}\lambda_1 \frac{V}{L} Z\right)\right)\widehat{u}_1 = 0\,. \tag{4.30}$$

Natural frequency can be now calculated:

$$\omega = \sqrt{\frac{E_1 \frac{V}{L^2} + \frac{1}{2}\lambda_1 \frac{V}{L} Z}{\frac{1}{3}\rho V}}\,. \tag{4.31}$$

At this point, it has been demonstrated that the natural frequency calculated by a thermo-mechanical analysis is higher than the one calculated by a pure mechanical analysis (without thermo-mechanical coupling $Z = 0$). In other words, the thermo-mechanical coupling impact the structure by increasing its stiffness.
This conclusion can be extended for all the natural frequencies of generic structures: similar examples can be arranged in case of Multi degree Of Freedoms (MDOFs) systems and different FEs. The same reasoning can be applied to demonstrate that also the electro-mechanical (or magneto-mechanical) coupling leads to a certain increase in structure's stiffness.
Dimensionless analysis shows that the dimensionless factor responsible of the natural frequency variation in this one dimensional thermo-mechanical system is the following:

$$\digamma = \frac{\alpha_1^2 E_1 \theta_{ref}}{\rho C}, \tag{4.32}$$

where $\alpha_1 = \lambda_1 / E_1$.
In particular, accounting the dimensionless frequencies $\widetilde{\omega}$ as $\widetilde{\omega} = \omega\sqrt{\frac{\rho L^2}{E_1}}$, the difference between the natural frequency calculated in the pure mechanical case $\widetilde{\omega}_{PM}$ respect to the frequency $\widetilde{\omega}_{TM}$ found in the thermo-mechanical coupled case is given by the following relation:

$$\widetilde{\omega}_{TM} = \sqrt{\widetilde{\omega}_{PM}^2 + \frac{9}{4}\digamma}, \tag{4.33}$$

where $\widetilde{\omega}_{PM} = 3$.
It should be noted that $\digamma$ is always positive and consequently $\widetilde{\omega}_{TM} \geq \widetilde{\omega}_{PM}$. In addition, all factors in $\digamma$ are positive in nature, apart $\alpha = 0$[2]. It follows that the condition $\widetilde{\omega}_{TM} = \widetilde{\omega}_{PM}$ is

[2]E.g. dealing with certain carbon fiber composite materials.

possible in physics only when $\alpha = 0$.
Substituting numbers in formulas, it can be found that, for an aluminium rod, such difference is slightly lower than 2% in absolute value.
Such value can be slightly exceeded if the temperature at the node 1 is considered free to vary (clamp mechanical and not thermal). To solve such different problem, it is necessary to start from a nucleus of dimension 3×3, since primary unknowns are now 3: θ_1, u_2, θ_2. It can be found out that $\theta_1 = \theta_2$. After some calculations, Eq. 4.33 changes to Eq. 4.34:

$$\widetilde{\omega}_{TM} = \sqrt{\widetilde{\omega}_{PM}^2 + 3\digamma}. \tag{4.34}$$

Apart these simple exercises that can be solved by hands and that concern very simplified cases, FEM simulations show that, in case of aluminium structures of many DOFs and of more general geometries and boundary conditions, the difference between $\widetilde{\omega}_{PM}$ and $\widetilde{\omega}_{TM}$ can be far from the before mentioned value of 2% (Sec. 6.4). In addition, in case of particular materials, this effect depends on which/how many fields are considered in coupling (Sec. 7.1).

Part II

Numerical Results

Figure 4.4. MUL2 logo

In next chapters FEM results obtained in present activity are illustrated. Results are obtained in MUL2 FEM code, which is an academic code developed coherently with the theory presented in this work. The selective reduced integration is employed in MUL2 to overcome the shear locking phenomenon. As alternative to the selective reduced integration, the Mixed Interpolated Tensorial Components (MITC) technique has been recently implemented and assessed in work [19]. The penalty technique is used to impose boundary conditions, to numerically erase the contribution of particular DOFs or to artificially increase the stiffness related to particular constitutive coefficients (e.g. to obtain FSDT or CLT modeling starting form the ED1 kinematic description).

Chapter 5

Mechanical results

In this chapter, PVD (D in acronyms) stands for PVD-u_x,u_y,u_z and RMVT (M in acronyms) stands for RMVT-u_x,u_y,u_z(σ_{zz},σ_{xz},σ_{yz}) in order to simplify the notation.

5.1 Static analysis

5.1.1 Convergence study

A three layer thin square plate of unitary side ($a = 1$ $[m]$) loaded by a sinusoidal unitary pressure at the top face ($\widehat{p}_z = 1$ $[N/m^2]$) is considered. The plate is simply supported at the two opposite sides with zero pressure (cylindrical bending). The layers are of equal thickness and they are made of the same orthotropic material. The total thickness ratio is $a/h = 100$ and the lamination scheme is [0/90/0]. Material properties are: $E_1 = 25$, $E_2 = 1$, $E_3 = 1$, $G_1 = 0.5$, $G_2 = 0.5$, $G_3 = 0.2$ (all in $[GPa]$); $\nu_{12} = 0.25$, $\nu_{13} = 0.25$, $\nu_{25} = 0.25$. Convergence results concerning the midplane transverse displacement at the center of the plate are shown in Fig. 5.1 for LDn and EDn Q4 FEs (Q4 stands for four-nodes Quadrangular finite elements). Regular $n \times 1$ meshes are considered. Following remark can be made. LMn FEs have good convergence properties. It can be noticed that, even when calculating a displacement, simple FEs like ED1 and ED2 converge to a value different from the exact solution. Such difference decreases as the order of the thickness expansion increases.

5.1.2 Meyer-Piening benchmark

A sandwich-thin, rectangular plate loaded by a transverse pressure applied to a small rectangular region located at the plate centers, is considered [20]. The plate is simply supported in correspondence to their four edges. The plate geometry is as follows: width a=100 [mm], length b=200 [mm], total thickness h=12 [mm]. The faces of the same material have different thicknesses: top face thickness $h_3 = .1$ [mm], bottom face thickness $h_1 = .5$ [mm]. The core thickness is $h_1 = 11.4$ [mm]. The load consists of a transverse 1 [MPa] pressure applied to a rectangular zone at the center of the plate, which has dimensions of 5×20 [mm] (Fig. 5.2). Such a loading situation is very common in practice. It occurs each time a concentrated loading is applied to a sandwich structure. The two faces have the following material data: $E_1 = 70000$ [MPa], $E_2 = 71000$ [MPa], $E_3 = 71000$ [MPa], $G_{13} = 26000$ [MPa], $G_{23} = 26000$ [MPa], $G_{12} = 26000$ [MPa], $\nu_{13} = 0.3$, $\nu_{23} = 0.3$, $\nu_{12} = 0.3$. The core consists of metallic foam. Its material properties are: $E_1 = 3$ [MPa], $E_2 = 3$ [MPa], $E_3 = 2.8$ [MPa], $G_{13} = 1$ [MPa], $G_{23} = 1$ [MPa], $G_{12} = 1$

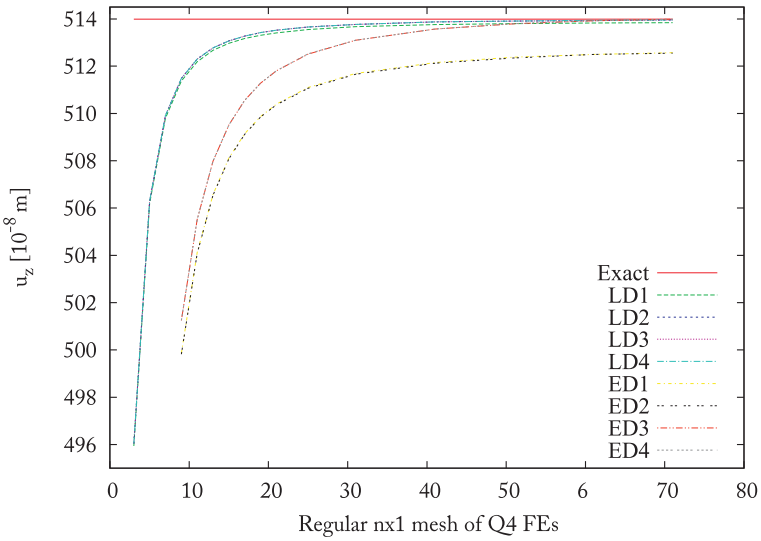

Figure 5.1. Midplane transverse displacement at the center of the plate: convergence study

[MPa], $\nu_{13} = 0.25$, $\nu_{23} = 0.25$, $\nu_{12} = .25$. In Figs. 5.3 are the two different meshes (named a and b) employed in the FEM analysis. The localized pressure load at the top of the plate causes some local effects which are clear in Figs. 5.4,5.5: the dip at the top face of the plate is more evident and more pronounced than the corresponding deformation at the bottom of the plate. This phenomenon is due to the softness of the core and it is directly related to the value of ϵ_z through the thickness of the plate. Theories with classical kinematics, like the CLT or the FSDT, are not suitable to model the described local effect. The reason of that is the assumption of $\epsilon_z = 0$. Results in numbers are collected in Tabs. 5.1,5.2 where comparisons among 3D analytical, 3D NASTRAN and two-dimensional plate FE results are discussed.

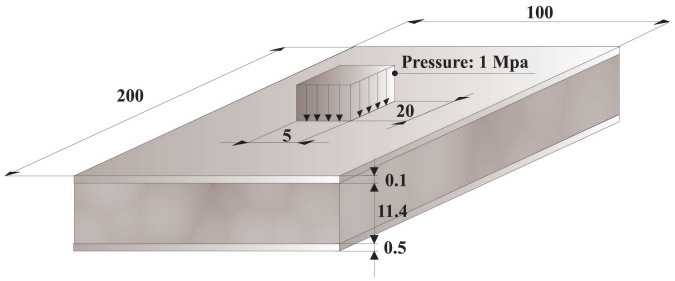

Figure 5.2. Meyer–Piening rectangular sandwich plates subjected to transverse pressure located at the plate center

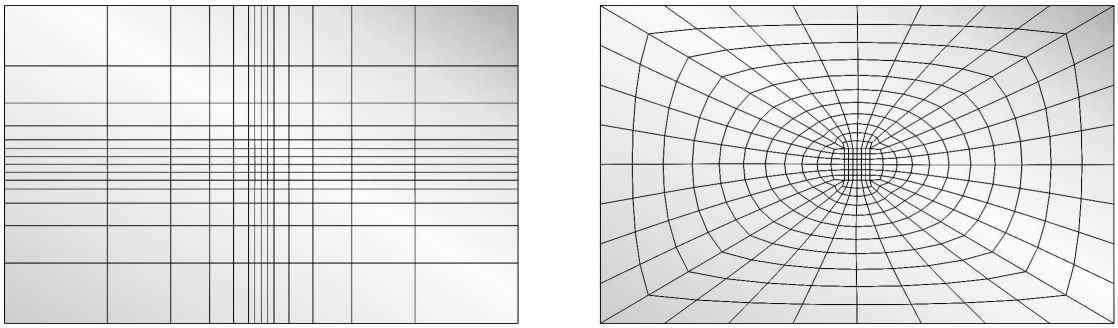

Figure 5.3. Two different meshes of Q4 FEs employed in the analysis: mesh *a* and mesh *b*

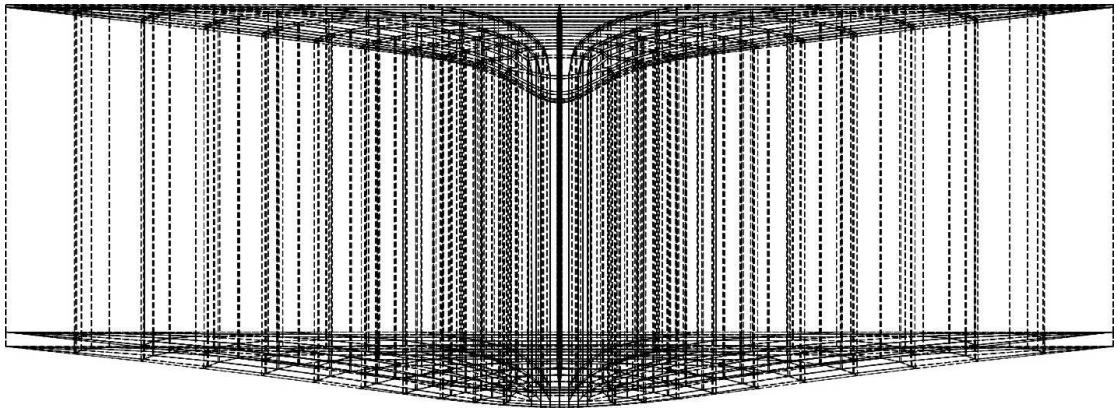

Figure 5.4. Static deformation with evident the different displacements between top and bottom surface

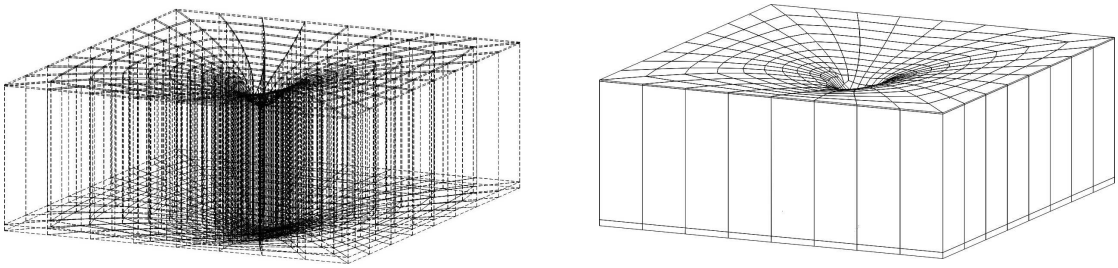

Figure 5.5. Structure under static deformation: transparent and opaque assonometric view

	u_z - top plate	u_z - bottom plate
3D Analytical [20]	-3.78	-2.14
3D-NASTRAN [20]	-3.84	-2.19
2D-LD1 (mesh a)	-3.30	-2.13
2D-LD2 (mesh a)	-3.51	-2.14
2D-LD3 (mesh a)	-3.52	-2.14
2D-LD4 (mesh a)	-3.52	-2.14
2D-LD1 (mesh b)	-3.33	-2.13
2D-LD2 (mesh b)	-3.54	-2.13
ESAComp	-3.12	-3.12

Table 5.1. Comparison of different analysis

	z	$u_3\,[mm]$	$\sigma_{22}\,[MPa]$	$\sigma_{11}\,[MPa]$	$\sigma_{12}\,[MPa]$
	Upper Face				
3D Analytical [20]	top	-3.78	-241	-624	0
	bottom		211	580	0
3D-NASTRAN [20]	top	-3.84	-237	-628	0
	bottom		102	582	0
2D-LM2	top	-3.7628	-223.93	-595.56	0
	bottom		196.37	556.00	0
2D-ED1	top	-0.0187	-23.99	-29.46	0
	bottom		-23.75	-29.17	0
	Lower Face				
3D Analytical [20]	top		-121	-138	0
	bottom	-2.14	127	146	0
3D-NASTRAN [20]	top		-120	-140	0
	bottom	-2.19	127	148	0
2D-LM2	top		-118.99	-136.20	0
	bottom	-2.1403	125.00	144.03	0
2D-ED1	top		3.32	4.87	0
	bottom	-0.0181	4.50	6.36	0

Table 5.2. Comparison of different analysis

5.2 Modal analysis

5.2.1 Convergence study

A fully simply supported square plate of aluminium alloy $2024-T6$ is considered under PVD analysis with a regular meshes of QUAD elements, where a regular mesh is a mesh of the same number of equally-spaced elements along the two plate's directions. Material properties are those in Tab. 5.3. The plate thickness ratio is 1/100. Different through-the-thickness expansion are

	$E[GPa]$	$G[GPa]$	$\nu_{12}[-]$	$\rho[kg/m^3]$
Al 2024-T6	73	27.239	0.34	2800

Table 5.3. Material properties of the aluminium alloy Al 2024-T6

employed for primary variables (form one to fourth order). Pure mechanical case is addressed to. In the following, the undamped natural frequencies calculated by FEM are compared with those calculated analytically, when available. Frequencies ($\overline{\omega}$) are dimensionless according to $\overline{\omega} = \omega\sqrt{\frac{a^4\rho}{h^2E}}$, where a is the plate dimension along the x-axis, ρ is the material density, h is the thickness and E is the Young's modulus.
By comparisons between analytical and FEM results, it in the following is proved that the FEM results converges to the analytical solution. For sake of conciseness, only a subset of the implemented FEs are considered in present convergence study.

Convergence study for the Q4 - ED1 finite element

frequency number	*analytical*	FEM mesh (Q4 - ED1 element) (3×3)	(6×6)	(9×9)	(12×12)	(15×15)
1	7.0664	7.9941	7.2827	7.1614	7.1196	7.1004
2	17.655	30.483	19.801	18.554	18.150	17.969
3	17.655	30.483	19.801	18.554	18.150	17.969
4	28.230	48.912	31.925	29.789	29.092	28.777

Table 5.4. Plate undamped dimensionless natural frequencies calculated for the pure mechanical case: convergence study of the ED1-Q4 (affected by thickness locking) finite element to the corresponding analytical solution - see the graphic view in Fig. 5.6

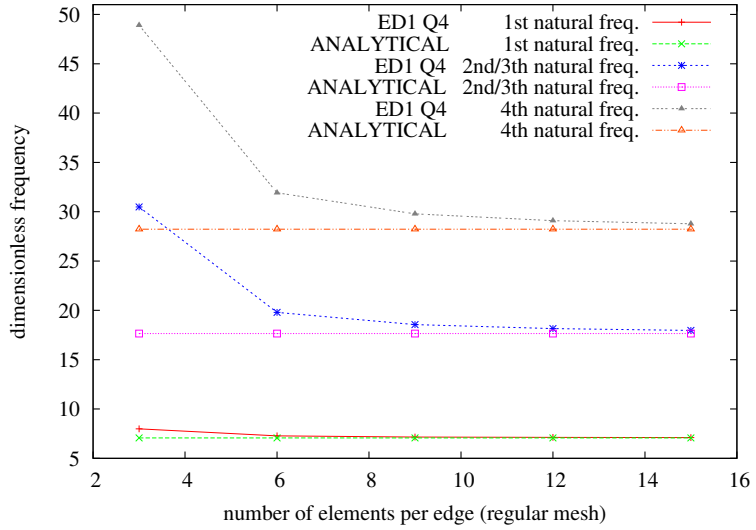

Figure 5.6. Graphical view of Tab. 5.4

Results in Tab. 5.4 and in Fig. 5.6 are affected by thickness locking. In order to obtain a solution free of thickness locking the remedy illustrated in Eqs. 2.7 and in [21] is employed: Tab. 5.5 and Fig. 5.7.

frequency number	*analytical*	FEM mesh (Q4 - ED1 element) (3×3)	(6×6)	(9×9)	(12×12)	(15×15)
1	-	6.8680	6.2458	6.1399	6.1035	6.0868
2	-	26.244	16.991	15.912	15.563	15.407
3	-	26.244	16.991	15.912	15.563	15.407
4	-	42.547	27.437	25.567	24.957	24.682

Table 5.5. Plate undamped dimensionless natural frequencies calculated for the pure mechanical case: convergence study of the ED1-Q4 (free of thickness locking) finite element to the corresponding analytical solution - see the graphic view in Fig. 5.7

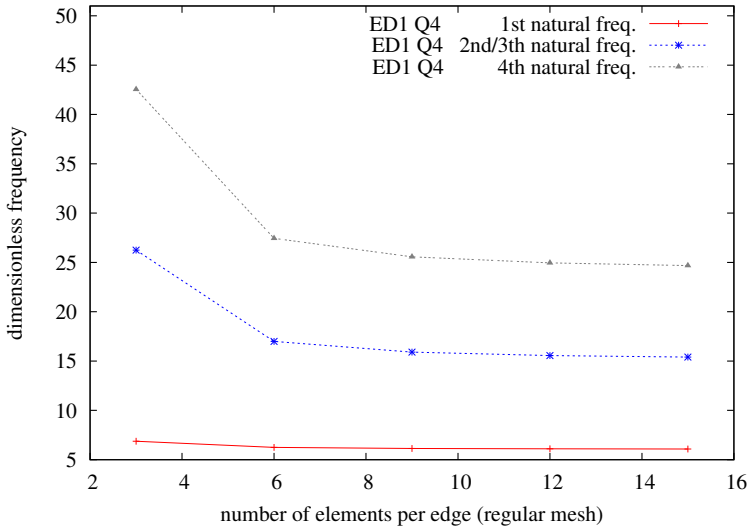

Figure 5.7. Graphical view of Tab. 5.5

Convergence study for the Q4 - ED2 finite element

frequency number	*analytical*	FEM mesh (Q4 - ED2 element)			
		(3×3)	(6×6)	(9×9)	(12×12)
1	6.0572	6.9319	6.2591	6.1457	6.1067
2	15.135	28.064	17.199	15.992	15.607
3	15.135	28.064	17.199	15.992	15.607
4	24.205	44.773	27.692	25.665	25.010

Table 5.6. Plate undamped dimensionless natural frequencies calculated for the pure mechanical case: convergence study of the ED2-Q4 finite element to the corresponding analytical solution - see the graphic view in Fig. 5.8

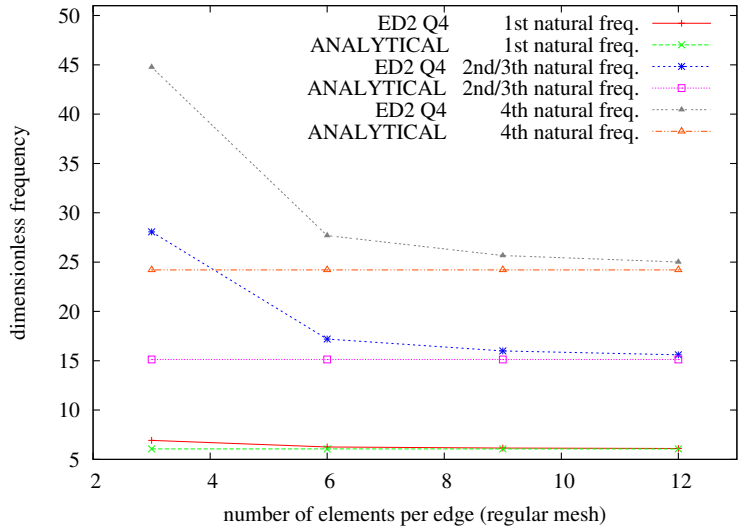

Figure 5.8. Graphical view of Tab. 5.6

Convergence study for the Q4 - ED3 finite element

frequency number	*analytical*	FEM mesh (Q4 - ED3 element)			
		(3×3)	(6×6)	(9×9)	(12×12)
1	6.0570	6.9316	6.2588	6.1454	6.1065
2	15.134	28.054	17.197	15.991	15.605
3	15.134	28.054	17.197	15.991	15.605
4	24.202	44.733	27.687	25.661	25.006

Table 5.7. Plate undamped dimensionless natural frequencies calculated for the pure mechanical case: convergence study of the ED3-Q4 finite element to the corresponding analytical solution - see the graphic view in Fig. 5.9

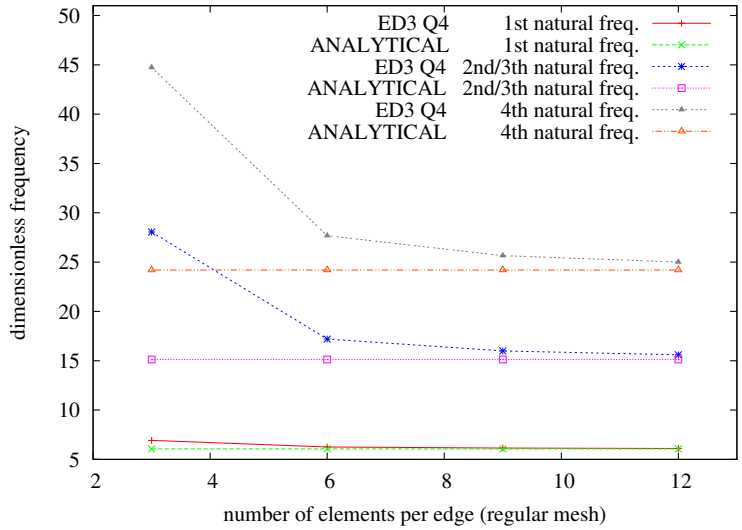

Figure 5.9. Graphical view of Tab. 5.7

Convergence study for the Q4 - ED4 finite element

frequency number	*analytical*	FEM mesh (Q4 - ED4 element)		
		(3×3)	(6×6)	(9×9)
1	6.0570	6.9316	6.2588	6.1454
2	15.134	28.054	17.197	15.991
3	15.134	28.054	17.197	15.991
4	24.202	44.733	27.687	25.661

Table 5.8. Plate undamped dimensionless natural frequencies calculated for the pure mechanical case: convergence study of the ED4-Q4 finite element to the corresponding analytical solution - see the graphic view in Fig. 5.10

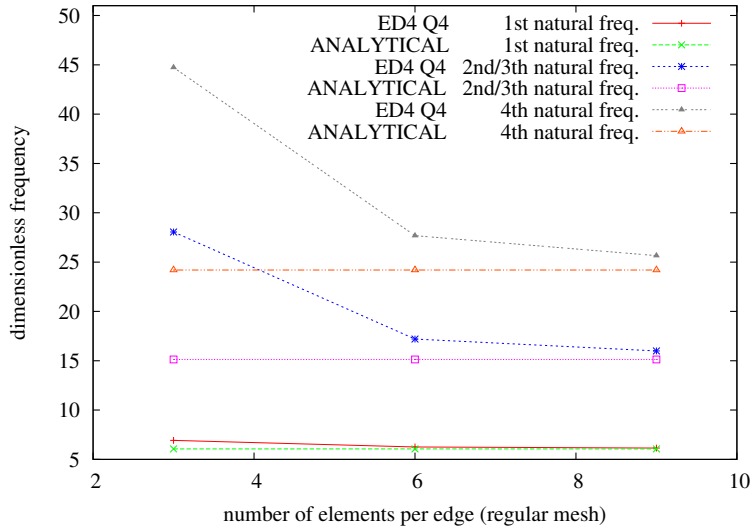

Figure 5.10. Graphical view of Tab. 5.8

Convergence study for the Q9 - ED1 finite element

frequency number	*analytical*	FEM mesh (Q9 - ED1 element) (3×3)	(6×6)	(9×9)	(12×12)	(15×15)
1	7.0664	7.0812	7.0674	7.0666	7.0665	7.0665
2	17.655	18.117	17.687	17.662	17.657	17.656
3	17.655	18.117	17.687	17.662	17.657	17.656
4	28.230	29.062	28.289	28.242	28.234	28.232

Table 5.9. Plate undamped dimensionless natural frequencies calculated for the pure mechanical case: convergence study of the ED1-Q9 (affected by thickness locking) finite element to the corresponding analytical solution - see the graphic view in Fig. 5.11

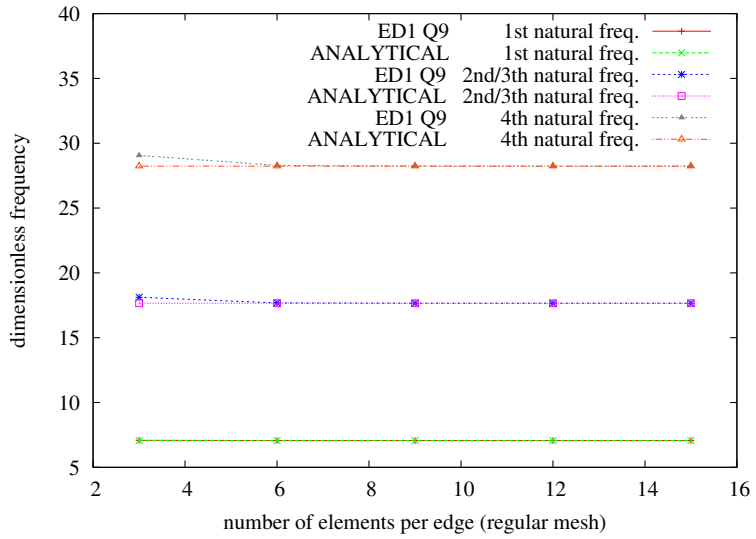

Figure 5.11. Graphical view of Tab. 5.9

Results in Tab. 5.9 and in Fig. 5.11 are affected by thickness locking. In order to obtain a solution free of thickness locking the remedy illustrated in Eqs. 2.7 and in [21] is employed: Tab. 5.10 and Fig. 5.12.

frequency number	*analytical*	FEM mesh (Q9 - ED1 element) (3×3)	(6×6)	(9×9)	(12×12)	(15×15)
1	-	6.0701	6.0580	6.0573	6.0572	6.0572
2	-	15.534	15.163	15.141	15.137	15.136
3	-	15.534	15.163	15.141	15.137	15.136
4	-	24.928	24.256	24.215	24.208	24.206

Table 5.10. Plate undamped dimensionless natural frequencies calculated for the pure mechanical case: convergence study of the ED1-Q9 (free of thickness locking) finite element to the corresponding analytical solution - see the graphic view in Fig. 5.12

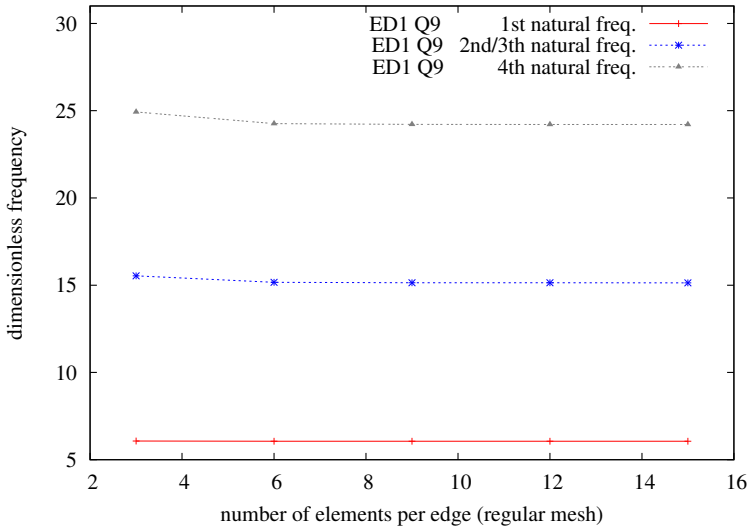

Figure 5.12. Graphical view of Tab. 5.10

Convergence study for the Q9 - ED2 finite element

frequency number	*analytical*	FEM mesh (Q9 - ED2 element)			
		(3×3)	(6×6)	(9×9)	(12×12)
1	6.0572	6.0703	6.0580	6.0574	6.0573
2	15.135	15.564	15.164	15.141	15.137
3	15.135	15.564	15.164	15.141	15.137
4	24.205	24.972	24.257	24.215	24.208

Table 5.11. Plate undamped dimensionless natural frequencies calculated for the pure mechanical case: convergence study of the ED2-Q9 finite element to the corresponding analytical solution - see the graphic view in Fig. 5.13

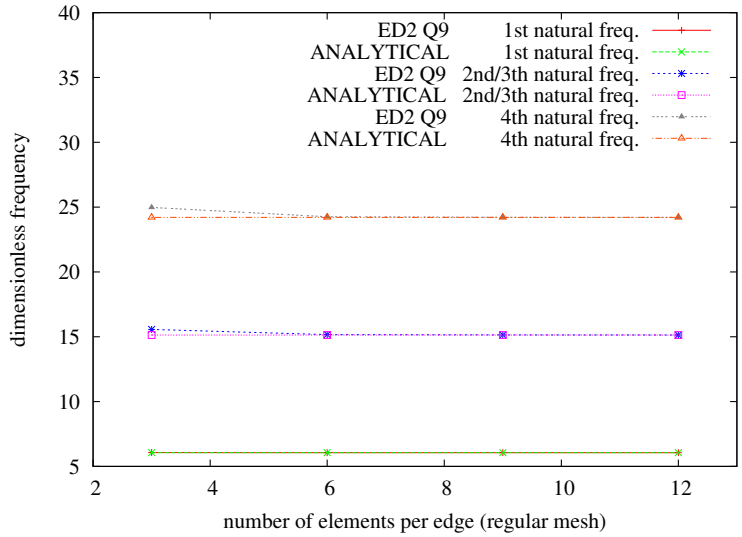

Figure 5.13. Graphical view of Tab. 5.11

Convergence study for the Q9 - ED3 finite element

frequency number	*analytical*	FEM mesh (Q9 - ED3 element)			
		(3×3)	(6×6)	(9×9)	(12×12)
1	6.0570	6.0701	6.0578	6.0572	6.0570
2	15.134	15.563	15.163	15.140	15.136
3	15.134	15.563	15.163	15.140	15.136
4	24.202	24.968	24.254	24.212	24.205

Table 5.12. Plate undamped dimensionless natural frequencies calculated for the pure mechanical case: convergence study of the ED3-Q9 finite element to the corresponding analytical solution - see the graphic view in Fig. 5.14

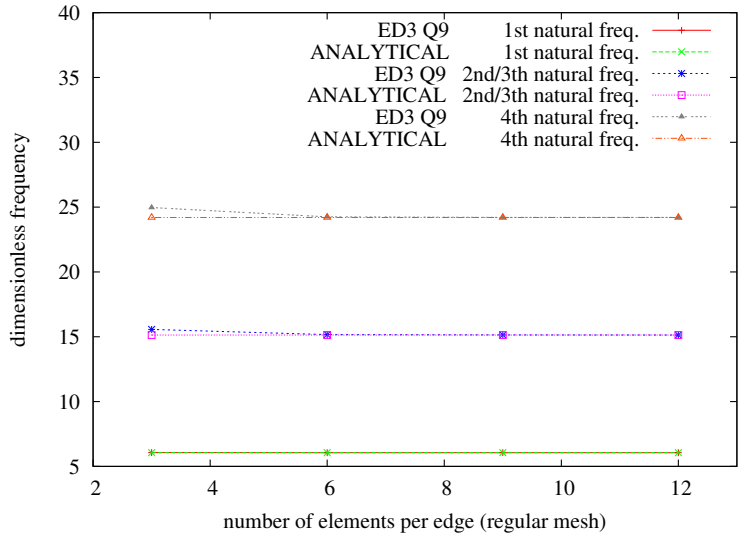

Figure 5.14. Graphical view of Tab. 5.12

Convergence study for the Q9 - ED4 finite element

frequency number	*analytical*	FEM mesh (Q9 - ED4 element) (3×3)	(6×6)	(9×9)
1	6.0570	6.0701	6.0578	6.0572
2	15.134	15.563	15.163	15.140
3	15.134	15.563	15.163	15.140
4	24.202	24.968	24.254	24.212

Table 5.13. Plate undamped dimensionless natural frequencies calculated for the pure mechanical case: convergence study of the ED4-Q9 finite element to the corresponding analytical solution - see the graphic view in Fig. 5.15

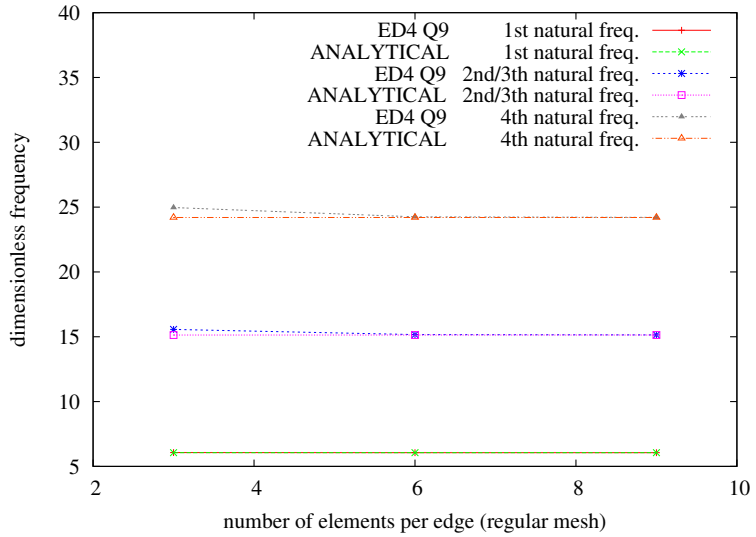

Figure 5.15. Graphical view of Tab. 5.13

5.2.2 Assessment by comparison with exact, experimental and NASTRAN results

In [22], experiments have been carried out to determine the free vibration frequencies and mode shapes of 3.2 mm thick, pultruded Glass Reinforced Plastic (GRP), square plates with six combinations of clamped (C), simply supported (S) and free (F) edge supports. Finite-element (FE) frequency and mode shape predictions based on orthotropic plate theory were shown to be in reasonable agreement with the experimental frequencies and modes.
In the following, results obtained by the ED1 Q4 FE are illustrated next to results published in [22] for comparison purpose.

Pultruded GRP plate material properties

In Tab. 5.14 are material properties of a Pultruded GRP plate of thickness equal to 3.2 $[mm]$. It should be appreciated that the given manufacturer's moduli values, are minimum values for use in design. Experience has shown that they may be up to 20% lower than the value measured in a single coupon test. Therefore, as an important aspect of the work presented here is to compare theoretical and experimental vibration frequencies, it is sensible to use moduli determined from coupon tests rather than design values. However, as no shear modulus tests were undertaken on the 3.2 $[mm]$ thick pultruded plate, it has been necessary to use the manufacturer's value for the shear modulus in the numerical analyses. The mass density per unit area of the pultruded GRP plate is required for the closed-form and finite-element (FE) orthotropic and anisotropic plate analyses. The manufacturer's density value of 1771.5 $[kg/m^3]$ is used.

E_1 $[N/m^2]$	E_2 $[N/m^2]$	G_{12} $[N/m^2]$	ν_{12} $[N/m^2]$	ν_{21} $[N/m^2]$	Comments
14.21E9	8.91E9		0.28	0.21	Tension coupon values
14.13E9	8.85E9		0.31	0.20	
12.40E9	4.83E9	2.93[a]	0.31	0.29	Manufacturer's min. values

[a] Value for a pultruded section

Table 5.14. Material properties of a Pultruded GRP plate

Parameters investigated in plate vibration tests

In this study, the effects of three principal types of parameter on the free vibration frequencies of 3.2 $[mm]$ thick pultruded GRP square ($a = b = 30$ $[mm]$) plates are investigated. The parameters are: the degree of material orthotropy (defined in terms of the orientation of the rovings with respect to one of the plate edges), the combination of plate edge support conditions. Three cases of orthotropy/anisotropy were investigated: (1) longitudinal (rovings parallel to the xaxis); (2) transverse (rovings at 90° to the x-axis) and (3) 45° (rovings oriented at 45° to the x and y axes). These three cases are shown in Fig. 5.16. Cases (1) and (2) correspond to the two extremes of orthotropy and case (3) corresponds to the situation in which the plate's anisotropy is a maximum. The effects of the three orthotropy/anisotropy cases were investigated for six combinations of plate edge support conditions. The latter are illustrated in Fig. 5.17 and range from plates with all edges clamped (C-C-C-C) to cantilever plates (C-F-F-F).

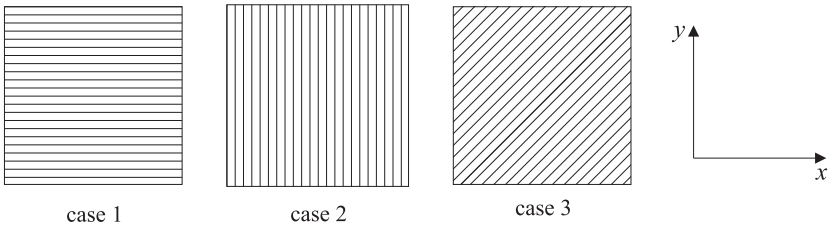

Figure 5.16. The three degree of material orthotropy/anisotropy considered

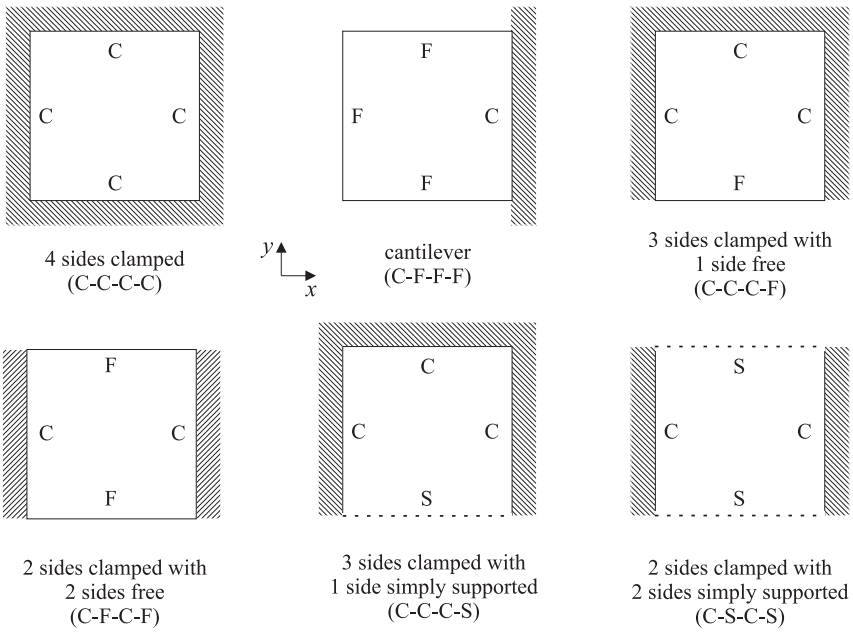

Figure 5.17. Combination of plate edge support conditions

Computation of free vibration frequencies in closed form

The free vibration frequencies of the pultruded GRP, square plates are computed on the basis of homogeneous orthotropic and anisotropic thin plate theory. Approximate closed-form expressions is referred to, in order to have the natural frequencies of the plates without free edges [22].

Computation of free vibration frequencies in MSC/Nastran

The MSC/NASTRAN FE software is used to compute the free vibration frequencies of the square pultruded GRP plates. The plates are modeled with the CQUAD4 element, which is a four node, shear deformable general quadrilateral plate element with five degrees of freedom per node - three translations and two out-of-plane rotations. With this element, the clamped edge (C) condition is simulated by setting all five degrees of freedom to zero at a boundary node. Likewise, the simply supported edge (S) condition is defined by setting the three translations to zero at a boundary node. For the free edge (F) condition, all five degrees of freedom remain unconstrained at a boundary node. The MSC/NASTRAN FE software was first used to compute the free vibration

frequencies of a square simply supported isotropic thin plate for a range of uniform mesh sizes. The purpose of these computations was to establish a suitable mesh size for the subsequent pultruded plate vibration frequency analyses. The simply supported isotropic plate is chosen, because its natural frequency is known exactly. The frequency of this plate was determined using square meshes ranging from 2×2 (coarse) to 32×32 (fine) extending over the whole plate. The FE analysis frequencies for the first six vibration modes are shown in comparison to the exact frequency values in Tab. 5.15. The rate of convergence with mesh refinement for the first mode of vibration is also shown in Fig. 5.18. It is evident from Tab. 5.15 that when an 8×8 mesh is used, the computed frequency differs by less than 1 Hz from the exact frequency. Furthermore, Fig. 5.18 shows that as the mesh is refined beyond 16×16, the FE analysis predicts a frequency lower than the exact value. This is because the exact frequency is based on thin and not shear deformation plate theory. Based on the results of this frequency convergence study for the simply supported, isotropic, square plate, it was decided to use a uniform 32×32 mesh for all of the FE free vibration analyses of pultruded GRP plates.

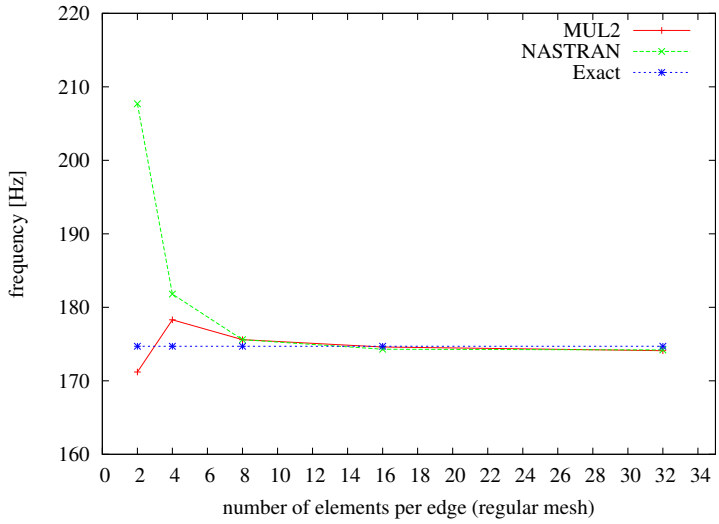

Figure 5.18.

Computation of free vibration frequencies in MUL2

The MUL2 FE software has been used to analyze the same problems previously solved in MSC/NASTRAN (Sec. 5.2.2). Present work has thus the additional worthiness of assessment for MUL2: the accuracy of results is illustrated by comparison with MSC/NASTRAN and with the closed-form solutions.
In MUL2, the plates are modelled with the ED1 Q4 element, which is a four node, shear deformable general quadrilateral plate element with six degrees of freedom per node. The physical meaning of nodal unknowns depends on the employed thickness function. In this case the Taylor expansion is employed: the first three degrees of freedom are the three nodal displacement and the other three are rotations. The clamped edge (C) condition is simulated setting by penalty all six degrees of freedom to zero at a boundary node. Likewise, the simply supported edge (S) condition is defined setting by penalty to zero the translations to zero at a boundary node. For the free edge (F) condition, all six degrees of freedom remain unconstrained at a boundary node.

For the analyses, the meshes were not uniform, but each mesh was arranged so that the elements were roughly similar in shape and did not have any large obtuse angles.

Uniform mesh size	Vibration mode number (M=MUL2/N=NASTRAN)											
	1 (M)	1 (N)	2 (M)	2 (N)	3 (M)	3 (N)	4 (M)	4 (N)	5 (M)	5 (N)	6 (M)	6 (N)
2×2	171.2	207.7	11569.8	11188.8	11569.8	11188.8	11570.0		11781.5		11781.5	
4×4	178.3	181.8	566.6	517.5	566.6	517.5	936.2	871.8	1858.7	1311.7	1858.7	1311.7
8×8	175.6	175.6	463.1	452.8	463.1	452.8	746.7	725.3	1022.2	965.2	1022.2	965.2
16×16	174.6	174.3	422.0	439.1	422.0	439.1	707.0	700.0	905.2	891.8	905.2	891.8
32×32	174.1	174.2	436.9	436.4	436.9	436.4	697.8	696.5	879.1	876.1	879.1	876.1
Exact sol.[a]	174.7	174.7	436.8	436.8	436.8	436.8	698.9	698.9	873.6	873.6	873.6	873.6

[a] Based on thin (shear-rigid) plate theory

Table 5.15. Convergence of approximate FE frequency $[Hz]$ with mesh refinement for an isotropic, simply supported, square plate ($a = b = 0.3$ $[m]$, $t = 0.0032$ $[m]$, $E = 210E9$ $[N/m^2]$, $\nu = 0.3$ and $\rho = 7860$ $[Kg/m^3]$)

Comparison of experimental and computed frequencies

The free vibration frequencies of square GRP plates are presented and discussed in this section. The results encompass the three levels of orthotropy/anisotropy defined in terms of the orientation of the rovings, i.e., longitudinal, transverse and 45°, with respect to the x-axis of the plate, and the six combinations of edge support conditions. Frequencies for the first seven modes of vibration are presented in Tab. 5.16. For plates with combinations of clamped (C) and simply supported (S) edges, generally four frequencies are listed for each vibration mode: the theoretical frequency ([22]), the MU2 FE frequency, MSC/NASTRAN FE frequency and the experimentally determined frequency. However, for the plates with combinations of clamped (C) and free (F) edges, in general only three frequency values are given in Table 5.16, because a simple closed-form expression was not available. It is evident from 5.16 that both FE analyses predict similar frequency values for all cases and that these values are slightly higher respect to the closed-form solution. In commercial SW, this may be attributable to one or more of the following factors: the use of a coarser mesh, an element based on thin plate theory and the Guyan reduction technique, which uses lumped masses at the master degrees of freedom. The experimentally determined frequencies appear, for the most part, to be in reasonable agreement with both the theoretical and FE frequency predictions, especially for the lower vibration modes and when all of the plate edges are supported. For plates with one or more free edges, some of the experimental frequencies for the first vibration mode differ significantly from the FE values, but show much better agreement for higher modes. It is also evident that a number of the third mode frequencies were missed in the experiments, which is not altogether surprising given that only a simple experimental vibration test rig was available. The gaps in the sixth and seventh vibration mode columns of 5.16 arise, because only five frequencies were determined in the vibration tests. Due to some missed third mode frequencies and occasional diffculties in determining the nodal line patterns, vibration frequencies and mode shapes were computed for the first seven vibration modes in order to permit a more comprehensive comparison between theory and experiment. The difference between the theoretical/numerical and experimental frequencies in 5.16 is generally less than 10% and suggests that orthotropic/anisotropic thin plate theory provides a sound basis for modelling the free vibration response of pultruded GRP plates under a variety of edge support conditions.

Support conditions	Anal./Exp.	Vibration mode number						
		1	2	3	4	5	6	7
C-C-C-C	Exact	150.39	284.49	330.18	444.91	502.75	610.52	646.42
(Long./Transv.)	MUL2	149.26	282.91	328.57	441.29	503.35	611.37	643.35
	NASTRAN	149.09	281.87	327.51	439.11	499.82	607.41	638.27
	Exp.	140.00	268.00	305.00	441.00	497.00		
C-C-C-S (Long.)	Exact	136.26	247.23	322.66	418.39	444.20	597.88	605.25
	MUL2	135.18	245.51	321.30	415.38	443.81	594.44	606.68
	NASTRAN	135.13	245.01	320.37	413.85	441.73	591.01	602.89
	Exp.	132.00	232.00		376.00	400.00	521.00	
C-C-C-S (Transv.)	Exact	127.54	271.22	278.94	403.69	493.65	533.63	613.90
	MUL2	126.73	270.34	277.66	401.72	495.33	534.07	613.98
	NASTRAN	126.66	269.43	277.22	400.25	491.96	531.87	609.80
	Exp.	125.00	261.00		385.00	465.00	555.00	
C-S-C-S (Long.)	Exact	126.73	216.17	316.63	391.71	397.28	556.22	600.40
	MUL2	125.79	213.98	315.94	389.88	394.16	551.33	602.95
	NASTRAN	125.79	213.84	315.10	388.85	393.06	549.13	599.27
	Exp.	125.00		203.00	344.00	370.00	506.00	
C-S-C-S (Transv.)	Exact	112.60	235.41	261.64	370.94	464.27	486.28	584.40
	MUL2	111.40	233.79	261.46	368.99	463.46	489.22	581.71
	NASTRAN	111.36	233.72	260.61	367.97	462.50	485.95	579.56
	Exp.	113.00	214.00		352.00	446.00		529.00
C-C-C-C (45°)	Exact	149.54	304.30	304.30	458.77	541.15	541.15	647.21
	MUL2	147.08	290.96	308.12	445.33	534.23	542.63	658.56
	NASTRAN	146.80	289.77	306.77	442.26	530.33	538.67	652.28
	Exp.	150.00	292.00		428.00	505.00		616.00
C-C-C-S (45°)	Exact	133.21	264.73	294.69	428.48	479.96	534.13	645.14
	MUL2	130.71	257.76	292.04	415.19	477.00	531.46	617.25
	NASTRAN	130.56	257.06	290.99	412.93	474.55	527.86	612.48
	Exp.	129.00	240.00		390.00	437.00	556.00	
C-S-C-S (45°)	Exact	121.08	230.91	285.41	402.49	424.33	525.64	598.77
	MUL2	119.18	224.98	283.63	387.61	423.64	525.51	575.03
	NASTRAN	119.09	224.63	282.73	386.04	422.16	522.14	571.57
	Exp.	114.00	207.00		375.00	397.00	543.00	
C-F-C-F (Long.)	MUL2	105.86	117.44	172.96	293.03	303.76	309.05	369.70
	NASTRAN	105.82	117.37	172.89	292.20	303.44	308.14	368.60
	Exp.	70.00	94.00		172.00	208.00	230.00	
C-F-C-F (Trans.)	MUL2	83.75	97.97	172.80	231.94	252.05	330.03	346.40
	NASTRAN	83.63	97.82	172.74	231.07	251.09	238.93	346.23
C-F-C-F (45°)	MUL2	86.81	107.02	181.10	240.95	269.66	324.05	367.42
	NASTRAN	105.82	117.37	172.89	292.20	303.44	308.14	368.60
	Exp.	70.00	94.00		172.00	208.00	230.00	
C-C-C-F (Long.)	MUL2	110.66	161.62	293.66	298.53	349.18	467.53	511.19
	NASTRAN	110.61	161.48	292.97	297.67	348.05	465.58	508.68
	Exp.	76.00	152.0	246.00	287.00	305.00		
C-C-C-F (Trans.)	MUL2	90.40	161.34	239.22	307.21	337.72	465.38	467.62
	NASTRAN	90.27	161.21	238.32	306.10	337.10	462.15	465.74
C-C-C-F (45°)	MUL2	95.08	165.16	251.03	309.21	336.83	478.79	488.18
	NASTRAN	95.02	168.84	250.34	308.22	335.36	475.94	485.32
	Exp.	98.00	161.00	241.00	296.00	331.00		
C-F-F-F (Long.)	MUL2	16.58	32.89	96.91	107.74	130.24	209.02	244.41
	NASTRAN	16.61	32.92	96.89	107.86	130.29	209.07	244.23
	Exp.	15.00	32.00	77.00	114.00		210.00	
C-F-F-F (Trans.)	MUL2	13.10	30.70	81.47	113.92	119.23	207.73	232.39
	NASTRAN	13.11	30.72	81.40	113.90	119.38	207.74	231.89
C-F-F-F (45°)	MUL2	13.46	36.18	81.49	108.92	129.19	223.14	241.36
	NASTRAN	13.48	36.17	81.51	108.98	129.15	222.89	241.13
	Exp.	27.00	38.00	85.00	110.00	125.00		

Table 5.16. The free vibration frequencies of square GRP plates in differently combined plate edge support conditions and fiber orientation

Concluding remarks

A series of small amplitude vibration tests have been found on literature on 3.2 [mm] thick, square pultruded GRP plates with three orientations of the principal material axes and six edge support combinations. The free vibration frequencies and mode shapes observed in the tests have been compared with corresponding frequencies and mode shapes, obtained from approximate closed-form expressions and numerical FE analysis. MUL2 FE SW and MSC/NASTRAN SW have been employed to obtain FE numerical results. By comparison, it has been showed that results provided by MUL2 SW are in general closer to the exact solution respect to those obtained by MSC/NASTRAN SW, on equal mesh. The theoretical/numerical and experimental results have been shown to be in reasonably good agreement with, in general, corresponding frequency values differing by less than 10%. Consequently, it can be confirmed that thin orthotropic/anisotropic plate theory provides a sound basis for modelling the free vibration response of pultruded GRP plates, despite their relatively heterogeneous fibre architectures. It has also been shown, both numerically and experimentally, that, irrespective of the degree of material orthotropy, the first mode vibration frequencies of square, pultruded GRP plates decrease as the rotational and translational edge restraint is successively relaxed. Moreover, it has been demonstrated that there is a very large reduction in frequency when the number of supported edges reduces from two to one.

5.2.3 Buckling analysis

A fast overview of the buckling analysis that can be performed in MUL2 is presented in the following. In Fig. 5.19 a compressed beam is considered under undamped frequency analysis and buckling analysis. The details of the problems are in the label of the figure itself. LD1 Q4 FEs are used in the FEM model and thus the beam is considered as a narrow plate. It can be noted that the FEM results are in good agreement with the exact solutions of the undamped natural frequencies and of the buckling loads. If pre-loading is not applied to the structure, the undamped natural frequencies are computed through the system in Eq. 7.2. In case of pre-loading, the system in 4.24 has to be solved. The i-th buckling load corresponds to the pre-loading such that the i-th natural frequency goes to zero. In agreement with such definition, buckling loads can be calculated in direct way solving the system in 4.23. Some interesting

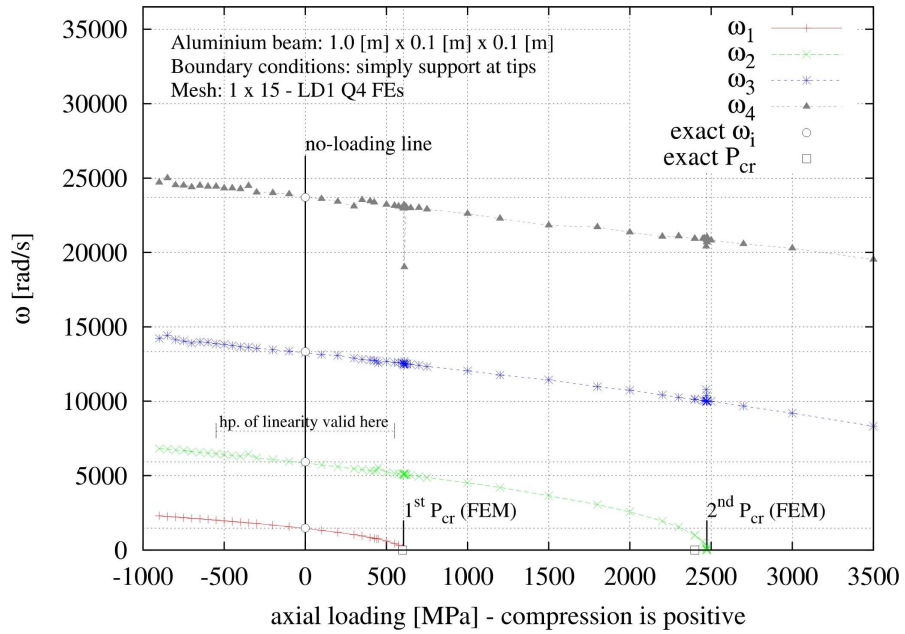

Figure 5.19. Variation of undamped natural frequencies in pre-loading condition - assessment with exact points

research studies could be planned to study the buckling, the natural frequencies and the mode shape of plates subjected to in-plane combined loading, where shear and normal stresses are simultaneously present. It is understood that this subject is crucial in aerospace applications, where panels works almost always in pre-loaded configuration during their operational life. The investigation could easily encompass anisotropic multilayered structures in multifield approach, according to the advanced two-dimensional modeling proposed in this work.
In Fig. 5.20 the first five mode shapes of a square plate calculated without pre-loading are compared with the corresponding mode shape found imposing a normal pre-loading close to the first buckling load. The colored edge is the loaded one. Material properties are those of aluminium in Tab. 5.3, the dimension of the edges $a = b$ is 0.1 $[m]$ and the thickness ratio is $a/h = 100$. It is evident that the pre-loading deeply affects the mode shapes of the structure. As a consequence, this effect should be taken into account when panels are employed as structural elements in aerospace applications or, more in general, when dynamic effects are relevant.

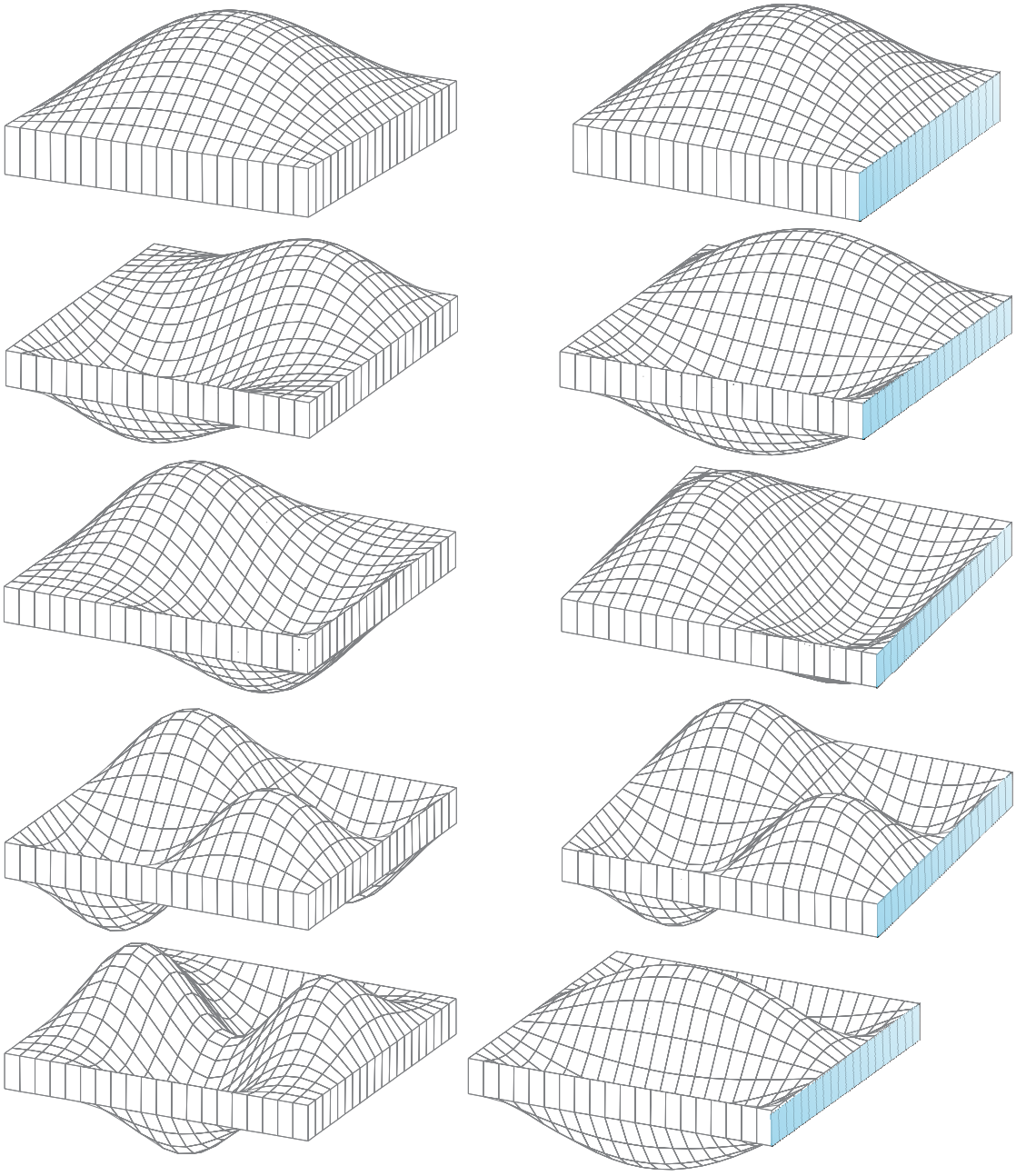

Figure 5.20. First five mode shape without pre-loading (on the left); first five mode shape with pre-loading equal to the 9.99% of buckling normal load, applied on the colored edge (on the right)

5.3 The application of Failure Criteria

Composite materials are characterized by a mechanics and a failure mechanics which are more complicate in comparisons with conventional materials. A correct design requires an accurate and effective prediction of failure parameters, such as failure loadings, failure locations and failure indices. Highly accurate mechanical models are therefore needed to effectively describe the mechanics of composites and predict their failure. The RMVT model presented in this work is able to calculate all stresses with very high accuracy, and then particularly suitable for failure forecast. In this work, the maximum stress failure criterion has been adopted and is introduced. Further investigations could be part of future works, including other failure criteria, i.e. the criterion for composite laminates of Puck.

5.3.1 Maximum stress failure criterion

The idea of Maximum Stress criterion is to compare the lamina stress status with the lamina normal and shear strength. Failure occurs when the ratio is greater or equal to 1:

$$\begin{array}{ll} \frac{|\sigma_{11}|}{X} \geq 1; & \frac{|\sigma_{23}|}{R} \geq 1; \\ \frac{|\sigma_{22}|}{Y} \geq 1; & \frac{|\sigma_{13}|}{S} \geq 1; \\ \frac{|\sigma_{33}|}{Z} \geq 1; & \frac{|\sigma_{12}|}{T} \geq 1. \end{array} \tag{5.1}$$

X, Y, and Z represent the lamina normal strengths while R, S, and T are the lamina shear strengths in the material reference system (subscripts 23, 13, 12). Normal strengths depend on the sign of the corresponding stress component. In the case of tensile stresses, the tensile strengths X_T, Y_T and Z_T must be used in Eq. (5.1). For negative values of the normal stress components the compressive strengths X_C, Y_C and Z_C have to be used. Due to the linearity of the problem, a relation of proportionality holds between the applied loading $p_{zz}^{(0)}$ and every stress component. This means that, for every form of Eq. (5.1), a failure loading $p_{zz}^{(F)}$ can be calculated with the following formula:

$$\begin{array}{ll} p_{zz,11}^{(F)} = p_{zz}^{(0)} \frac{X}{|\sigma_{11}|}; & p_{zz,23}(F) = p_{zz}^{(0)} \frac{R}{|\sigma_{23}|}; \\ p_{zz,22}^{(F)} = p_{zz}^{(0)} \frac{Y}{|\sigma_{22}|}; & p_{zz,13}(F) = p_{zz}^{(0)} \frac{S}{|\sigma_{13}|}; \\ p_{zz,33}^{(F)} = p_{zz}^{(0)} \frac{Z}{|\sigma_{33}|}; & p_{zz,12}(F) = p_{zz}^{(0)} \frac{T}{|\sigma_{12}|}. \end{array} \tag{5.2}$$

The minimum failure load is the minimum value of Eq. (5.2). Failure indices can be computed along the thickness z considering the minimum failure load as reference.

5.3.2 Benchmarks

Two different plate problems are considered in the subsequent numerical investigations which are devoted to the calculation of the stress field and the failure index. The exact 3D solution of reference is provided by Pagano in work [23]. FEM results are obtained in the MUL2 software with a regular 15×15 mesh of Q4 FEs.

Problem I

A four-edge simply supported orthotropic square plate with three layers made of the $T300/5208$ graphite/epoxy material is analyzed. Symmetric [0/90/0] and [0/45/0] as well as anti-symmetric [0/90/0/90] configurations are considered. The stacking sequence starts from the plate top; ply

angles are measured with respect to the x-axis. In order to deal with thin and moderately thick plates, three different thickness ratios are considered: $a/h = 100, 50, 10$. A bi-sinusoidal pressure loading with a half wave for each side is addressed to. The mechanical properties of the material are listed below:

$$E_L = 132.5\,\text{MPa}, E_T = 10.8\,\text{MPa}, G_{LT} = 5.7\,\text{MPa},$$

$$G_{TT} = 3.4\,\text{MPa}, \nu_{LT} = 0.24, \nu_{TT} = 0.49. a = 1.0\,\text{m}.$$

The material strengths are:

$$X_t = 1515\,\text{MPa}, X_c = 1697\,\text{MPa}, Y_t = 43.8\,\text{MPa},$$

$$Y_c = 43.8\,\text{MPa}, Z_t = 43.8\,\text{MPa}, Z_c = 43.8\,\text{MPa},$$

$$R = 86.9\,\text{MPa}, S = 67.6\,\text{MPa}, T = 86.9\,\text{MPa}.$$

Problem II

A four-edge simply supported orthotropic square plate consisting of two layers [90/0] and three layers [0/90/0] with bi-sinusoidal pressure loading is considered. The thickness ratio $a/h = 10$. The geometric and material properties are:

$$a = 1.0\,\text{m}, E_L = 132.5\,\text{MPa}, E_T = 10.8\,\text{MPa},$$

$$G_{LT} = 5.7\,\text{MPa}, G_{TT} = 3.4\,\text{MPa},$$

$$\nu_{LT} = 0.24, \nu_{TT} = 0.49.$$

Stress field evaluation: Comparison between PVD and RMVT results

The results of different stresses of problem II are first considered in Tab. 5.17, where ζ is introduced as dimensionless plate-thickness coordinate with zero placed at the middle surface level. Emphasis is placed on the top and bottom of the plate as well as on the interfaces between the layers. It can be noted that the results of transverse stresses obtained with the mixed formulation are almost exactly the same as Pagano's 3D solution. 3D results can also be obtained with the FEM solution for in-plane stresses. Results with models based on PVD show discontinuities for transverse stresses at the layer interfaces. Figs. 5.21-5.24 confirm the advantage of the "a priori" calculation of transverse stresses with RMVT. Concerning problem I, it can also be underlined that, in Fig. 5.21, the transverse shear stresses σ_{13} appear with the classical PVD modeling, where it should be zero due to reasons of symmetry. This can have a significant effect on the calculation of failure (Sec. 5.3.2).

	σ_{33}	σ_{33}	σ_{33}	σ_{33}	σ_{11}	σ_{11}	σ_{11}	σ_{11}
ζ	ED2	LD2	LM2	3D Pagano	ED2	LD2	LM2	3D Pagano
1.000000	1.028	1.116	1.009	1.000	46.53	48.78	48.73	48.74
0.866667	0.957	1.021	0.990	0.987	40.30	40.93	40.92	40.88
0.733333	0.886	0.945	0.954	0.950	34.08	33.43	33.38	33.47
0.600000	0.816	0.887	0.901	0.894	27.86	26.28	26.23	26.42
0.466667	0.745	0.849	0.831	0.822	21.64	19.48	19.45	19.66
0.333333	0.675	0.830	0.746	0.739	15.43	13.03	13.05	13.10
0.333333	0.638	0.754	0.746	0.739	1.86	1.69	1.74	1.74
0.200000	0.584	0.653	0.648	0.647	1.21	1.11	1.13	1.13
0.066667	0.530	0.552	0.551	0.549	0.56	0.52	0.53	0.52
-0.066667	0.477	0.452	0.454	0.449	-0.09	-0.06	-0.07	-0.09
-0.200000	0.423	0.352	0.357	0.351	-0.75	-0.65	-0.67	-0.70
-0.333333	0.370	0.252	0.261	0.260	-1.40	-1.23	-1.27	-1.31
-0.333333	0.326	0.177	0.261	0.260	-15.60	-13.20	-13.22	-13.28
-0.466667	0.257	0.156	0.175	0.177	-21.80	-19.63	-19.60	-19.82
-0.600000	0.188	0.118	0.105	0.106	-27.99	-26.40	-26.35	-26.56
-0.733333	0.119	0.061	0.052	0.050	-34.18	-33.53	-33.48	-33.58
-0.866667	0.050	-0.015	0.016	0.013	-40.37	-41.00	-40.99	-40.97
-1.000000	-0.019	-0.108	-0.002	0.000	-46.56	-48.81	-48.77	-48.79

Table 5.17. σ_{33} and σ_{11} at the center of the plate along thickness ζ; $a/h = 10$, [0/90/0]; Problem I

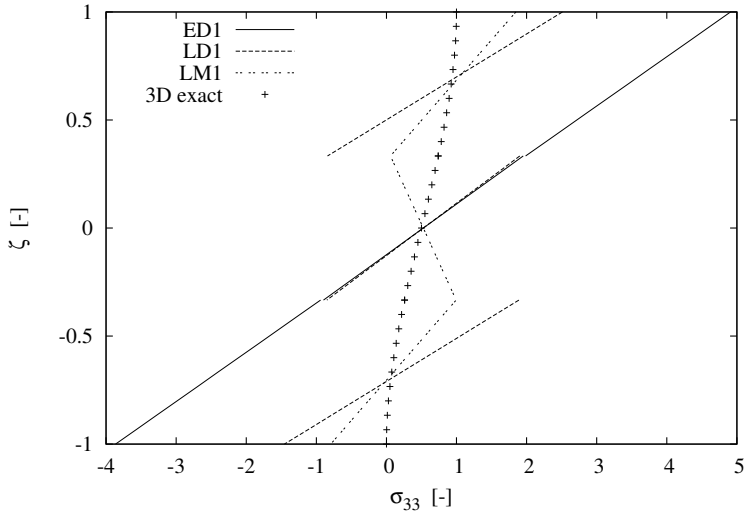

Figure 5.21. σ_{33} in the center of the plate along thickness ζ; $a/h = 10$, [0/90/0]; Problem I

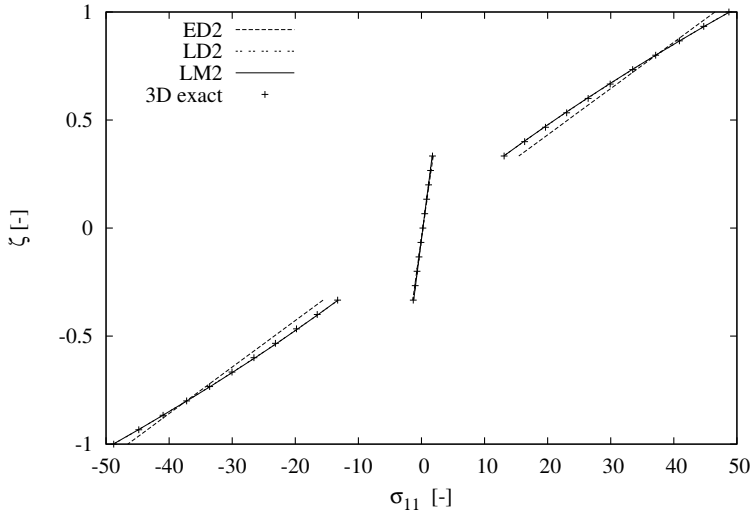

Figure 5.22. σ_{11} in the center of the plate along thickness ζ; $a/h = 10$, [0/90/0]; Problem I

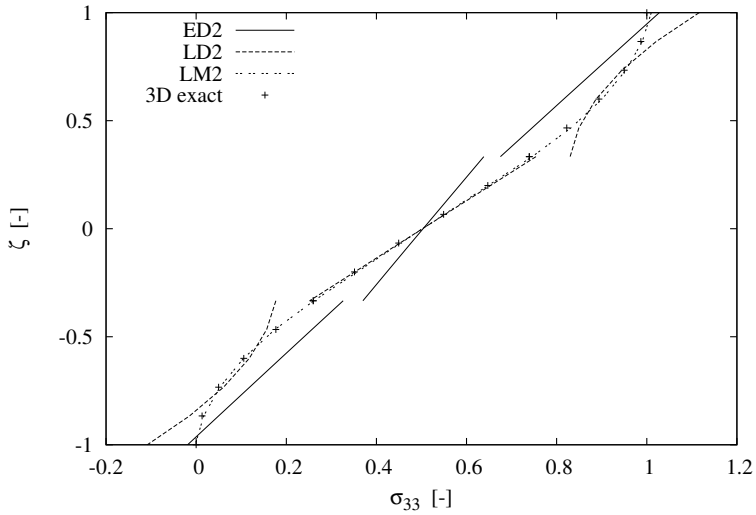

Figure 5.23. σ_{33} in the center of the plate along thickness ζ; $a/h = 10$, [0/90/0]; Problem I

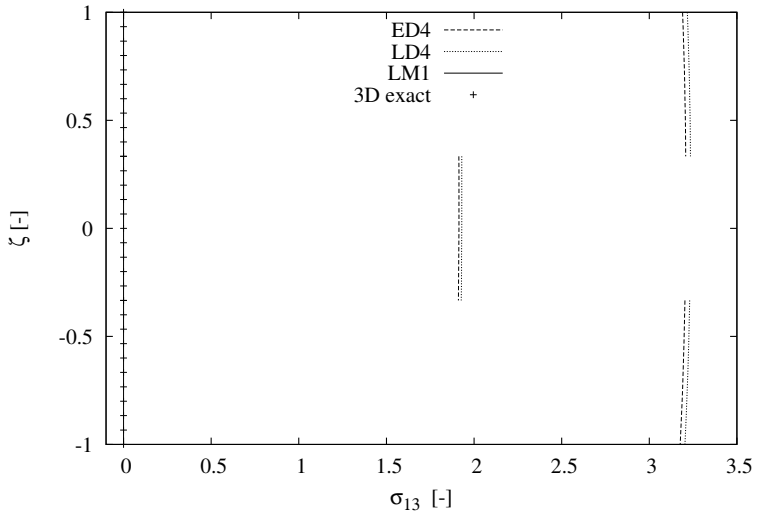

Figure 5.24. σ_{13} in the center of the plate along thickness ζ; $a/h = 10$, [0/90/0]; Problem I

Results on maximum stress failure criteria

The results show the necessity of using mixed formulations for failure analysis. With PVD models, the wrong transverse shear stresses σ_{13} and σ_{23} appear in the center of the plate, which should be zero for problem II. These wrong stresses can be so high for thin plates that they reach the minimum failure load and lead to wrong results. The minimum failure load is not affected for thicker plates, but the numbers in the distribution of the failure index along the z-direction become not longer reasonable in some areas where these wrong transverse stresses are too high. Therefore, only mixed models should be used for running failure analysis. The results of the minimum first-ply failure loading values are presented in Tab. 5.18. LM models achieve very accurate results even with second order expansions. For most of the addressed cases, minimum failure load occurs in the central point of the plate. These locations along the z-direction can be dissimilar for different stacking-sequences. For the [0/45/0] case, the critical points are found in the layer interfaces which can be identified in Fig. 5.25, while for [0/90/0] and [0/90/0/90] failure occurs at the top of the plate (Figs. 5.26,5.27). The results of [0/90/0] and [0/90/0/90] are compared with Pagano's 3D exact solution of reference [3]. Convergence for the minimum first-ply failure load is shown in Tab. 5.19. Furthermore, many analysis have been performed for the 3-layer case, with a step wise change of 15 deg. in the orientation of the middle layer. The results are shown in Fig. 5.28. It can be concluded that the most critical point for failure in the z-direction depends to a great extent on the ply angles of the laminate and can change from the top to the interfaces of the lamination.

a/h	100	50	10
[MPa]	$\times 10^{-2}$	$\times 10^{-1}$	$\times 1$
Analytical			
3D Pagano	9.1838	3.6434	7.2858
MUL2, Q4, 8×8			
Classical ESL models			
ED1	3.6496*	2.6682*	5.9578
ED2	3.4410*	2.7355*	7.7215
ED3	3.4386*	2.7280*	7.1818
ED4	3.4386*	2.7280*	7.3307
Classical LW models			
LD1	3.4620*	2.7470*	6.5592
LD2	3.4382*	2.7268*	7.2457
LD3	3.4382*	2.7267*	7.2847
LD4	3.4382*	2.7267*	7.2901
Mixed LW models			
LM1	8.2752	3.2824	6.5338
LM2	9.2822	3.6798	7.2344
LM3	9.2829	3.6805	7.2579
LM4	9.2829	3.6807	7.2613

(*)Minimum failure loading due to wrong transverse shear stresses

Table 5.18. Minimum first-ply failure loading values; [0/90/0] stacking sequence; Problem I

[MPa]	$a/h = 100$ $\times 10^{-2}$	$a/h = 50$ $\times 10^{-1}$	$a/h = 10$ $\times 1$
3D Pagano	9.1838	3.6434	7.2858
$Q4$, 6×6	9.3656	3.7106	7.2115
$Q4$, 8×8	9.2822	3.6798	7.2344
$Q4$, 10×10	9.2455	3.6660	7.2432

Table 5.19. Convergence of first-ply failure loading values with Maximum Stress Criterion; [0/90/0] stacking sequence, LM2 results; Problem I

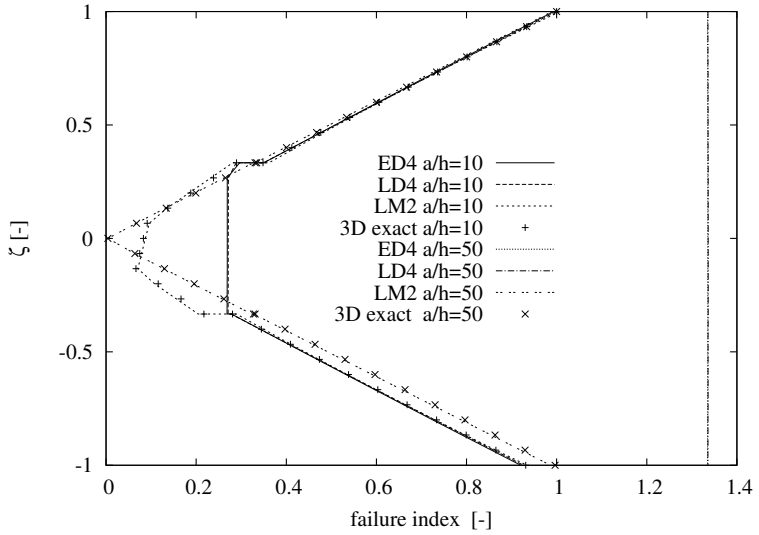

Figure 5.25. Failure index via max stress criterion along thickness ζ; [0/90/0], $a/h = 10$, $a/h = 50$; Problem I

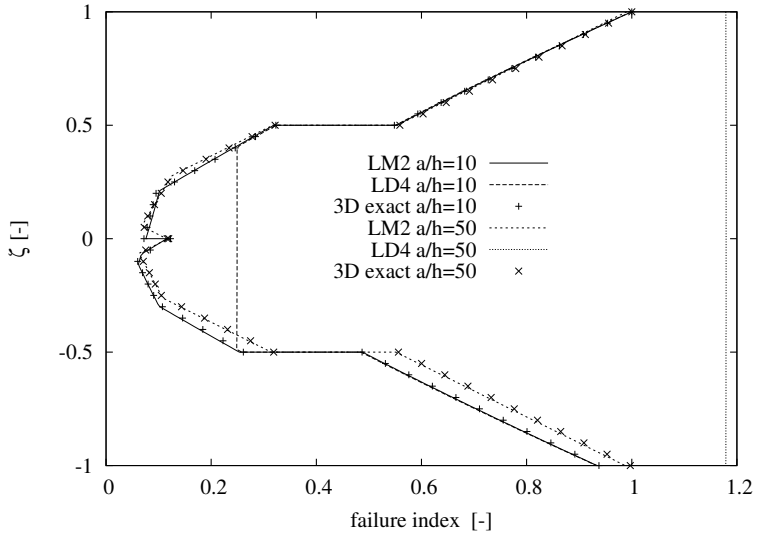

Figure 5.26. Failure index via max stress criterion along thickness ζ; [0/90/0/90], $a/h = 10$ and $a/h = 50$; Problem I

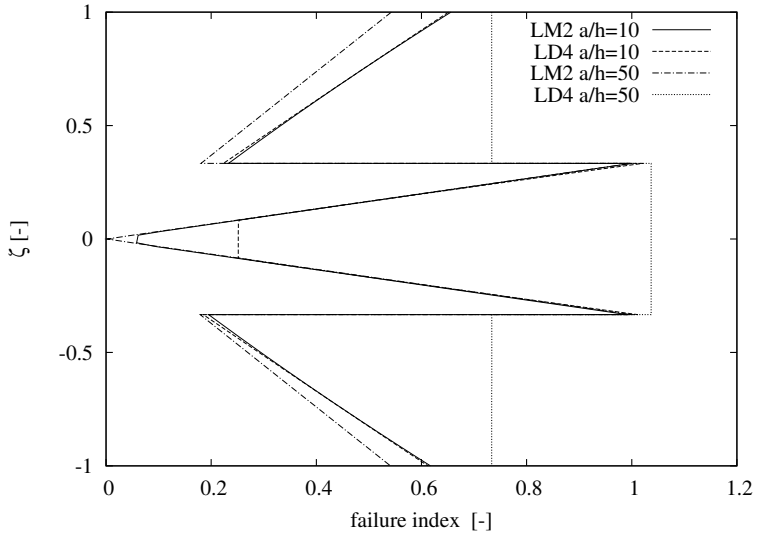

Figure 5.27. Failure index via max stress criterion along thickness ζ; [0/45/0], $a/h = 10$, $a/h = 50$; Problem I

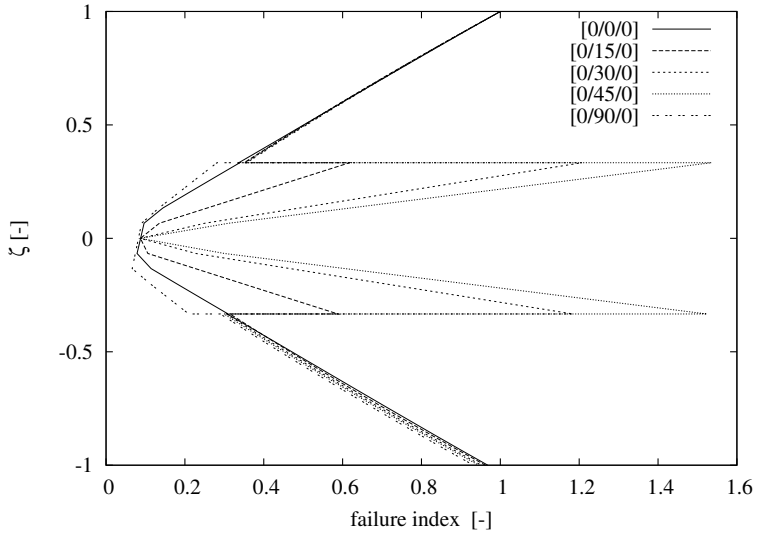

Figure 5.28. Failure index via max stress criterion along ζ for various lamination angles; $a/h = 10$, minimum failure load at the top; LM2 model; Problem II

A global/scalar parameter for stress accuracy evaluation

In order to describe the performance of modelling stresses with a FEM model, it is necessary to consider all six stresses σ_{11}, σ_{22}, σ_{12}, σ_{13}, σ_{23}, σ_{33} and their distribution along z. If just particular stresses or particular locations in the thickness-direction are considered, the quality of a model cannot be described satisfactorily. Therefore, a simple global parameter for the accuracy of stresses of different FEM models has been adopted. The idea is to consider all six stresses and give their accuracy in comparison with a reference solution: the squared difference between the FEM and the reference solution is integrated numerically along z and the results is divided by the integral along z of the squared reference solution. This for each one of the six stress components. The result is multiplied by a factor of 100 in order to obtain the normalized percent error ***ER*** as a final value. The errors of all the stresses can then be summed to have a global indicator of solution fairness. According to this criterion, the results close to zero confirm a very accurate modelling (low error), while high values indicate that the model is not appropriate for the stress/failure index calculation. Tabs. 5.20,5.21 show the results of ***ER*** for problem II. The results are very accurate for plane stresses as nearly all the models provide an error of about 1% or even less. Considering transverse stresses, the error rises for all the PVD models, especially for ED1, whose solution is totally out of range (although the thickness locking correction is active). RMVT-based models are able to provide a very accurate description of transverse stresses. In particular, higher orders provide almost the exact solution for all six stresses. The ED1 results are the worst and the other theories all lie in-between. The dependency of ***ER*** on the lamination angle for different theories is also shown in Fig. 5.29. Different behaviors can be obtained with other theories.

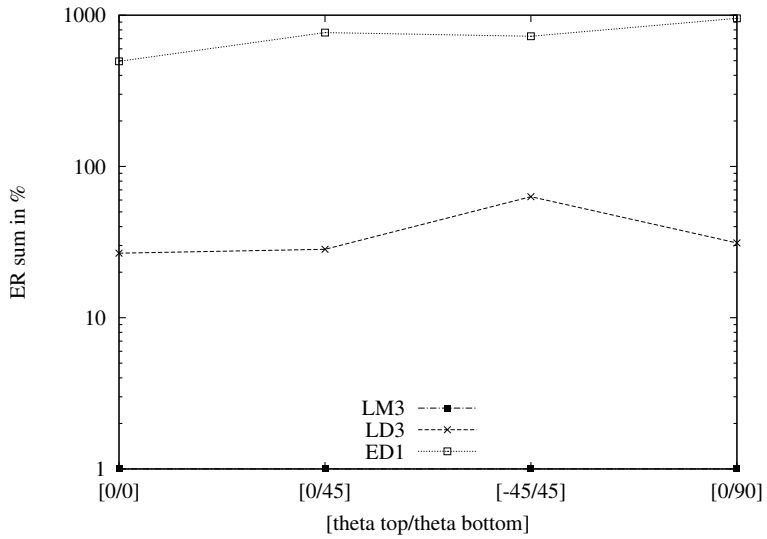

Figure 5.29. Dependency of ER on the lamination angle theta, LM3 results as reference; Problem II

	$ER(\sigma_{11})$ $(a/2,a/2)$	$ER(\sigma_{22})$ $(a/2,a/2)$	$ER(\sigma_{12})$ (0,0)	$ER(\sigma_{13})$ $(0,a/2)$	$ER(\sigma_{23})$ $(a/2,0)$	$ER(\sigma_{33})$ $(a/2,a/2)$	sum
Classical ESL							
ED1	1.85	1.95	1.65	37.74	37.38	873.07	953.6
ED2	1.33	1.31	0.61	34.22	34.19	46.07	117.7
ED3	0.72	0.73	0.35	18.78	19.20	38.69	78.5
ED4	0.62	0.63	0.22	17.75	18.07	33.43	70.7
Classical LW							
LD1	3.73	3.79	2.38	34.56	34.54	371.59	450.6
LD2	0.79	0.80	0.43	22.74	23.17	8.19	56.1
LD3	0.13	0.13	0.02	13.08	13.33	4.55	31.2
LD4	0.12	0.12	0.02	13.08	13.33	3.63	30.3
Mixed LW							
LM1	5.82	5.94	1.11	30.71	30.44	8.59	82.6
LM2	0.88	0.89	0.49	14.15	14.41	2.51	33.3
LM3	0.46	0.46	0.39	0.92	0.92	0.36	3.5

Table 5.20. ER in % for all the six stresses; stacking sequence [90/0] (top-to-bottom); Pagano 3D solution as reference; Problem II

	$ER(\sigma_{11})$ $(a/2,a/2)$	$ER(\sigma_{22})$ $(a/2,a/2)$	$ER(\sigma_{12})$ (0,0)	$ER(\sigma_{13})$ $(0,a/2)$	$ER(\sigma_{23})$ $(a/2,0)$	$ER(\sigma_{33})$ $(a/2,a/2)$	sum
Classical ESL							
ED1	4.76	4.98	2.77	49.51	40.35	403.17	505.5
ED2	4.46	4.25	2.89	48.41	36.34	13.01	109.4
ED3	0.83	0.93	0.71	20.55	21.70	17.18	61.9
ED4	0.91	0.43	0.71	20.57	21.75	4.63	49.0
Classical LW							
LD1	1.37	4.80	0.95	23.47	30.13	140.56	201.3
LD2	0.19	0.55	0.15	5.68	21.16	4.03	31.8
LD3	0.05	0.24	0.09	4.79	19.52	2.02	26.7
LD4	0.05	0.24	0.09	4.79	19.52	1.97	26.7
Mixed LW							
LM1	2.46	5.93	1.38	4.92	22.06	71.29	108.0
LM2	0.41	0.63	0.44	3.01	7.53	0.52	12.5
LM3	0.21	0.33	0.35	0.42	0.63	0.31	2.3

Table 5.21. ER in % for all the six stresses; stacking sequence [0/90/0]; Pagano 3D solution as reference; Problem II

Chapter 6

Thermo-mechanical results

In order to simplify the notation, in this chapter PVD (D in acronyms) stands for PVD-u_x,u_y,u_z or for PVD-u_x,u_y,u_z,θ if pure mechanical or thermo-mechanical analysis is addressed to, respectively.

6.1 Mechanical loading: static instantaneous thermo-mechanical analysis

A simply supported square aluminum plate is considered to investigate the "full" coupling between temperature and mechanical fields. To the authors' best knowledge no results are available on that topic. The reason of this absence lies on the fact that such a coupling is negligible for those materials which are normally employed in thermal structures. The analysis of a simple isotropic plate is proposed. Results are shown in dimensional form so that numbers can be judged by engineering sense. The mechanical properties are: $E = 73$ $[GPa]$, $\nu = 0.3$, $\alpha = 25E\text{-}6$ $[K^{-1}]$, $C = 897$ $[J/(kg \cdot K)]$, $\rho = 2800$ $[kg/m^3]$.
The plate dimensions are: length and width $a = b = 10$ $[m]$, thickness $h = 1$ $[m]$. The plate is loaded at the top face by the bi-sinusoidal pressure of peak value $p_m = 2E7$ $[Pa]$. Such load leads to a stress condition very close to the material elastic limit: $\sigma_{xx} = \sigma_{yy} \simeq 404E6$ $[Pa]$. Present case study is organized in order to provide an example of the maximum thermal variation caused by a mechanical loading, within the frame of a linear static analysis. A 23×23 mesh of LD4 Q4 elements is employed. In general there is not substantial difference in terms of displacements between those two analysis for the displacements u_x and u_y. A slight difference can be seen in Fig. 6.1 for u_z. Such distinction is still very small and it is justified by the fact that for a fully coupled thermo-mechanical analysis, a small part of work is employed to modify the temperature of the plate. The u_z displacement for this kind of analysis results to be smaller than the one obtained by a simple mechanical analysis because a part of work is used to develop the temperature variation. The same amount of work is subtracted from the work used to deform the plate. It can be demonstrated that only a small part of work has been used to modify the temperature. In fact, Fig. 6.2 shows that the maximum thermal variation is lower than 2.5 $[K]$ (with the stresses close to the elastic limit). Fig. 6.3 gives a three dimensional representation of the thermal field calculated at the top/bottom face of the plate (the thickness axis is scaled unequally in order to make the temperature field more visible). It is understood that the calculated temperature profile concerns the first moment in which the *static* load is applied to the structure. In fact, after the transient heat change into the plate itself, the temperature variation would be equal to

zero wherever in the plate and the displacement field will become coincident to the one calculated in a pure mechanical analysis.

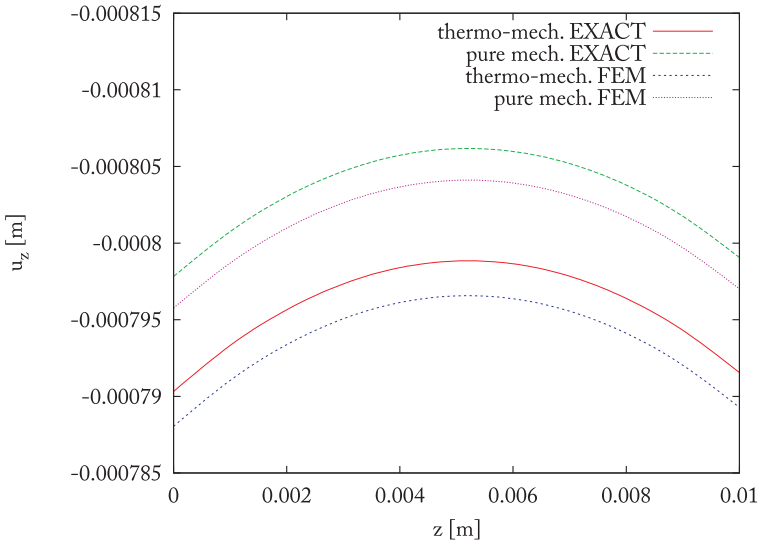

Figure 6.1. Through-the-thickness displacement at the plate position $(\frac{a}{2}, \frac{b}{2})$ - a regular 23×23 mesh of Q4 LD4 FEs is employed

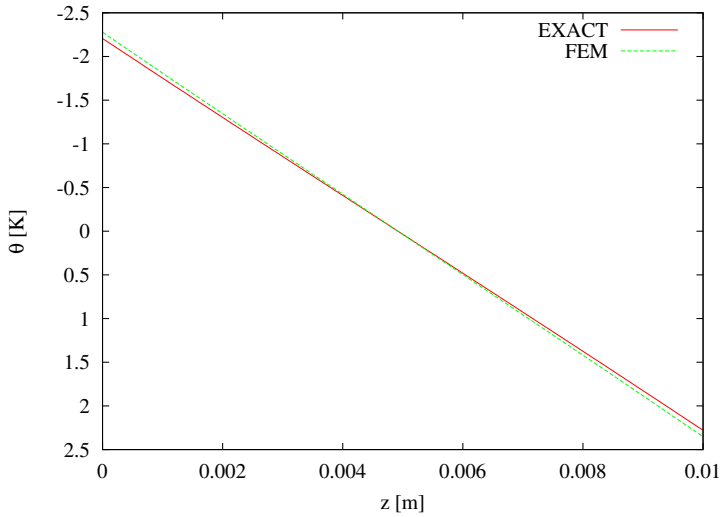

Figure 6.2. Through-the-thickness temperature profile at the plate position $(\frac{a}{2}, \frac{b}{2})$ - a regular 23×23 mesh of Q4 LD4 FEs is employed

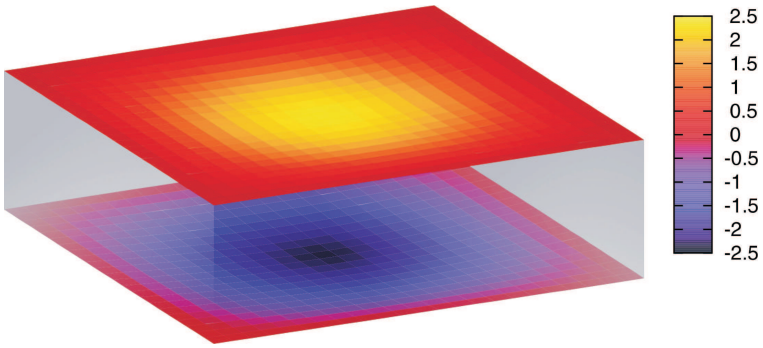

Figure 6.3. View of the plate under static deformation; the colors at the top and bottom faces indicate the instantaneous temperature variation - unit of measurement $[K]$

6.2 Thermal loading: static displacement and stress assessment

In this section several FEM results of thermo-mechanical static analysis of multilayered anisotropic plates obtained in MUL2 are compared to the 3D exact solutions found by Bhaskar and Varadan [24]. Numerical results are presented for the bending of a $(0°/90°/0°)$ square (a=b) laminate due to the temperature field given by

$$\theta = \overline{\theta}(2z/h)sin(\frac{\pi x}{a})sin(\frac{\pi y}{b}), \tag{6.1}$$

where h is the total thickness of the laminate. The following material properties, typical of high-modulus graphite/epoxy, are assumed:

$$\begin{aligned} &E_L/E_T = 25; \\ &G_{LT}/E_T = 0.5; \\ &G_{TT}/E_T = 0.2; \\ &\nu_{LT}/\nu_{TT} = 0.25; \\ &\alpha_T/\alpha_L = 1125, \end{aligned}$$

where L and T refer to directions parallel and perpendicular, respectively, to the fibres. In the FEM analysis, the dimensional values given for material properties are though coherently with the above given dimensionless ratios.
Note that the distribution of temperature along the thickness, for given thermal boundary conditions at the top and at the bottom surfaces, can be obtained by solution of the heat conduction equation (see, for example, the work of Tungikar and Rao [25]). However, only simple linear antisymmetric (with respect to z) thermal variation is considered as this would lead to bending (without stretching) of a symmetric laminate and would be adequate to bring out the importance of non-classical influences such as shear deformation and thickness stretch.
The deflections and stresses are presented in terms of the following dimensionless parameters (sign $\widetilde{}$):

$$\widetilde{u}_z = \frac{u_z}{h\alpha_L\overline{\theta}(\frac{a}{h})^2}, \qquad (\widetilde{u}_x,\widetilde{u}_y) = \frac{(u_x,u_y)}{h\alpha_L\overline{\theta}\frac{a}{h}}, \qquad \widetilde{\sigma}_{ij} = \frac{\sigma_{ij}}{E_T\alpha_L\overline{\theta}}.$$

In Tabs. 6.1,6.2 there is a comparisons between the 3D exact solution of the above described problem [24] and the FEM results obtained by multifield FEs of different accuracy along the

thickness. Results in Tab. 6.1 are free of thickness locking since the reduction of the constitutive relations (Eqs. 2.7). Even if the employed mesh is not particularly refined, LD4 FEM results are in very good agreement with the exact solution, both for displacement and for in-plane stresses. In the other side, results obtained by LD1 FEs are in general accurate only for thin plates.
Results of the convergence study for displacements and for in-plane stresses can be found in Figs. 6.4,6.5. It can be noticed that FEM solutions converge to the 3D exact values [24] and that accurate results for displacements and in-plane stresses are obtained by Q9 FEs even with a poor mesh. Moreover, it is conformed that the convergence is much faster for displacements than for stresses. Additional details on the thermo-mechanical coupling effect can be found in a previous work [26].

$\frac{a}{h}$	*sol.*	$\widetilde{u}_x(\mp\frac{h}{2})$	$\widetilde{u}_y(\mp\frac{h}{2})$	$\widetilde{u}_z(\mp\frac{h}{2})$	$\widetilde{\sigma}_{xx}(\pm\frac{h}{2})$	$\widetilde{\sigma}_{yy}(\mp\frac{h}{2})$	$\widetilde{\sigma}_{xy}(\mp\frac{h}{2})$
2	3D[24]	±20.04	±151.4	96.79	±1390	±635.4	±269.3
2	FEM	±12.88	±162.4	90.38	±672.3	±711.3	±281.5
4	3D[24]	±18.11	±81.83	42.69	±1183	±856.1	±157.0
4	FEM	±16.51	±86.08	41.82	±916.0	±960.2	±164.9
10	3D[24]	±16.61	±31.95	17.39	±1026	±1014	±76.29
10	FEM	±17.31	±33.47	17.84	±945.3	±1134	±81.65
20	3D[24]	±16.17	±20.34	12.12	±982.0	±1051	±57.35
20	FEM	±17.29	±21.59	12.82	±936.4	±1173	±62.55
50	3D[24]	±16.02	±16.71	10.50	±967.5	±1063	±51.41
50	FEM	±17.26	±17.92	11.27	±931.7	±1186	±56.55
100	3D[24]	±16.00	±16.17	10.26	±965.4	±1065	±50.53
100	FEM	±17.25	±17.40	11.05	±930.1	±1187	±55.65
CLT	EX.[24]	±15.99	±15.99	10.18	±964.6	±1065	±50.24

Table 6.1. z values are given in parentheses; (x,y) values are: ($a/2$,$a/2$) for $\widetilde{u}_z$, $\widetilde{\sigma}_{xx}$ and $\widetilde{\sigma}_{yy}$; (0,$a/2$) for $\widetilde{u}_x$; ($a/2$,0) for $\widetilde{u}_y$ and (0,0) for $\widetilde{\sigma}_{xy}$ - a regular 6×6 mesh of Q9 LD1 FEs is employed

$\frac{a}{h}$	*sol.*	$\widetilde{u}_x(\mp\frac{h}{2})$	$\widetilde{u}_y(\mp\frac{h}{2})$	$\widetilde{u}_z(\mp\frac{h}{2})$	$\widetilde{\sigma}_{xx}(\pm\frac{h}{2})$	$\widetilde{\sigma}_{yy}(\mp\frac{h}{2})$	$\widetilde{\sigma}_{xy}(\mp\frac{h}{2})$
2	3D[24]	±20.04	±151.4	96.79	±1390	±635.4	±269.3
2	FEM	±20.09	±151.4	96.74	±1432	±624.2	±275.3
4	3D[24]	±18.11	±81.83	42.69	±1183	±856.1	±157.0
4	FEM	±18.16	±81.82	42.68	±1220	±850.2	±160.5
10	3D[24]	±16.61	±31.95	17.39	±1026	±1014	±76.29
10	FEM	±16.66	±31.91	17.39	±1059	±1012	±78.05
20	3D[24]	±16.17	±20.34	12.12	±982.0	±1051	±57.35
20	FEM	±16.21	±20.29	12.12	±1013	±1050	±58.69
50	3D[24]	±16.02	±16.71	10.50	±967.5	±1063	±51.41
50	FEM	±16.05	±16.68	10.50	±997.4	±1061	±52.58
100	3D[24]	±16.00	±16.17	10.26	±965.4	±1065	±50.53
100	FEM	±16.01	±16.16	10.26	±994.3	±1063	±51.66
CLT	EX.[24]	±15.99	±15.99	10.18	±964.6	±1065	±50.24

Table 6.2. z values are given in parentheses; (x,y) values are: ($a/2$,$a/2$) for $\widetilde{u}_z$, $\widetilde{\sigma}_{xx}$ and $\widetilde{\sigma}_{yy}$; (0,$a/2$) for $\widetilde{u}_x$; ($a/2$,0) for $\widetilde{u}_2$ and (0,0) for $\widetilde{\sigma}_{xy}$ - a regular 6×6 mesh of Q9 LD4 FEs is employed

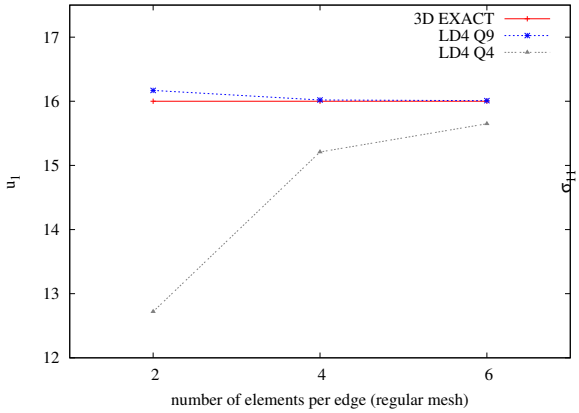

Figure 6.4. Convergence study for displacement u_x

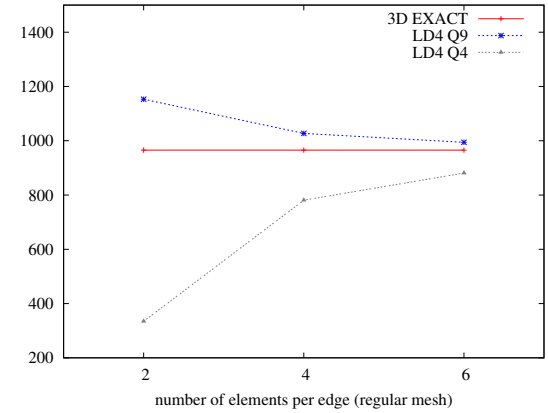

Figure 6.5. Convergence study for stress σ_{xx}

6.3 Thermal loading: assessment of temperature profile, steady-state solution

A simply supported three layered square plate of edge $a = 0.1$ $[m]$ is considered. The top and bottom layer are made of alluminium, having equal tickness h_1. The middle layer is made of steel and has thickness $2 \times h_2$ (Fig. 6.6). Alluminium material properties are $E = 73.0E9$ $[Pa]$, $G = 27.239E9$ $[Pa]$, $\nu = 0.34$, $\alpha = 25.D - 6$ $[K^{-1}]$, $\kappa = 180$ $[W/(m \cdot K)]$, $\rho = 2800$ $[kg/m^3]$ and $C = 897$ $J/(K \cdot kg)$, where α is the coefficient of thermal expansion. Steel coefficients are $E = 210.0E9$ $[Pa]$, $G = 80.77E9$ $[Pa]$, $\nu = 0.3$, $\alpha = 11.1E - 6$ $[K^{-1}]$, $\kappa = 13$ $[W/(m \cdot K)]$, $\rho = 7860$ $[kg/m^3]$, $C = 450$ $J/(K \cdot kg)$. The T_{ref} is set to 298.15 $[K]$. A temperature variation respect to T_{ref} is imposed at the top and at the bottom face of the panel: $+10$ $[K]$ and -10 $[K]$ respectively.
The coupled thermo-mechanical static analysis was run with a regular mesh of 11×11 LD1 FEs to calculate the through-the-thickness temperature profile and the plate displacement caused by the imposed temperatures, at steady-state condition. The attention is restricted to the central point of the plate $(\frac{a}{2}, \frac{a}{2})$.
Each curve in Fig. 6.7, shows a temperature profile along the thickness of the plate. Different geometrical configurations are considered by the variation of h_1 and h_2 mutual dimensions, keeping the same total thickness. The calculated temperatures profiles are in very good agreement to the exact solution obtained applying the Fourier's law (interface points θ_{exact}). In Fig. 6.8 is illustrated the middle plate displacement u_z for the various choices of h_1/h_2 ratios. It can be noted an optimal region for minimum displacement, which is minor than the displacement pertaining to the extreme case of full alluminium/steeel panel. Fig. 6.9 shows the variation of the temperature profile when κ_2 goes progressively from a value appropriate for steel to a value typical of aluminium. The agreement with the exact solution is reconfirmed and it can be noticed that for κ_1/κ_2 the temperature profile becomes linear, as usual for a single-layer panel. Fig. 6.10 shows the variation of u_z for different $\kappa_2 = \kappa_1$ ratios, with κ_1 kept constant. It is visible that the ideal configuration of maximum displacement is for $\kappa_2 = 0$, while any increase in κ_2 leads to a decrease in displacement (until an asymptotic value not present in the figure for scaling reasons). Concluding, present case study shows the usefulness of the formulated thermo-mechanical FEs, which are able to calculate in one single run the steady-state static deformation/stress field of

a structure under thermal loading. The separate application of the Fourier's law to obtain the trough-the-thickness temperature profile is not required. In fact, the temperature distribution through all the layers of the structure is automatically calculated using the information of thermal conductivities, besides the pure mechanical constitutive coefficients.

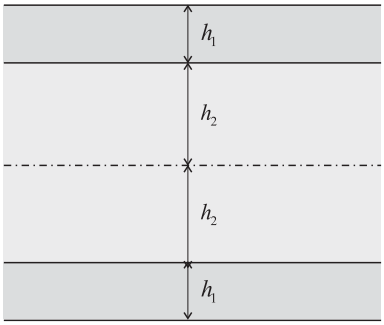

Figure 6.6. Plate-thickness geometry description

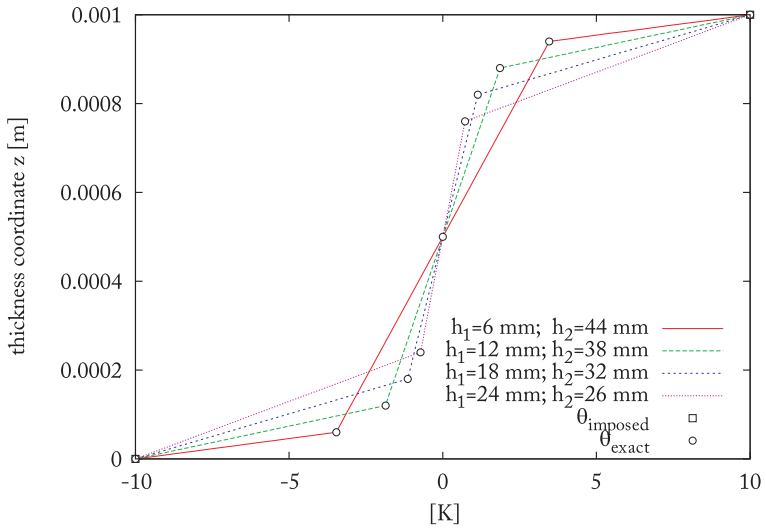

Figure 6.7. Variation of the plate-thickness temperature profile with the ratio h_1/h_2, total thickness constant - point $(\frac{a}{2}, \frac{a}{2})$

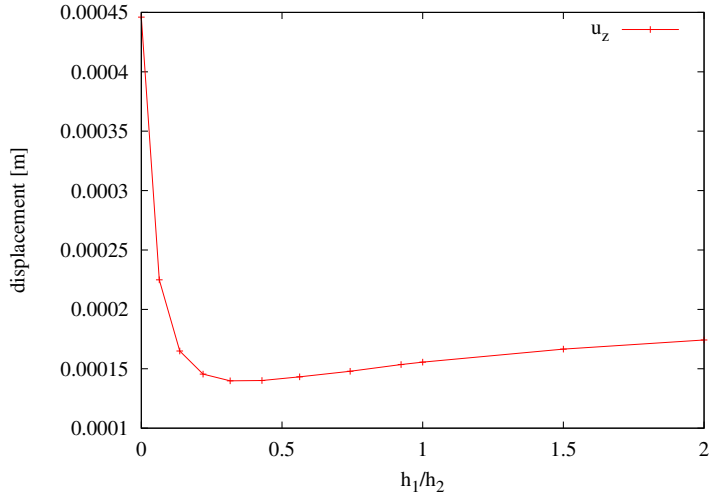

Figure 6.8. Variation of the displacement uz with the ratio h_1/h_2, total thickness constant - middle plate point

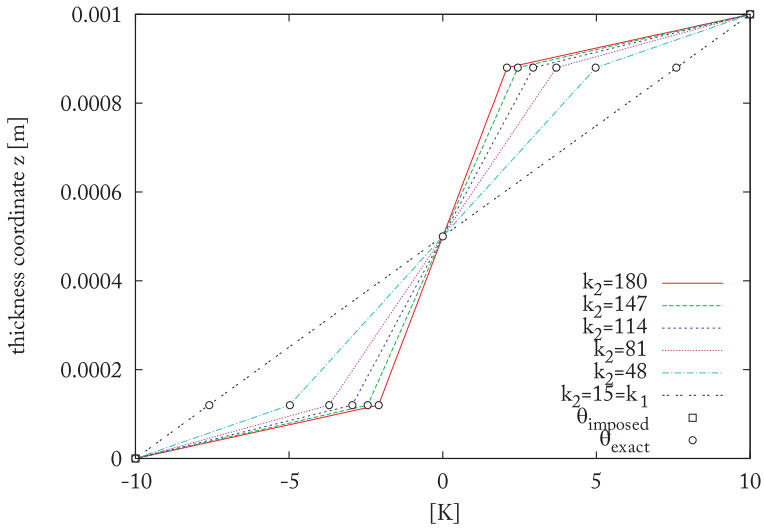

Figure 6.9. Variation of the plate-thickness temperature profile with the ratio κ_2/κ_1, κ_1 constant - point $(\frac{a}{2}, \frac{a}{2})$

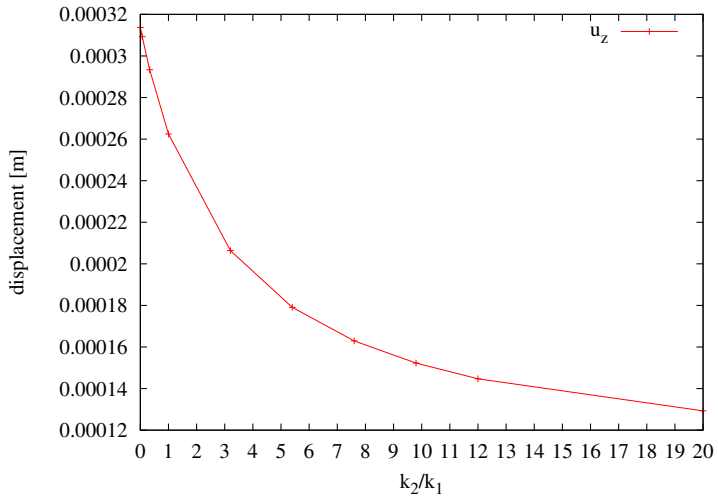

Figure 6.10. Variation of the displacement u_z with the ratio κ_2/κ_1, κ_1 constant - middle plate point

6.4 Thermo-mechanical dynamic analysis of aluminium plate

A mechanically fully clamped square plate of aluminium (material properties in Sec. 6.3) is considered with a regular 20×20 mesh of Q4 ED1 FEs. Two plate thickness ratios are considered: 1/10 and 1/20, with thickness equal to 0.01 $[m]$ and 0.005 $[m]$ respectively. Pure mechanical and thermo-mechanical coupled cases are addressed to. In Tab. 6.3 is the comparison between the undamped natural frequencies calculated in each analysis. It can be noted that natural frequencies are sensitive to thermo-mechanical coupling effects. Moreover it is shown that the percentage error depends not only on thermal coefficients but also, in small quantity, on the thickness ratio (and consequently on the impact of boundary conditions). As conclusion, aluminium can be considered as one of those materials requiring the thermo-mechanical coupling in the modeling, if very accurate results are needed for plate dynamic analysis. Anyway, in the majority of mechaniclal/aerospace engineering applications, the here showed phenomenon can be neglected. In fact, factors of safety usually applied in design largely cover eventual errors like those in Tab. 6.3.

	thickness ratio = 1/10			*thickness ratio* = 1/20		
freq. n.	*pure mech.*	*th.-mech.*	difference	*pure mech.*	*th.-mech.*	difference
1	51740.9	52331.3	+1.14 %	27663.1	28018.1	+1.28 %
2	99963.2	100893	+0.93 %	55888.7	56513.3	+1.12 %
3	99963.2	101094	+1.13 %	55888.7	56649.8	+1.36 %
4	140360	141719	+0.97 %	81005.2	81986.6	+1.21 %
5	167999	168575	+0.34 %	99246.7	100378	+1.14 %
6	168310	168860	+0.33 %	99864.7	101075	+1.21 %
7	168310	169498	+0.71 %	121925	123248	+1.09 %

Table 6.3. Undamped natural frequencies calculated for the pure mechanical case and for the thermo-mechanical coupled case $[Hz]$ - a regular 20×20 mesh of Q4 ED1 FEs is employed

Chapter 7

Electro-mechanical results

In this chapter, PVD (D in acronyms) stands for PVD-u_x,u_y,u_z,ϕ and RMVT-D_z (M in acronyms) stands for RMVT-u_x,u_y,u_z,$\phi(D_z)$ in order to simplify the notation. Results related to RMVT-u_x,u_y,u_z,$\phi(\sigma_{zz}$,σ_{xz},σ_{yz},$D_z)$ are not listed in the following for sake of conciseness: the FEM application of this last particular case of RMVT leads to better convergence properties for transverse stresses respect to RMVT-u_x,u_y,u_z,$\phi(D_z)$ and to PVD-u_x,u_y,u_z,ϕ, but it involves a higher number of DOFs. Moreover, modeling transverse stresses via RMVT does not significantly improve the accuracy of results for D_z.

7.1 Smart structure in various multifield analysis

A mechanically fully clamped piezoelectric multilayered square plate of thickness ratio 3/100 is considered under PVD layer-wise analysis with a regular 4×4 mesh of QUAD-9 elements. Thickness of each layer is equal to 0.1 $[mm]$. A first order through-the-thickness expansion is employed for primary variables. The three layers are orthotropic and of same thickness. Moreover, the material and the laminate system of reference are coincident. The properties of the top and of the bottom layers are those of PZT-4 (piezoelectric mean) while properties of the middle layer are those of the composite material made from graphite fibers preimpregnated with an epoxy resin matrix (Gr/Ep). See Tab. 7.1 for material properties. A comparison is made between the undamped natural frequencies calculated for different cases of coupling. A complete analysis would take into account the coupling between mechanic, electric, magnetic and thermal fields. Since the two considered material don't exhibit significant magnetic properties, magnetic interactions are here neglected, while mechanic, electric and thermal fields are considered in several combination of coupling. From results in Tab. 7.2, it can be noticed that the shift in natural frequencies due to the electro-mechanical coupling contributions is significant. On the contrary, frequencies differences, due to thermal field coupling interactions with the other fields, are relatively small. That is, in this case, materials thermal properties are negligible (see the case of aluminium in Sec. 6.4, in which thermal effects are remarkable). It is understood that, in the most general case, mutual interactions between mechanical, thermal, electrical and magnetic fields should not be ignored "a priori" and that the here proposed formulation can take the part of a tool able to identify which field interactions are relevant or not, when modeling of structures with significant multifield properties is required (e.g. dealing with smart structures).

	PZT-4	Gr/Ep		PZT-4	Gr/Ep		PZT-4	Gr/Ep
$E_1[GPa]$	81.3	132.4	$\varepsilon_{11}[C^2/(N\,m^2)]$	1.306E-8	3.099E-11	$\rho[kg/m^3]$	7500	1550
$E_2[GPa]$	81.3	10.76	$\varepsilon_{22}[C^2/(N\,m^2)]$	1.306E-8	2.656E-11	$\theta_{ref}[K]$	298.15	298.15
$E_3[GPa]$	64.5	10.76	$\varepsilon_{33}[C^2/(N\,m^2)]$	1.151E-8	2.656E-11	$\alpha_1[-]$	4E-6	0.02E-6
$G_{12}[GPa]$	30.6	5.654	$e_{31}[C/m^2]$	-5.2	0	$\alpha_2[-]$	4E-6	0.02E-6
$G_{13}[GPa]$	25.6	5.654	$e_{32}[C/m^2]$	-5.2	0	$\alpha_3[-]$	4E-6	5E-6
$G_{23}[GPa]$	25.6	3.606	$e_{33}[C/m^2]$	15.08	0	$p_1[C/(K\,m^2)]$	4E-4	
$\nu_{12}[-]$	0.33	0.24	$e_{15}[C/m^2]$	12.72	0	$p_2[C/(K\,m^2)]$	4E-4	
$\nu_{13}[-]$	0.43	0.24	$e_{24}[C/m^2]$	12.72	0	$p_3[C/(K\,m^2)]$	4E-4	
$\nu_{23}[-]$	0.43	0.49	$C\,[J/(kg\,K)]$	420	879			

Table 7.1. Material properties of PZT-4 and Gr/Ep

natural	*coupled fields* :			
frequency n.	*pure mechanical*	*thermal-mechanical*	*electrical-mechanical*	*thermal-electrical-mechanical*
1	81.84	81.91	90.61	90.67
2	132.64	132.76	146.08	146.20
3	140.83	141.97	154.22	154.36
4	180.38	180.57	204.46	204.64

Table 7.2. Undamped natural frequencies calculated considering different fields in coupling $[Hz]$

7.2 Comparisons between FEM results and 3D closed form solutions

In this section a few FEM results are compared with the exact solution provided by Heyliger [27]. A three layer thin square plate of unitary side ($a = 1$ $[m]$) loaded by a sinusoidal unitary pressure at the top face ($\widehat{p}_z = 1$ $[N/m^2]$) is considered in the following mechanical assessment. The plate is simply supported at the two opposite sides with zero pressure (cylindrical bending). The layers are of equal thickness and they are made of the same orthotropic material. The total thickness ratio is $a/h = 100$ and the lamination scheme is [0/90/0]. Material properties are: $E_1 = 25$, $E_2 = 1$, $E_3 = 1$, $G_1 = 0.5$, $G_2 = 0.5$, $G_3 = 0.2$ (all in $[GPa]$); $\nu_{12} = 0.25$, $\nu_{13} = 0.25$, $\nu_{25} = 0.25$. Regular $n \times 1$ meshes are considered. Following remark can be made. LMn FEs have good convergence properties. It can be noticed that, even when calculating a displacement, simple FEs like ED1 and ED2 converge to a value different from the 3D solution. Such difference decreases as the order of the thickness expansion increases. The obtained convergence properties are preserved for electrical quantities, when piezoelectric materials are included in the lamination. For sake of conciseness this analysis is not quoted.
A simply supported cross-ply [0/90] laminate composed of an elastic material with piezoelectric layers bonded to the upper and lower surfaces is considered for the following electromechanical case study. The elastic layer of the [0] fiber-angle is on the top. The plate is square with a side length a. The total thickness is h. The elastic layers have a thickness of $0.4h$, while the thickness of the piezoelectric layers is $0.1h$. The plate aspect ratio is $a/h = 4$. The elastic material is modeled as a fiber-reinforced composite and has the properties $E_{11} = 132.38$ (all in $[GPa]$), $E_{22} = 10.756$, $E_{33} = 10.756$, $G_{12} = 3.606$, $G_{13} = 5.654$, $G_{23} = 5.654$, $\nu_{12} = 0.24$, $\nu_{13} = 0.24$, $\nu_{23} = 0.49$, $\varepsilon_{11}/\varepsilon_0 = 3.5$, and $\varepsilon_{22}/\varepsilon_0 = \varepsilon_{33}/\varepsilon_0 = 3.0$. The material of the piezoelectric layers is PZT-4 and the material properties are $E_{11} = E_{22} = 81.3$ (all in $[GPa]$), $E_{33} = 64.5$, $G_{44} = G_{55} = 25.6$, $G_{66} = 30.6$, $\nu_{12} = 0.329$, $\nu_{13} = \nu_{23} = 0.432$, $e_{31} = e_{32} = -5.20$ (all in $[C/m^2]$), $e_{33} = 15.08$, $e_{24} = e_{15} = 12.72$, and $\varepsilon_{11}/\varepsilon_0 = \varepsilon_{22}/\varepsilon_0 = 1475$, $\varepsilon_{33}/\varepsilon_0 = 1300$. The piezoelectric layer thickness is taken as 0.1 $[m]$. Both the sensor case and actuator case are considered in the following (see the two configurations in Fig. 7.1, where p_z indicates a pressure $[N/m^2]$ and ϕ_t indicates the potential $[V]$ imposed on the top face and $\widehat{p}_z = \widehat{\phi}_t = 1$). The analysis will be restricted to LW cases. These last are, in fact, capable to furnish reliable results at each layer interface. A second order thickness expansion is considered to properly calculate the through-the-thickness electric displacement, which clearly shows a parabolic-like trend through the external layers (see Fig. 7.4).

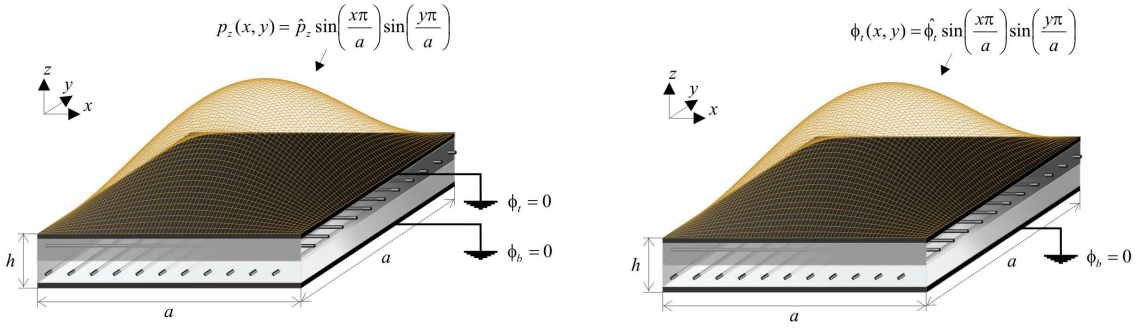

Figure 7.1. On the left the plate in sensor configuration (applied pressure); on the right the plate in actuator configuration (applied potential)

7.2.1 Sensor case

The applied double sinusoidal pressure loading p_z is considered on the top plate surface (sensor configuration). The load amplitude is equal to 1 $[N/m^2]$. The top and bottom laminate surfaces are fixed at zero potential. The FEM results are obtained with a regular 10×10 mesh of LD2 (or LM2) Q4 FEs to minimize computational costs keeping a good accuracy. The exact midplane transverse displacement at the center of the plate is 30.027 $[m]$, while the value calculated by the LD2 or LM2 FEs is 30.119 $[m]$. Additional comparisons between the exact solution [28] and the FEM results are shown in Tabs.7.3-7.5 and in Figs. 7.2-7.4.
A comparison between the 3D-exact solution, PVD and RMVT-D_z results is provided in Tab. 7.3 for displacement u_2 and for the electric potential ϕ: the PVD and RMVT-D_z results are very close and they are in good agreement with the exact solution (see also Figs. 7.2,7.3). In other words, when D_z is modeled by RMVT, the calculated primary variables do not change significantly with respect to PVD. However, if a slight difference is detected, the RMVT results are closer to the exact solution.
A comparison between the 3D-exact solution, PVD and RMVT-D_z results is provided in Tab. 7.4 for the transverse stress σ_{33} and for the in-plane stresses σ_{22} and σ_{12}: the PVD and RMVT-D_z results are close to the exact solutions. It has been confirmed that, even for stresses, the difference between PVD and RMVT-D_z is negligible.
The advantages of RMVT-D_z implementation are evident in Tab. 7.5, where the evaluation of transverse displacement is referred to. The results are compared with 3D-exact and to PVD solutions. It should be underlined that RMVT-D_z leads to an almost 3D-exact description, while PVD results can be affected by very large errors (see also Fig. 7.4). In the RMVT-D_z* column, the D_z is calculated by using the physical constitutive relations in the RMVT-D_z analysis. It can be noted that the RMVT-D_z* results are very close to the PVD ones.
The charge Q, calculated on the top surface of the top layer of the plate through the plate surface integration of D_z, is shown in Tab. 7.6. It is important to underline that RMVT-D_z provides a different charge value from PVD (almost 15% different) and this would encourage the use of RMVT-D_z, which appears mandatory in the sensor case.

	$u_2 \times 10^{12}$	$u_2 \times 10^{12}$	$u_2 \times 10^{12}$	$\phi \times 10^1$	$\phi \times 10^1$	$\phi \times 10^1$
Height	$3D$[28]	PVD	$RMVT\text{-}D_z$	$3D$[28]	PVD	$RMVT\text{-}D_z$
1.000	-47.549	-45.593	-45.594	0.0000	0.0000	0.0000
0.975	-41.425	-39.527	-39.528	0.0189	0.0181	0.0181
0.950	-35.424	-33.567	-33.569	0.0358	0.0336	0.0336
0.925	-29.531	-27.715	-27.772	0.0488	0.0464	0.0464
0.900	-23.732	-21.969	-21.970	0.0598	0.0567	0.0567
0.800	-10.480	-10.058	-10.577	0.0589	0.0560	0.0559
0.700	0.1413	-0.0836	-0.0836	0.0589	0.0560	0.0559
0.600	9.8917	9.5104	9.5108	0.0596	0.0567	0.0567
0.500	20.392	18.205	18.206	0.0611	0.0583	0.0583
0.400	24.768	22.149	22.150	0.0634	0.0606	0.0605
0.300	29.110	26.700	26.703	0.0665	0.0637	0.0637
0.200	33.819	31.860	31.863	0.0706	0.0677	0.0677
0.100	39.309	37.628	37.632	0.0756	0.0726	0.0726
0.075	44.492	42.930	42.934	0.0602	0.0581	0.0581
0.050	49.772	48.341	48.346	0.0425	0.0411	0.0411
0.025	55.163	53.863	53.867	0.0224	0.0218	0.0218
0.000	60.678	59.494	59.499	0.0000	0.0000	0.0000

Table 7.3. PVD and RMVT-D_z results: comparison between LD2 and LM2 FEM solutions with the 3D-exact solution, sensor case. Displacements are in $[m]$; electric potential is in $[V]$. $u_2 = u_2(a/2,0)$; $\phi = \phi(a/2,b/2)$.

	$\sigma_{33} \times 10^1$	$\sigma_{33} \times 10^1$	$\sigma_{33} \times 10^1$	σ_{22}	σ_{22}	σ_{22}	σ_{12}	σ_{12}	σ_{12}
Height	$3D$[28]	PVD	$RMVT\text{-}D_z$	$3D$[28]	PVD	$RMVT\text{-}D_z$	$3D$[28]	PVD	$RMVT\text{-}D_z$
1.000	10.000	9.6313	9.6381	6.5643	6.2392	6.2387	-2.4766	-2.3547	-2.3546
0.975	9.9657	9.4336	9.4354	5.8201	5.5033	5.5030	-2.1824	-2.0680	-2.0679
0.950	9.8682	9.3631	9.3598	5.0855	4.7857	4.7856	-1.8942	-1.7866	-1.7864
0.925	9.7154	9.4197	9.4112	4.3595	4.0865	4.0866	-1.6114	-1.5103	-1.5102
0.900	9.5151	9.6034	9.5898	3.6408	3.4057	3.4059	-1.3332	-1.2393	-1.2392
0.900	9.5151	10.163	10.163	2.8855	3.8364	3.8362	-0.2463	-0.2290	-0.2290
0.800	8.5199	8.7018	8.7018	1.4499	2.0094	2.0093	-0.1534	-0.1475	-0.1474
0.700	7.3747	7.4395	7.4395	0.2879	0.3332	0.3332	-0.0817	-0.0776	-0.0775
0.600	6.1686	6.3764	6.3764	-0.7817	-1.1923	-1.1922	-0.0212	-0.0193	-0.0193
0.500	4.9831	5.5124	5.5124	-1.9266	-2.5670	-2.5669	0.0369	0.0274	0.0274
0.500	4.9831	4.9178	4.9179	0.0991	0.0527	0.0527	0.0369	0.0274	0.0274
0.400	3.8045	3.9244	3.9244	-0.0149	-0.0683	-0.0683	0.0965	0.0771	0.0771
0.300	2.6137	2.8259	2.8259	-0.1280	-0.2049	-0.2049	0.1529	0.1335	0.1335
0.200	1.4821	1.6223	1.6223	-0.2426	-0.3571	-0.3570	0.2139	0.1966	0.1966
0.100	0.4868	0.3136	0.3136	-0.3616	-0.5248	-0.5247	0.2882	0.2663	0.2663
0.100	0.4868	0.8251	0.8365	-4.2348	-3.9325	-3.9325	1.5603	1.4415	1.4413
0.075	0.2845	0.9872	0.9436	-4.8806	-4.5636	-4.5634	1.8105	1.6933	1.6931
0.050	0.1312	1.0311	1.0339	-5.5337	-5.2123	-5.2119	2.0651	1.9499	1.9498
0.025	0.0340	0.9568	0.9553	-6.1951	-5.8785	5.8780	2.3246	2.2115	2.2113
0.000	0.0000	0.7641	0.7583	-6.8658	-6.5623	-6.5617	2.5899	2.4779	2.4777

Table 7.4. PVD and RMVT-D_z results: comparison between LD2 and LM2 FEM solutions with the 3D-exact solution, sensor case. Stresses are in $[Pa]$. $\sigma_{33} = \sigma_{33}(a/2,b/2)$; $\sigma_{11} = \sigma_{11}(a/2,b/2)$; $\sigma_{12} = \sigma_{12}(0,0)$.

	$D_z \times 10^{13}$			
Height	3D[28]	$RMVT\text{-}D_z$	PVD	$RMVT\text{-}D_z^*$
1.000	160.58	160.22	239.57	234.38
0.975	149.35	148.27	204.92	203.62
0.950	117.23	117.53	161.38	163.98
0.925	66.568	68.003	108.95	115.44
0.900	-0.3382	-0.3044	47.621	58.008
0.900	-0.3382	-0.3044	-0.2990	-0.3101
0.800	-0.1276	-0.0969	-0.0977	-0.1027
0.700	0.0813	0.1064	0.1037	0.1048
0.600	0.2913	0.3058	0.3051	0.3123
0.500	0.5052	0.5010	0.5065	0.5198
0.500	0.5052	0.5010	0.4943	0.4815
0.400	0.7259	0.7228	0.7236	0.7165
0.300	0.9563	0.9495	0.9529	0.9515
0.200	1.1995	1.1812	1.1821	1.1865
0.100	1.4587	1.4179	1.4114	1.4215
0.100	1.4587	1.4179	-50.162	-58.915
0.075	-58.352	-59.178	-105.53	-111.00
0.050	-103.66	-103.15	-152.63	-154.82
0.025	-132.40	-130.50	-191.45	-190.36
0.000	-142.46	-141.23	-222.00	-217.63

Table 7.5. Comparison between FEM and 3D-exact solutions, sensor case. LD2 and LM2 FEs are employed for PVD and RMVT case, respectively. The electric displacement is in $[c/m^2]$. $D_z = D_z(a/2,b/2)$. The D_z RMVT-$D_z{}^*$ is calculated by constitutive relations in the RMVT-D_z analysis.

$Q \times 10^{11}(RMVT - D_z)$	$Q \times 10^{11}(PVD)$	$Q \times 10^{11}(RMVT - D_z*)$
10.219	8.8763	8.5457

Table 7.6. Comparison between PVD and RMVT-D_z results, sensor case. LD2 or LM2 FEs are employed. Q is the charge at the top surface of the top layer and it is expressed in $[c]$. RMVT-D_z* result is computed starting from the D_z calculated by constitutive relations in the RMVT-D_z analysis.

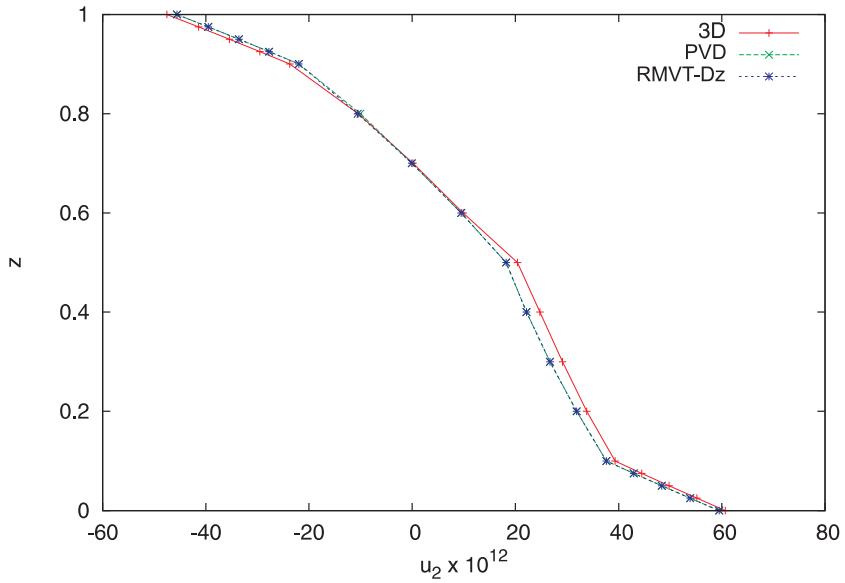

Figure 7.2. Comparison between LD2 FEM and 3D-exact solutions, sensor case; displacements are in $[m]$; $u_2 = u_2(a/2,0)$

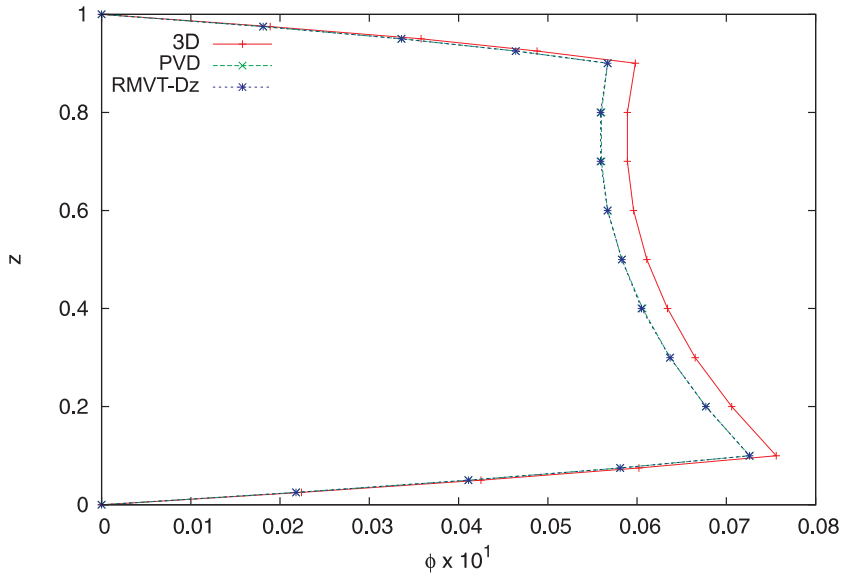

Figure 7.3. Comparison between LD2 FEM and 3D-exact solutions, sensor case; electric potential is in $[V]$; $\phi = \phi(a/2,b/2)$

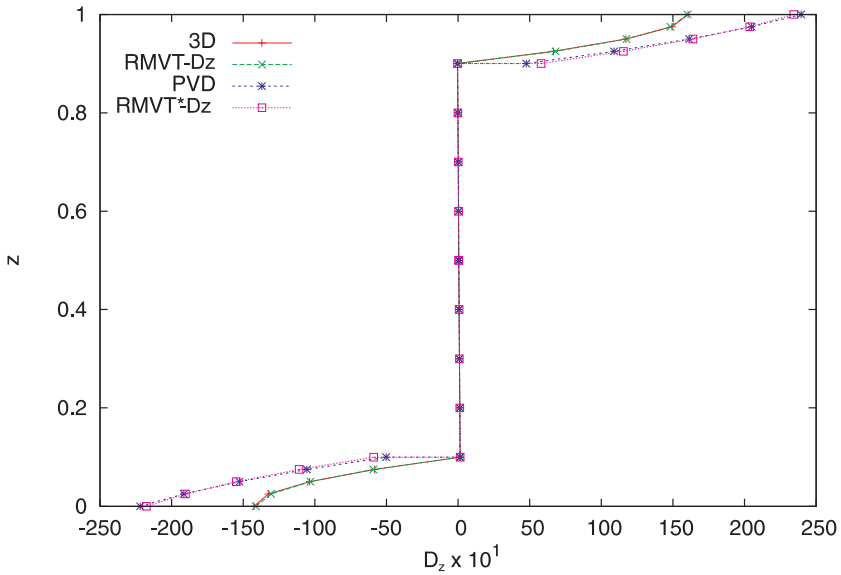

Figure 7.4. Comparison between FEM and 3D-exact solutions, sensor case; the electric displacement is in $[c/m^2]$; $D_3 = D_3(a/2,b/2)$; the D_z RMVT-D_z* is calculated by constitutive relations in the RMVT-D_z analysis

7.2.2 Actuator case

The applied double sinusoidal potential p_z is considered in the top plate surface (actuator configuration). The load amplitude is equal to 1 $[V]$. The bottom laminate surfaces is fixed at zero potential. The FEM results are obtained with a regular 10×10 mesh of LD2 (or LM2) Q4 FEs. The exact midplane transverse displacement at the center of the plate is -14.711×10^{-12} $[m]$, while the value calculated by the LD2 and LM2 FEs are -14.151×10^{-12} $[m]$ and -14.152×10^{-12} $[m]$, respectively. Other comparisons between the exact solution [28] and the FEM results are shown in Tabs.7.7-7.9.
The following remarks can be made. Tab. 7.7 shows that the primary variables, u_2 and ϕ, calculated by FEM are in good agreement with the exact solution provided by Heyliger [28]. As far as Tab. 7.8 is concerned, the in-plane stresses are also calculated with good accuracy, while the normal stress does not have reasonable values around the top and the bottom face of the plate. It is clear, from Tab. 7.9, that the RMVT-D_z modeling, compared to the PVD modeling, does not significantly improve the solution for the actuator case.

	$u_2 \times 10^{12}$	$u_2 \times 10^{12}$	$u_2 \times 10^{12}$	$\phi \times 10^{1}$	$\phi \times 10^{1}$	$\phi \times 10^{1}$
Height	$3D$[28]	PVD	$RMVT\text{-}D_z$	$3D$[28]	PVD	$RMVT\text{-}D_z$
1.000	-32.764	-33.951	-33.951	1.0000	1.0000	1.0000
0.975	-23.349	-24.377	-24.377	0.9971	0.9972	0.9972
0.950	-13.973	-14.826	-14.826	0.9950	0.9951	0.9951
0.925	-4.6174	-5.2983	-5.2977	0.9936	0.9936	0.9936
0.900	4.7356	4.2064	4.2069	0.9929	0.9929	0.9929
0.800	2.9808	2.5445	2.5448	0.8415	0.8423	0.8422
0.700	1.7346	1.2546	1.2548	0.7014	0.7011	0.7011
0.600	0.8008	0.3368	0.3368	0.5707	0.5695	0.5695
0.500	0.0295	-0.2091	-0.2091	0.4476	0.4473	0.4475
0.400	-0.4404	-0.5745	-0.5745	0.3305	0.3310	0.3311
0.300	-0.8815	-0.9518	-0.9517	0.2179	0.2177	0.2177
0.200	-1.3206	-1.3409	-1.3408	0.1081	0.1073	0.1073
0.100	-1.7839	-1.7419	-1.7418	-0.0001	-0.0001	-0.0001
0.075	-2.0470	-1.9963	-1.9963	-0.00009	-0.00009	-0.00009
0.050	-2.3140	-2.2554	-2.2554	-0.00008	-0.00007	-0.00007
0.025	-2.5856	-2.5191	-2.5191	-0.00004	-0.00004	-0.00004
0.000	-2.8625	-2.7875	-2.7876	0.00000	0.00000	0.00000

Table 7.7. PVD and RMVT-D_z results: comparison between LD2 and LM2 FEM solutions with the 3D-exact solution, actuator case. Displacements are in $[m]$; electric potential is in $[V]$. $u_2 = u_2(a/2,0)$; $\phi = \phi(a/2,b/2)$.

	$\sigma_{33} \times 10^1$	$\sigma_{33} \times 10^1$	$\sigma_{33} \times 10^1$	σ_{22}	σ_{22}	σ_{22}	σ_{12}	σ_{12}	σ_{12}
Height	$3D$[28]	PVD	$RMVT\text{-}D_z$	$3D$[28]	PVD	$RMVT\text{-}D_z$	$3D$[28]	PVD	$RMVT\text{-}D_z$
1.000	0.0000	-55.800	-55.419	111.81	113.28	113.26	-146.03	-148.30	-148.30
0.975	-0.8333	-43.279	-43.183	63.736	66.186	66.175	-100.77	-103.03	-103.03
0.950	-2.8471	-28.385	-28.574	15.833	19.448	19.447	-55.693	-57.858	-57.855
0.925	-5.3241	-11.118	-11.592	-32.001	-26.932	-26.923	-10.698	-12.781	-12.778
0.900	-7.5482	8.5218	-7.7627	-79.865	-72.955	-72.935	34.295	32.198	32.221
0.900	-7.5482	-15.579	-15.581	-51.681	-68.096	-68.104	6.3365	5.9489	5.9494
0.800	-12.957	-11.567	-11.569	-33.135	-41.748	-41.753	4.6631	4.2950	4.2954
0.700	-15.245	-11.713	-11.714	-19.840	-21.342	-21.345	3.3247	2.9062	2.9064
0.600	-15.510	-16.014	-16.016	-9.7737	-6.8792	-6.8808	2.2096	1.7823	1.7825
0.500	-14.612	-24.473	-24.475	-1.3905	1.6408	1.6397	1.2286	0.9237	0.9238
0.500	-14.612	-17.335	-17.337	-1.3089	-1.2973	-1.2975	1.2287	0.9237	0.9238
0.400	-12.524	-12.937	-12.939	-0.5782	-3.3075	-3.3091	0.5227	0.3400	0.3401
0.300	-9.2558	-9.2086	-9.2096	0.1348	5.7883	5.7872	-0.0572	-0.1927	-0.1926
0.200	-5.5018	-6.1487	-6.1495	0.8463	1.4314	1.4313	-0.5840	-0.6744	-0.6744
0.100	-1.8733	-3.7579	-3.7583	1.5723	2.2270	2.2270	-1.1220	-1.1051	-1.1051
0.100	-0.8733	-3.3555	-2.8333	14.529	14.007	13.988	-6.0731	-5.9813	-5.9814
0.075	-1.1074	-4.1098	-3.7838	17.801	17.041	17.030	-7.3455	-7.1917	-7.1918
0.050	-0.5162	-4.3795	-4.2493	21.098	20.148	20.144	-8.6346	-8.4220	-8.4222
0.025	-0.1351	-4.1645	-4.2299	24.428	23.328	23.331	-9.9437	-9.6723	-9.6726
0.000	0.0000	-3.4647	-3.7256	27.795	26.581	26.591	-11.276	-10.942	-10.943

Table 7.8. PVD and RMVT-D_z results: comparison between LD2 and LM2 FEM solutions with the 3D-exact solution, actuator case. Stresses are in $[Pa]$. $\sigma_{33} = \sigma_{33}(a/2,b/2)$; $\sigma_{11} = \sigma_{11}(a/2,b/2)$; $\sigma_{12} = \sigma_{12}(0,0)$.

	$D_z \times 10^{13}$		
Height	$RMVT\text{-}D_z$	PVD	$RMVT\text{-}D_z^*$
1.000	-2.4431	-2.4382	-2.4385
0.975	-1.8416	-1.8388	-1.8388
0.950	-1.2408	-1.2395	-1.2394
0.925	-6.4070	-6.4043	-6.4007
0.900	-4.1321	-4.1504	-4.0924
0.900	-4.1321	-4.1274	-4.1294
0.800	-3.8746	-3.8751	-3.8757
0.700	-3.6205	-3.6228	-3.6220
0.600	-3.3700	-3.3705	-3.3682
0.500	-3.1229	-3.1182	-3.1145
0.500	-3.1229	-3.1275	-3.1313
0.400	-3.0498	-3.0492	-3.0515
0.300	-2.9732	-2.9709	-2.9718
0.200	-2.8931	-2.8925	-2.8920
0.100	-2.8095	-2.8142	-2.8123
0.100	-2.8095	-2.8425	-2.8823
0.075	-2.8409	-2.8144	-2.8393
0.050	-2.8384	-2.7898	-2.7997
0.025	-2.8020	-2.7685	-2.7635
0.000	-2.7316	-2.7507	-2.7307

Table 7.9. Comparison between FEM and 3D-exact solutions, actuator case. LD2 and LM2 FEs are employed for PVD and RMVT case, respectively. The electric displacement is in $[c/m^2]$. $D_z = D_z(a/2,b/2)$. The D_z RMVT-$D_z{}^*$ is calculated by constitutive relations in the RMVT-D_z analysis.

7.3 Comparisons between experimental and FEM results

A dynamic test on a one-side clamped composite multilayered plate with four piezoelectric patches is considered. One of these patches is an actuator. Remaining patches are sensors. An additional sensor is given by measurements with a laser vibromiter at a fixed point. Three natural frequencies are detected from the response of the excited structure. Two different softwares, MUL2 and Nastran, are employed to perform the linear modal analysis of the structure. A critical comparison between numerical and experimental frequencies is proposed. Investigations on the electro-mechanical coupling effect and on the higher-order effects are performed in MUL2.

Test description

A dynamic test on a composite multilayered plate with four piezoelectric patches is considered. The plate is clamped at one side. See the picture and the scheme of the system in Figs. 7.5,7.6.

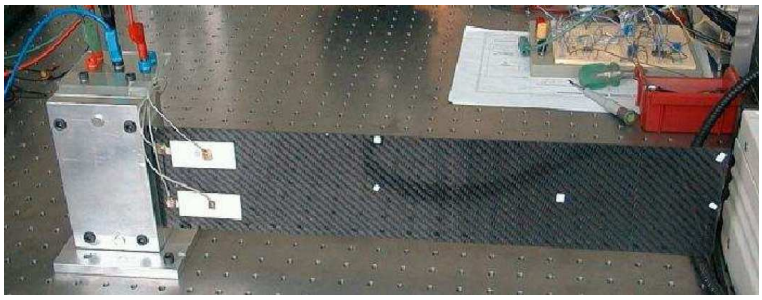

Figure 7.5.

Geometry

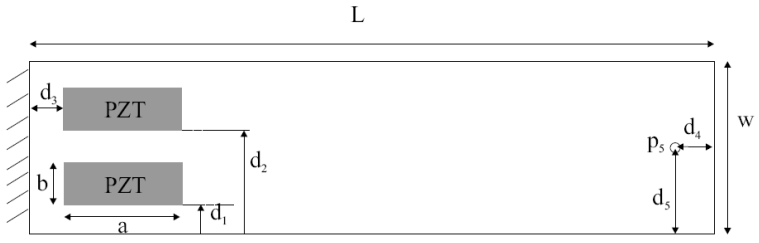

Figure 7.6.

$L = 463$ $[mm]$;
$a = 55$ $[mm]$;
$b = 25$ $[mm]$;
$d_1 = 13$ $[mm]$;
$d_2 = 64$ $[mm]$;
$d_3 = 15$ $[mm]$;
$d_4 = 5$ $[mm]$;
$d_5 = 50$ $[mm]$;
$w = 100$ $[mm]$;
$thickness = 1{,}3$ $[mm]$.

See Fig. 7.7 for a more detailed scheme of the patches. The thickness of each patch is 0.25 $[mm]$.

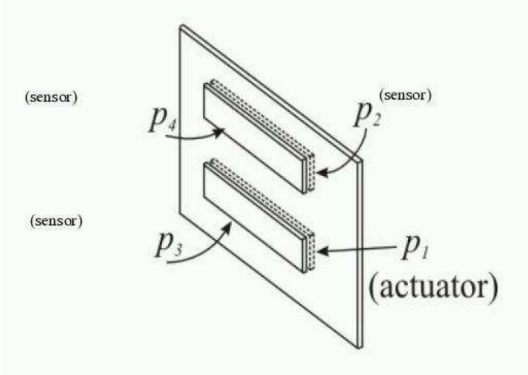

Figure 7.7.

Material properties

The composite is made of six layers of equal thickness and properties (total thickness is 1,3 $[mm]$):

$E_x = 41.5$ $[GPa]$;
$E_y = 41.5$ $[GPa]$;
$G_{xy} = 3.35$ $[GPa]$;
$\nu_{xy} = 0.042$;
$\rho = 1490$ $[Kg/m^3]$.

Material properties of the patches are the followings:

$E = 65$ $[GPa]$;
$d_{31} = d_{32} = -205 \times 10^{-12}$ $[m/V]$;
$\nu = 0.3$;
$\rho = 7800$ $[Kg/m^3]$;
$\varepsilon = 2600$ $[Kg/m^3]$.

Experimental results

The focus id on the velocity-data acquired at point p_5. From Fig. 7.8 three natural frequencies are detected: the first is around 6 $[Hz]$; the second is around 33 $[Hz]$ and the third is around 92 $[Hz]$.

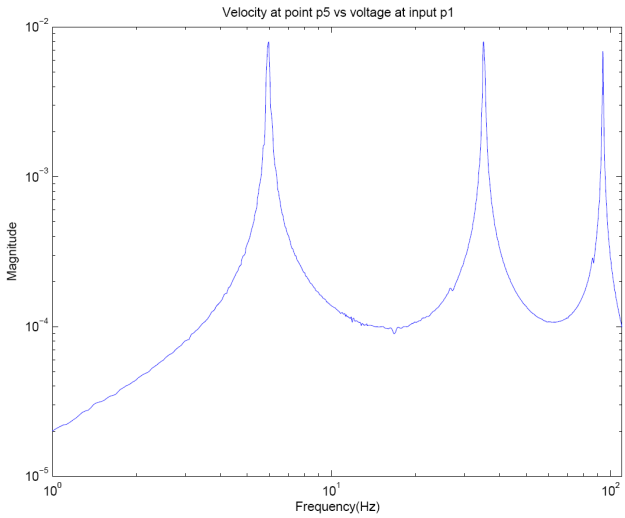

Figure 7.8.

Modeling and comparison of results

The aim of this section is to show how to obtain by modeling the three natural frequencies found during the experiment. Undamped natural frequencies are computed under the common assumption of low damping ratio. Rigorously, a frequency response analysis would be performed, but undamped natural frequencies are calculated by linear modal analysis for computational reasons. In order to retain the consistency with the real system, the stiffness of the actuator patch P_1 is set to zero.
Mechanical modeling has been performed both in $MUL2$ and in Nastran softwares for comparative reasons. ESL theory is employed and the PVD is applied. After a convergence study a regular mesh of 30×10 Q4 FEs is chosen, with a first order through-the-thickness expansion.
In Tab. 7.10 undamped natural frequencies of the composite panel calculated in MUL2 are compared with those calculated in Nastran. The two set of frequencies are in good agreement. Almost all the calculated frequencies slightly increase if the patches are considered in the analysis (the structure is more rigid, compare Tab. 7.11 with 7.10). The Laminate tool has been employed to model the patches in Nastran. Results in Tab. 7.11 are reasonably close to the experimental ones regardless the electro-mechanical coupling is not addressed to in the FEM analysis.
The influence of coupling in the system is summarized in Tab. 7.12, where results of mechanical analysis are compared to results of an electro-mechanical fully coupled analysis. Since a multifield analysis cannot be performed in Nastran, only MUL2 results are presented in Tab. 7.12. It is clear that the stiffening effect due to the electro-mechanical coupling is negligible in this case-study and the reason is in the fact that the piezoelectric patches represent a very small percentage of the structure. In Figs. 7.9-7.20 are represented the mechanical mode shapes calcu-

freq. $[Hz]$	MUL2	Nastran
1	5.1715	5.1682
2	23.812	23.570
3	32.486	32.340
4	77.216	76.198
5	91.399	90.416
6	146.82	143.98

Table 7.10. Undamped natural frequencies of the plate without patches, regular mesh of 30×10 Q4 FEs, first order through-the-thickness expansion - mechanical analysis

frEq. $[Hz]$	MUL2	Nastran	experiment
1	6.3292	5.6742	$\cong 6$
2	25.092	24.458	-
3	36.831	32.563	$\cong 33$
4	80.766	77.288	-
5	99.146	87.056	$\cong 92$
6	152.70	142.04	-

Table 7.11. Undamped natural frequencies of the plate with patches, regular mesh of 30×10 Q4 FEs, first order through-the-thickness expansion - mechanical analysis

frEq. $[Hz]$	MUL2 no coupled	MUL2 coupled
1	6.3292	6.3298
2	25.092	25.093
3	36.831	36.832
4	80.766	80.768
5	99.146	99.149
6	152.70	152.71

Table 7.12. Undamped natural frequencies of the plate with patches, regular mesh of 30×10 Q4 FEs, first order through-the-thickness expansion

lated respectively in MUL2 and in Nastran. Patches are considered, also if they are not visible in Nastran images. It can be noticed that the two analysis are equivalent also concerning mode shapes.
From mode shapes it is clear why some natural frequencies cannot be detected from the experiment: transverse translation of point p_5 is not significantly excited by modes two, four and six. The contrary occurs for modes one, three and five, which are regularly detected during the test.

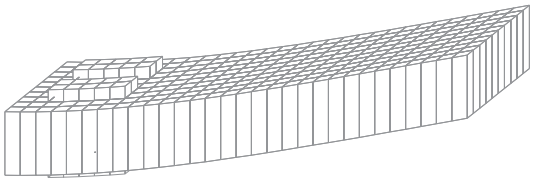

Figure 7.9. First mode shape (MUL2)

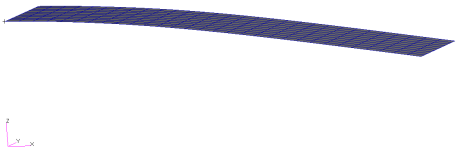

Figure 7.10. First mode shape (Nastran)

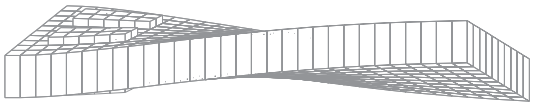

Figure 7.11. Second mode shape (MUL2)

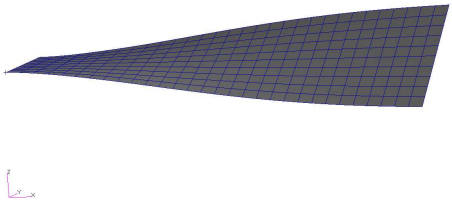

Figure 7.12. Second mode shape (Nastran)

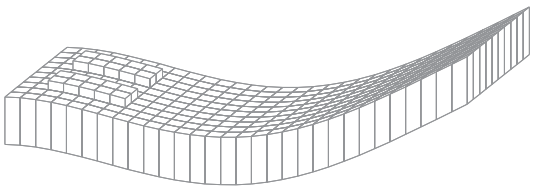

Figure 7.13. Third mode shape (MUL2)

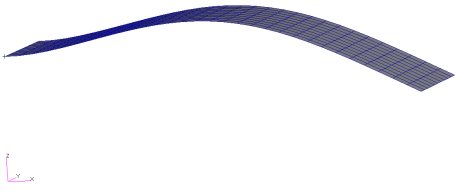

Figure 7.14. Third mode shape (Nastran)

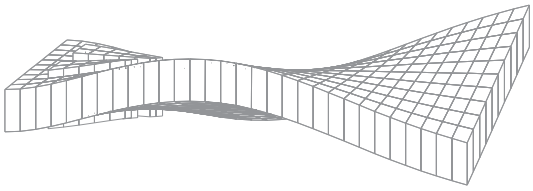

Figure 7.15. Fourth mode shape (MUL2)

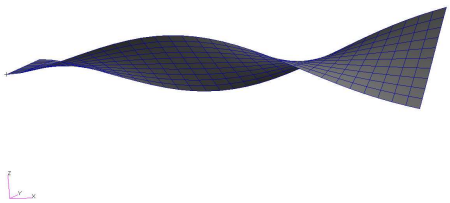

Figure 7.16. Fourth mode shape (Nastran)

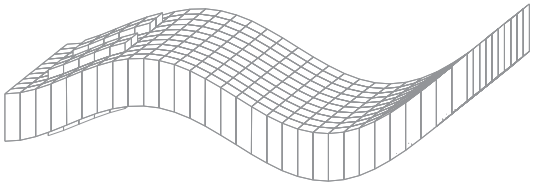

Figure 7.17. Fifth mode shape (MUL2)

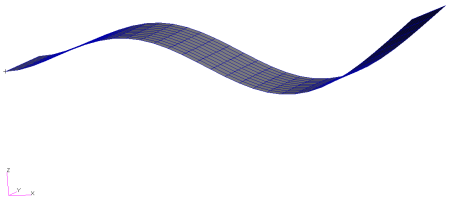

Figure 7.18. Fifth mode shape (Nastran)

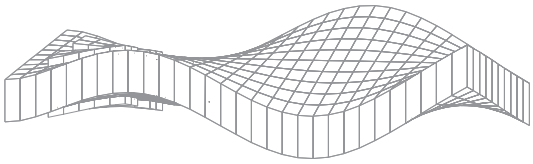

Figure 7.19. Sixth mode shape (Mul2)

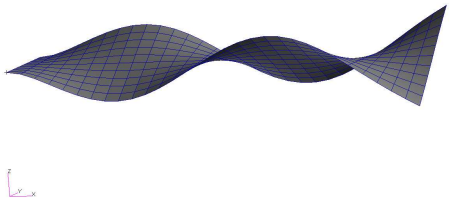

Figure 7.20. Sixth mode shape (Nastran)

Tab. 7.13 illustrates how higher order effects impact on the present analysis. Since the same frequencies are obtained with different order of through-the-thickness expansion, is clear that this case study is not significantly affected by higher order effects.

frEq. $[Hz]$	MUL2 1^{st}	MUL2 2^{nd}	MUL2 3^{rd}	MUL2 4^{th}
1	6.3292	6.3425	6.3338	6.3325
2	25.092	25.111	25.092	25.091
3	36.831	36.904	36.890	36.889
4	80.766	80.847	80.793	80.791
5	99.146	99.342	99.306	99.302
6	152.70	152.90	152.80	152.80

Table 7.13. Undamped natural frequencies of the plate with patches, regular mesh of 30×10 Q4 FEs, comparison between first, second third and fourth order through-the-thickness expansion

Chapter 8

Electro-magneto-mechanical results

In this chapter, PVD (D in acronyms) stands for PVD-u_x,u_y,u_z,ϕ,φ in order to simplify the notation.

8.1 Comparisons between FEM results and 3D closed form solutions

This chapter shows some numerical results obtained for the coupled magneto-electro-mechanical PVD application to assess the developed FEs for static magneto-electro-mechanical multilayered plate problems. Present FE analyses are compared with 3D exact solution by Pan [29]. Square plates which are loaded at the top layer surface and with simply supported edges are analyzed. Layered plates are build by using a combination of layers made of piezoelectric and magnetostrictive materials. The piezoelectric material consists of $BaTiO_3$ (called B for brevity) and the magnetostrictive one $CoFe_2O_4$ (called F for brevity). The physical properties of these two materials are given in Tab. 8.1 where C_{ij}, e_{ij}, q_{ij} are the stiffness, piezoelectric and piezomagnetic coefficients while ε_{ij} and μ_{ij} are the electric permittivity and the magnetic permeability respectively.
The considered stacking sequences are B/F/B and F/B/F, the load is a bi-sinusoidal pressure of peak 1 $[N/m^2]$, applied at the top face; each layer has the same thickness $h_k = 0.1$ $[m]$, plate length is $a = 1$ $[m]$ and all the quantities have been calculated with correspondence to the in-plane coordinate values: $x = 0.75$ $[m]$ and $y = 0.25$ $[m]$, as done in the referenced article [29]. The employed mesh is regular 4×4 of Q9 FEs. LW and ESL results are here compared with the exact solution. Linear, parabolic, 3-rd and 4-th order LW and ESL results are compared in Tabs. 8.2-8.5. Tabs. 8.2,8.3 collect results of mechanical electric and magnetic quantities, calculated for the B/F/B staking sequence; Tabs. 8.4,8.5 provide the same information in case F/B/F staking sequence.
At this point it is important to underline that in the FEM analysis the plate is considered as sensor. As a consequence, electric and magnetic potentials are set to zero both at the top and at the bottom face. Since such boundary condition is not imposed in the exact solution, FEM and exact potentials values are not in agreement. Anyway, this discrepancy does not affect results related to other quantities.
Displacements calculated by ESL theory are often (but not always) close to the exact solution,

but a high order through-the-thickness expansion is often required. With the LW approach good results for displacement can be reached even without a high order through-the-thickness expansion. In general, best results for stresses are obtained by LW theory with high order through-the-thickness expansion, while ESL approach can lead to unreasonable numbers. More details and results can be found in another work devoted to interactions between the magnetic field and the others [30].

Properties	$BaTiO_3$	$CoFe_2O_4$	Properties	$BaTiO_3$	$CoFe_2O_4$
C_{11}[GPa]	166	286	$e_{31}[C/m^2]$	-4.4	0
C_{22}[GPa]	166	286	$e_{32}[C/m^2]$	-4.4	0
C_{12}[GPa]	77	173	$e_{33}[C/m^2]$	18.6	0
C_{13}[GPa]	78	170.5	$e_{24}[C/m^2]$	11.6	0
C_{23}[GPa]	78	170.5	$e_{15}[C/m^2]$	11.6	0
C_{33}[GPa]	162	269.5	$q_{31}[N/(Am)]$	0	580.3
C_{44}[GPa]	43	45.3	$q_{32}[N/(Am)]$	0	580.3
C_{55}[GPa]	43	45.3	$q_{33}[N/(Am)]$	0	699.7
C_{66}[GPa]	44.5	56.5	$q_{24}[N/(Am)]$	0	550
			$q_{15}[N/(Am)]$	0	550
$\varepsilon_{11} \times 10^9[C^2/(Nm^2)]$	11.2	0.08			
$\varepsilon_{22} \times 10^9[C^2/(Nm^2)]$	11.2	0.08			
$\varepsilon_{33} \times 10^9[C^2/(Nm^2)]$	12.6	0.093			
$\mu_{11} \times 10^6[Ns^2/C^2]$	5	-590			
$\mu_{22} \times 10^6[Ns^2/C^2]$	5	-590			
$\mu_{33} \times 10^6[Ns^2/C^2]$	10	157			

Table 8.1. Properties of the materials employed in the Electro-magneto-mechanical problems

	σ_{zz} [Pa] top face	σ_{xz} [Pa] center	u_x [m] bottom face	u_z [m] bottom face
3D[29]	0.5	-3.96×10^{-1}	-2.01×10^{-12}	5.4×10^{-12}
LD1	0.74	-4.14×10^{-1}	-2.02×10^{-12}	5.5×10^{-12}
LD2	0.57	-4.31×10^{-1}	-2.05×10^{-12}	5.6×10^{-12}
LD3	0.55	-4.24×10^{-1}	-2.05×10^{-12}	5.6×10^{-12}
LD4	0.51	-4.23×10^{-1}	-2.05×10^{-12}	5.6×10^{-12}
ED1	1.38	-1.94×10^{0}	-1.24×10^{-13}	5.7×10^{-12}
ED2	3.95	-3.04×10^{-1}	-1.50×10^{-13}	6.4×10^{-12}
ED3	2.96	-1.00×10^{0}	-1.44×10^{-13}	6.72×10^{-12}
ED4	9.18	-4.78×10^{-2}	-1.45×10^{-13}	6.82×10^{-12}

Table 8.2. Electro-magneto-mechanical problem. Comparison of various kinematics for the B/F/B plate: evaluation of transverse stresses and displacements. The mesh is regular 4×4 of Q9 FEs

	ϕ_{max} [V]	φ_{max} [C/s]	σ_{xx} [Pa] top face	σ_{xy} [Pa] bottom face
3D[29]	1.54×10^{-3}	-2.61×10^{-6}	1.27	-5.77×10^{-1}
LD1	8.33×10^{-4}	-7.07×10^{-7}	1.43	-5.38×10^{-1}
LD2	8.39×10^{-4}	-7.15×10^{-7}	1.39	-5.47×10^{-1}
LD3	8.39×10^{-4}	-7.11×10^{-7}	1.38	-5.48×10^{-1}
LD4	8.39×10^{-4}	-7.12×10^{-7}	1.38	-5.48×10^{-1}
ED1	5.98×10^{-4}	-6.65×10^{-7}	2.67	-3.35×10^{-2}
ED2	1.01×10^{-3}	-8.22×10^{-7}	4.39	-3.06×10^{-2}
ED3	9.86×10^{-4}	-8.08×10^{-7}	5.76	-3.02×10^{-2}
ED4	9.97×10^{-4}	-1.01×10^{-6}	9.72	-2.65×10^{-2}

Table 8.3. Electro-magneto-mechanical problem. Comparison of various kinematics for the B/F/B plate: evaluation of in-plane stresses and electric and magnetic potentials. The mesh is regular 4×4 of Q9 FEs

	σ_{zz} [Pa] top face	σ_{xz} [Pa] center	u_x [m] bottom face	u_z [m] bottom face
3D[29]	0.5	-3.86×10^{-1}	-1.57×10^{-12}	4.38×10^{-12}
LD1	0.83	-3.97×10^{-1}	-1.55×10^{-12}	4.33×10^{-12}
LD2	0.53	-4.11×10^{-1}	-1.583×10^{-12}	4.40×10^{-12}
LD3	0.51	-4.06×10^{-1}	-1.584×10^{-12}	4.40×10^{-12}
LD4	0.51	-4.06×10^{-1}	-1.585×10^{-12}	4.40×10^{-12}
ED1	1.56	-1.25×10^{0}	-1.30×10^{-13}	4.00×10^{-12}
ED2	8.73	-3.22×10^{-1}	-1.57×10^{-13}	5.44×10^{-12}
ED3	3.91	-7.84×10^{-1}	-1.58×10^{-13}	5.56×10^{-12}
ED4	16.4	-1.95×10^{-1}	-1.59×10^{-13}	5.64×10^{-12}

Table 8.4. Electro-magneto-mechanical problem. Comparison of various kinematics for the F/B/F plate: evaluation of transverse stresses and displacements. The mesh is regular 4×4 of Q9 FEs

	ϕ_{max} [V]	φ_{max} [C/s]	σ_{xx} [Pa] top face	σ_{xy} [Pa] bottom face
3D[29]	2.30×10^{-3}	-1.88×10^{-6}	1.33	-5.69×10^{-1}
LD1	5.54×10^{-4}	-1.63×10^{-7}	1.6	-5.49×10^{-1}
LD2	5.56×10^{-4}	-1.53×10^{-7}	1.44	-5.74×10^{-1}
LD3	5.58×10^{-4}	-1.55×10^{-7}	1.42	-5.74×10^{-1}
LD4	5.58×10^{-4}	-1.55×10^{-7}	1.42	-5.74×10^{-1}
ED1	4.48×10^{-4}	-3.00×10^{-6}	2.65	-4.81×10^{-2}
ED2	4.84×10^{-4}	-1.90×10^{-6}	8.26	-4.18×10^{-2}
ED3	5.62×10^{-4}	-1.73×10^{-6}	6.89	-4.21×10^{-2}
ED4	5.10×10^{-4}	-1.41×10^{-6}	15.9	-3.61×10^{-2}

Table 8.5. Electro-magneto-mechanical problem. Comparison of various kinematics for the F/B/F plate: evaluation of in-plane stresses and electric and magnetic potentials. The mesh is regular 4×4 of Q9 FEs

Chapter 9

Conclusions and outlook

During this PhD an advanced modeling technique has been proposed for the analysis of multilayered structures in multifield approach. Referring to thermodynamics, the constitutive relations for mechanical, thermal, electrical and magnetic fields have been obtained considering the fully coupled interactions. Two principal variational statements have been considered (the PVD and the RMVT). Each variational statement has been customized to the particular subcases of coupling. A new condensed notation has been thought in order to make possible the use of a symbolic code to obtain the FE matrices appropriate to analyze each possible case-study. Within this framework, a set of new FEs have been formulated and assessed by comparisons to closed-form solutions.
The inedit $RMVT\text{-}D_z$ class of FEs seems particularly promising for the application to the closed-loop control of smart structures.
The usefulness of the higher order mixed layer-wise FEs (not available in commercial codes) has been discussed in reference to the accurate calculation of the stress field and to the application of failure criteria.
A few results of buckling analysis have been obtained and discussed together with results of undamped natural frequencies of plates in pre-loaded configuration. A future research could be planned to study the buckling, the natural frequencies and the mode shape of plates subjected to in-plane combined loading, where shear and normal stresses are simultaneously present. It is understood that this subject is relevant for aerospace applications, where panels works almost always in pre-loaded configuration during their operational life. The investigation could easily encompass anisotropic multilayered structures in multifield approach, according to the advanced two-dimensional modeling proposed in this work. The interest in this topic is due to the fact that thermo-mechanical coupled interactions play a crucial role in buckling phenomena.
Particular emphasis should be also devoted to the capabilities of the formulated thermo-mechanical FEs, which are able to calculate in one single run the steady-state static deformation of a structure under thermal loading. The separate application of the Fourier's law to obtain the trough-the-thickness temperature profile is not required. In fact, the temperature distribution through all the layers of the structure is automatically calculated using the information of thermal conductivities besides the pure mechanical constitutive coefficients.
Definitely, the work done during this PhD has contributed to enrich the spectrum of multifield plate FEs that can be implemented, according to a hierarchical approach. Results concerning many particular FEM applications of PVD/RMVT have not been illustrated for sake of conciseness, although the methodology to obtain corresponding fundamental nuclei has been detailed. In conclusion, results obtained in this PhD would suppose further market-oriented

FEM implementations, with the aim to propose advanced computational tools for engineering applications.

Appendix A

Obtaining other PVD possible fundamental nuclei

One of the goals in FEM analysis it to fast calculations as much as possible, without loosing accuracy in results. On top of this, is is understood that not all the multifield primary unknowns are necessary in a generic computation.
For instance, if thermal effect can be neglected, following procedure can be employed to erase the virtual variation $\delta\theta$:

- deletion of therm related to θ, in vector of primary unknowns (i.e. the 6^{th} term in Eqs. 1.32,4.3);
- deletion of column related to θ (the 6^{th}) in the differential operator of Eq. 1.34;
- deletion of the column and the row related respectively to θ and to η (which is the extensive variable associated to θ), in the consititutive matrix of Eq. 1.18;
- deletion of the cell related to θ (the 6^{th}) in vectors of Eqs. 1.15,1.16.

In so doing, nucleus $\boldsymbol{K}^{k\tau sij}$ results in a 5×5 matrix.
The same reasoning can be followed and automatized to neglect the others primary unknowns'virtual variations (i.e. u_x, u_y, u_z, ϕ or φ).
At this point it is clare the reason of authors'choice to group al the multifield primary variables in just one vector and multifield constitutive and geometrical relations in single matrices: in this way it is possible to obtain, always with the same automatized passages, nuclei involving whatever combination of primary unknowns (even neglecting displacements, for example in case of just thermal analysis). The aim is to show an easy-to-implement way to consider the chosen coupling interactions in FEM codes. Fundamental nucleus concerning the PVD pure mechanical case can be obtained deleting $\delta\phi$, $\delta\varphi$ and $\delta\theta$ contributions.
PVD Fundamental nucleus with mechanical-thermo coupling See consists in a 4×4 matrix and can be obtained deleting ϕ and φ contributions.
Modus operandi above described is the rigorous one. For the PVD case, all the nuclei can be obtained in a more simple way: starting from the 6×6 nucleus (which consider all primary unknowns), nuclei concerning all the other combinations of primary unknowns'virtual variations (in number less than 6) can be obtained simply erasing from the complete 6×6 $\boldsymbol{K}^{k\tau sij}$ matrix, all rows and columns which index is related to the primary unknowns to be excluded. The indices

are numbered as in the following:

$$\left\{ \begin{array}{cccccc} 1 & 2 & 3 & 4 & 5 & 6 \end{array} \right\} \tag{A.1}$$

$$\left\{ \begin{array}{cccccc} u_x & u_y & u_z & \phi & \varphi & \theta \end{array} \right\} \tag{A.2}$$

In Sec. 3.1 are a few examples of various PVD applications which leads to different fundamental nuclei.
The mass fundamental nucleus is be trivially obtained since it is only inclusive of contribution related to the mechanical field.

Appendix B

Obtaining other RMVT possible fundamental nuclei

As done for PVD in Appendix A, also with RMVT we can identify an automatic procedure to obtain all the other fundamental nuclei, when not all coupling are considered and even when less extensive variables are modeled in the thickness plate z-direction.
For instance, if thermal effect can be neglected, the same procedure described in Appendix A can be employed to erase virtual variation $\delta\theta$ from matrix involved by RMVT:

- deletion of therm related to θ, in vector of primary unknowns (i.e. the 6^{th} term in Eqs. 3.32,4.8;
- deletion of column related to θ (the 6^{th}) in the differential operator of Eq. 3.4.2;
- deletion of column related to θ (the 8^{th}) in vectors of Eqs. 3.59 and 3.59;
- deletion of the columns or rows related respectively to θ and to η (which is the extensive variable associated to θ), in consititutive matrix of Eqs. 3.4.2-3.4.2 (6^{th} row in Eqs. 3.4.2,3.47 and 6^{th} column in Eqs. 3.4.2,3.4.2).

In so doing, nucleus $\boldsymbol{K}^{k\tau si j}$ results in a 10×10 matrix.
The same reasoning can be followed and automatized to neglect the others primary unknowns'virtual variations (i.e. u_x, u_y, u_z, ϕ or φ).
Moreover, with the following example it is showed how to avoid the "a priori" modeling of a generic extensive variable between σ_{zz}, σ_{xz}, σ_{yz}, D_z and B_z.
The procedure to avoid the "a priori" modeling of the extensive variable D_z is illustrated in the following:

- to move from matrix of Eq. 3.41 the row related to D_z (next-to-last row), putting it to the end of matrix of Eq. 3.4.2;
- to erase from matrix of Eqs. 3.4.2 and 3.41 the null column related to D_z (next-to-last column);
- to erase the row and column related to D_z (next-to-last row and column) from matrix of Eq. 3.42, adding a column of zeros at the fist position;
- to move from vectors of Eqs. 3.59,3.59 the row related to D_z (next-to-last row), putting it to the end of vectors of Eqs. 3.59,3.59 respectively;

- to erase the row and column related to D_z (next-to-last row and column) from matrix of Eq. 3.4.2;
- to move from matrix of Eqs. 3.47 and 3.49 columns related to D_z (next-to-last row), putting it to the end of matrix of matrix in Eqs. 3.4.2 and 3.4.2 respectively;
- to move from matrix of Eqs. 3.4.2,3.49 rows related to D_z (next-to-last columns), putting it to the end of matrix matrix in Eqs. 3.4.2 and 3.47 respectively.

In so doing, nucleus $\boldsymbol{K}^{k\tau sij}$ results in a 9×9 matrix.
The same reasoning can be followed and automatized to avoid the "a priori" modeling of other extensive variable in the thickness plate z-direction, clarifying that in RMVT at list one variable must be modeled, otherwise PVD should be adopted. In Sec. 3.2 are a few examples of various RMVT applications which leads to different fundamental nuclei.
The mass fundamental nucleus is be trivially obtained since it is only inclusive of contribution related to the mechanical field and it is not conditioned by the "a priori" modeling of extensive variables.

Bibliography

[1] T. Ikeda. Fundamentals of piezoelectricity. *New York: Oxford Science Pubblications*, 1996.

[2] E. Carrera. Historical review of zig-zag theories for multilayered plates and shells. *Applied Mechanics Review*, 56:287–308, 2003.

[3] E. Carrera and S. Brischetto. Piezoelectric shell theories with a priori continuous transverse electromechanical variables. *JOMMS*, 2(2):377–399, 2007.

[4] E. Carrera and C. Fagiano. Mixed piezoelectric plate elements with continuous transverse electric displacements. *Journal of Mechanics of Materials and Structures*, 2(3):421–438, 2007.

[5] R.D. Mindlin. Forced thickness-shear and flexural vibrations of piezoelectric crystal plates. *Journal of Applied Physics*, 23:83–88, 1952.

[6] R.D. Mindlin H.F. Tiersten. Forced vibrations of piezoelectric cristal plates. *Quarterly of Applied Mathematics*, 20(2):107–119, 1962.

[7] E.P. EerNisse. Variational method for electroelastic vibrations analysis. *IEEE Transaction on Sonics and Ultrasonics*, SU-14(4):153–160, 1967.

[8] H.F. Tiersten. Linear piezoelectric plate vibrations. *Plenum Press, New York*, 1969.

[9] H. Allik and T.J.R. Hughes. Finite element method for piezoelectric vibration. *nternat. J. Numer. Methods Engrg.*, 2:151–157, 1970.

[10] R. D. Mindlin. Equation of high frequency vibration of thermopiezoelectric crystal plates. *Internat. J. Solids. and Structures*, 10:625–637, 1974.

[11] R. D. Mindlin. Theory of vibration of coated, thermopiezoelectric laminae. *J. Math. Phys.*, 19 (1):109–126, 1978.

[12] E. Carrera. Developments, ideas and evaluations based upon the reissner's mixed theorem in the modelling of multilayered plates and shells. *Applied Mechanics Review*, 54:301–329, 2001.

[13] E. Carrera. A class of two dimensional theories for multilayered plates analysis. *Atti Accademia delle Scienze di Torino, Mem Sci. Fis.*, 19-20:49–87, 1995.

[14] E. Carrera. Theories and finite elements for multilayered anisotropic, composite plates and shells. *Archives of Computational Method in Engineering, state of the art Reviews*, 9:87–140, 2002.

[15] E. Carrera and M. Boscolo. Classical and mixed finite elements for static and dynamics analysis of piezoelectric plates. *International Journal Numerical Methods in Engineering*, 70:253–291, 2007.

[16] G.A. Altay and M.C. Dökmeci. Some variational principles for linear coupled thermoelasticity. *International Journal of Solids and Structures*, 14(26):3937–3948, 1996.

[17] E. Reissner. On a certain mixed variational theory and a proposed application. *International journal for Numerical Methods in Engineering*, 20:1366–1368, 1984.

[18] E. Carrera, S. Brischetto, and P. Nali. Variational statements and computational models for multifield problems and multilayered structures. *Special Issue of MAMS*, 15(3):182–198, 2008.

[19] E. Carrera, M. Cinefra, and P. Nali. Mitc technique extended to variable kinematic multilayered plate elements. *Composite Structure*, 92:1888–1895, 2010.

[20] H.-R. Meyer-Piening. Experiences with 'exact' linear sandwich beam and plate analyses regarding bending, instability and frequency investigations. *Proceedings of the Fifth International Conference On Sandwich Constructions*, 1:37–48, Zurich, Switzerland, September 5-7, 2000.

[21] E. Carrera and S. Brischetto. Analysis of thickness locking in classical, refined and mixed multilayered plate theories. *Composite Structures*, 82:449–562, 2008.

[22] G.J. Turvey, N. Mulcahy, and M.B. Widden. Experimental and computed natural frequencies of square pultruded grp plates: effects of anisotropy, hole size ratio and edge support conditions. *Composite Structures*, 50:391–403, 2000.

[23] N.J. Pagano. Stress fields in composite laminates, international journal of solids structures. *International Journal of Solids Structures*, 14:401–406, 1978.

[24] K. Bhaskar, T. K. Varadan, and J. S. M. Ali. Thermoelastic solutions for orthotropic and anisotropic composite laminates. *Composites*, 27B:415–420, 1996.

[25] V.B. Tungikar and K.M. Rao. Three dimensional exact solution of thermal stresses in rectangular composite laminate. *Composite structures*, 27:419–430, 1994.

[26] E. Carrera, M. Boscolo, and A. Robaldo. Hierarchic multilayered plate elements for coupled multifield problems of piezoelectric adaptive structures: formulation and numerical assessment. *Archives of Computational Method in Engineering*, 14:383–430, 2007.

[27] P. Heyliger and D.A. Saravanos. Exact free-vibration analysis of laminated plates with embedded piezoelectric layers. *Journal of Acoustical Society of America*, 98(3):1547–1557, 1995.

[28] P. Heyliger. Static behavior of laminated elastic-piezoelectric plates. *AIAA Journal*, 32(12):2481–2484, 1994.

[29] E. Pan. Exact solution for simply supported and multilayered magneto-electro-elastic plates. *Journal of Applied Mechanics*, 68:608–618, 2001.

[30] E. Carrera, M. Di Gifico, P. Nali, and S. Brischetto. Refined multilayered plate elements for coupled magneto-electro-elastic analysis. *Multidisccipline Modeling in Materials and Structures*, 5:119–138, 2009.